YEAR-END TECHNICAL REPORT

September 29, 2023 to September 28, 2024

Environmental Remediation Science and Technology

Date submitted:

June 13, 2025

Principal Investigator:

Leonel E. Lagos, Ph.D., PMP®

Florida International University Collaborators:

Yelena Katsenovich, Ph.D.
Ravi Gudavalli, Ph.D.
Pieter Hazenberg, Ph.D.
Angelique Lawrence, M.S., GISP
Vadym Drozd, Ph.D.
DOE Fellows

Submitted to:

U.S. Department of Energy
Office of Environmental Management
Under Cooperative Agreement # DE-EM0005213

FIU | Applied Research Center
FLORIDA INTERNATIONAL UNIVERSITY

Addendum:

This document represents one (1) of five (5) reports that comprise the Year End Reports for the period of September 29, 2023 to September 28, 2024 prepared by the Applied Research Center at Florida International University for the U.S. Department of Energy Office of Environmental Management (DOE-EM) under Cooperative Agreement No. DE-EM0005213.

The complete set of FIU's Year End Reports for this reporting period includes the following documents:

Project 1: Chemical Process Alternatives for Radioactive Waste
Document number: FIU-ARC-2023-800012997-04b-009

Project 2: Environmental Remediation Science and Technology
Document number: FIU-ARC-2023-800013918-04b-006

Project 3: Waste and D&D Engineering and Technology Development
Document number: FIU-ARC-2023-800013919-04b-006

Project 4: DOE-FIU Science & Technology Workforce Development Initiative
Document number: FIU-ARC-2023-800013920-04b-015

Project 5: Long-Term Stewardship of Environmental Remedies: Contaminated Soils and Water and STEM Workforce Development
Document number: FIU-ARC-2023-800013922-04b-005

Each document will be submitted to OSTI separately under the respective project title and document number as shown above. In addition, the documents are available at the DOE Research website for the Cooperative Agreement between the U.S. Department of Energy Office of Environmental Management and the Applied Research Center at Florida International University: https://doeresearch.fiu.edu

TABLE OF CONTENTS

LIST OF FIGURES

LIST OF TABLES

PROJECT 2 EXECUTIVE SUMMARY

This project focuses on research to support environmental remediation and long-term monitoring of contaminated sediment, surface water, and groundwater at the Hanford Site, Savannah River Site (SRS), and the Waste Isolation Pilot Plant (WIPP). The primary objective is to reduce the potential for contaminant mobility or toxicity in surface and subsurface environments through the development and application of state-of-the-art environmental remediation technologies at DOE sites.

In FIU Year 4, the FIU Applied Research Center (ARC) provided research and technical support for contaminant remediation efforts at the Hanford Site under Task 1, at SRS under Tasks 2 and 3, and at the WIPP under Task 6. This research involved laboratory-scale studies employing novel analytical methods and advanced microscopy techniques for the characterization of various mineral samples. The tasks also included the implementation of hydrological models to predict the behavior and fate of existing and potential contaminants in surface and subsurface environments.

DOE Fellows supporting this project include Melissa Dieguez (Undergraduate, Biomedical Engineering), Aubrey Litzinger (Graduate, M.S., Environmental Engineering), Hannah Aziz (undergraduate, Environmental Engineering), Reann Nicolas, (undergraduate, Civil Engineering), Carolyn Grace Cooke (graduate, Ph.D., Chemistry), Ellie Risher (undergraduate, Environmental Engineering).

The following ARC researchers are supporting this project and mentoring the DOE-EM Fellows: Yelena Katsenovich (Ph.D., Env. Engineering, Tasks 1.5 & 5.2, Sr. Research Scientist, Project Manager), Ravi Gudavalli (Ph.D., Env. Engineering, Tasks 2.1 & 2.2, Sr. Research Scientist), Pieter Hazenberg (Ph.D., Hydrology and Quantitative Water Management, Tasks 3 & 6, Sr. Research Scientist), Angelique Lawrence (M.S., Environmental Science, Tasks 3 & 6, Research Specialist II), Vadym Drozd (Ph.D., Inorganic Chemistry, Task 1.4, Research Associate), Jose Rivera (B.S., Civil Engineering, Research Analyst), Leonel Lagos (Ph.D., PMP®, Mechanical Eng./Civil/Env. Engineering, PI).

Task 1: Remediation Research and Technical Support for the Hanford Site

The DOE EM faces a critical need to understand the biogeochemical processes influencing the behavior of contaminants such as uranium (U), iodine (I), technetium (Tc), chromium (Cr), and nitrate (NO_3^-) in the deep vadose zone (VZ) at the Hanford Site, as these contaminants significantly impact groundwater quality. These pollutants were released during atomic weapons production at the Hanford Site from 1944 through the late 1980s, leaving a complex legacy of radionuclide and chemical contamination in soil and groundwater.

This contamination presents unique and technically challenging cleanup issues for EM. The radioactive waste at the Hanford Site contains approximately 195 million curies of radioactivity and 220,000 metric tons of chemical contaminants. Of the 177 onsite tanks, 67 have leaked an estimated 3,800 cubic meters (1 million gallons) of liquid waste into the underlying sediment. In addition to the remaining tank waste, significant contamination persists in the soil, groundwater, and burial grounds (Gephart, 2003).

Most of this residual waste is concentrated in or near the 200 Area, where contaminant plumes pose a threat to groundwater due to downward migration through the unsaturated VZ sediment.

Among the fastest-moving subsurface contaminants are technetium-99, iodine-129, chromium, uranium, and nitrate (Gephart, 2003).

Task 1 provides an overview of subtasks supporting the Hanford Site's cleanup mission. These efforts complement ongoing work at PNNL to improve the understanding of long-term contaminant behavior in the subsurface.

Task 2. Remediation Research and Technical Support for Savannah River Site

Iodine-129 and uranium stand out as the major risk drivers among radiological acid waste contaminants released at the Savannah River Site's F-Area. Radionuclides, previously disposed of in unlined seepage basins as constituents of acidic aqueous waste, are migrating towards Fourmile Branch and Tims Branch wetlands through natural groundwater flow. Here, they may interact with natural organic materials in the wetland or with humic materials injected for remediation purposes.

There is a pressing need for the Savannah River Site (SRS) to collect results supplementing permit requirements associated with the Area Completion Project (ACP), specifically the Phase 2 strategy evaluating the performance of Phase 1, including areas downgradient of the F-Area inactive process sewer line and at Fourmile Branch. As per the corrective action plan's permitting requirements, ^{129}I concentrations must meet groundwater standards in Fourmile Branch by October 31, 2025, and in the F-Area plume in surface water at the seepline by October 31, 2030. Given the absence of DOE-approved technology for subsurface iodine remediation, understanding its long-term fate in plumes at SRS is crucial. Additionally, DOE-EM mandates further study of the fate of co-mingled contaminant plumes due to their complexity (McCabe, D., et al., 2017).

The experiments outlined in this task will contribute to our understanding of the interactions of ^{129}I with organic materials, study the factors controlling the attenuation of ^{129}I in wetlands, and assess the potential for U remediation through the injection of modified humic materials. These findings will provide essential data for meeting the aforementioned permitting requirements and DOE-EM goals.

SRS is undertaking synergistic research, funded by the Department of Energy's Environmental Management Office of Soil and Groundwater Remediation, as part of the Attenuation-Based Remedies for the Subsurface Applied Field Research Initiative (ABRS AFRI). This applied research aims to develop science-based approaches for cleaning and closing sites contaminated with combinations of metals, radionuclides, and other contaminants of concern.

The primary objective of this program is to devise attenuation-based remedies, specifically to investigate and validate the use of humate for subsurface stabilization of metals in contaminated groundwater plumes. SRS successfully conducted a field campaign demonstrating the viability of dissolving and injecting low-cost agricultural humate into the subsurface. The proposal suggests that this method may serve as a viable attenuation-based remedy for uranium and potentially for I-129 as well. Humic acid, with its numerous functional groups, plays a crucial role in ion exchange and acts as a metal complexing ligand with high complexation capacity, influencing the mobility of radionuclides in natural systems.

The fate and transport of uranium and iodine in the subsurface are influenced by various environmental factors, including pH, temperature, ORP, etc. A comprehensive understanding of the environmental conditions affecting these processes is crucial for a more realistic risk assessment. In FIU Performance Year 4, research was conducted to investigate the factors controlling the attenuation of iodine in the presence of wetland sediment and organoclays.

Additionally, ongoing research explored the impact of humic acid on uranium mobility at the Savannah River Site. Various types of humic substances, such as KW-30, were utilized in this research to assess their effect on co-contaminant removal.

The Task 2 component of this end-of-year report provides an overview of subtasks supporting the Area Completion Project to reduce iodine contamination, as well as the ABRS AFRI.

Task 3: Contaminant Fate and Transport Modeling for the Savannah River Site

This task involves the development and application of integrated hydrology and contaminant transport models for studying the fate of priority pollutants with emphasis on interactions between solute and sediment transport in the stream systems at SRS. The aim is to examine the response of these streams to historical discharges and environmental management remediation actions. The knowledge gained through these studies will provide a means of assessment, evaluation and post-closure long-term monitoring of water quality and environmental conditions following remedial activities. In general, hydrological models are the standard tools used for investigating surface/subsurface flow behavior. They provide uncertainty quantification, risk and decision support for water resource management, and evaluation of water quality, erosion, deposition, and transport. The models being developed by FIU will serve as long-term monitoring tools that provide simulation capabilities to economically assess the fate and transport of heavy metals and radionuclides of concern (e.g., uranium and I-129), that may have direct or indirect impact on the SRS environment. The models will provide information needed for informed decision-making in existing DOE-EM soil and groundwater remediation programs. Results obtained will provide DOE-EM suggestion of key locations for contaminant monitoring. Furthermore, the models can be utilized as forecasting tools to predict suspended sediment loads and the extent of remobilization regimes under different scenarios of extreme storm events and erosion conditions as well as the impact of long-term changes in climate.

Task 3 involves several subtasks that will assist DOE-EM in ensuring the achievement and maintenance of regulatory compliance goals for water quality in the SRS watersheds and in developing cost-effective remediation plans integrated into the SRS Area Completion Project (ACP) thus accelerating progress of the DOE EM environmental restoration mission.

Task 5: Research and Technical Support for WIPP

FIU has been engaged in basic research in collaboration with researchers from Los Alamos National Laboratory’s Actinide Chemistry and Repository Science Program (ACRSP) and the DOE Carlsbad Field Office (DOE-CBFO) to establish the scientific basis for the long-term disposition of nuclear waste in the WIPP repository. The solubility of actinides is a key factor influencing the fate and transport of radionuclides in the subsurface environment, particularly in the far field of a nuclear waste disposal site like the Waste Isolation Pilot Plant (WIPP).

In Year 4, FIU’s research was put on hold due to the loss of personnel, so there are no results to report. FIU will maintain communication with LANL scientists for potential future collaboration.

Task 6: Hydrology Modeling for Basin 6 of the Nash Draw near the WIPP

Scientists and researchers are concerned about the impact of climate on the karst region surrounding the Waste Isolation Pilot Plant (WIPP) and the long-term vulnerability, integrity and performance of this deep geologic transuranic waste repository due to the influence of characteristic surface features, such as sinkholes, swallets, and karst valleys, on groundwater recharge over time. Long-term changes in climate that are anticipated to occur within the south/southwestern USA are expected to result in more frequent intense precipitation events. It is currently unknown if this will lead to increased groundwater recharge or whether this results in increased surface flow and evapotranspiration. It is unclear whether groundwater recharge would be impacted and how, if impacted, this might affect the dissolution rate of halite within the subsurface. Task 6 was developed to support DOE-EM research and development activities at the Waste Isolation Pilot Plant (WIPP) by developing a high-resolution digital elevation model (DEM) of Basin 6 of the Nash Draw, just west of the repository, to more accurately delineate surface hydrological features and provide a foundation for development of a regional hydrological model using the DOE-developed Advanced Terrestrial Simulator (ATS). Using high-resolution surface elevation information will improve the ability of the coupled surface/subsurface flow model to simulate the hydrologic response to a range of storm events, compute the surface water balance and provide more accurate estimates of regional-scale infiltration rates/groundwater recharge. With improved estimates of the spatial and temporal patterns of recharge to force the groundwater model, predictions of halite dissolution and propagation of the shallow dissolution front will be made possible and the potential impact on repository performance quantified.

The research conducted under Task 6 evaluates the role of heavy precipitation events on groundwater recharge through surface depressions like sinkholes and the impact that this can have on the long-term stability of the WIPP.

MAJOR TECHNICAL ACCOMPLISHMENTS

Task 1: Remediation Research and Technical Support for the Hanford Site

Subtask 1.2: This subtask was completed in FIU Year 3.

- Submitted a paper titled "*The Reoxidation Behavior of Tc(IV) and U(IV) in Perched Water of the Hanford Site Vadose Zone after Treatment with Strong Reductants*" to the WM Symposia 2024.

Subtask 1.3: This task was completed in FIU Year 3

- Published a manuscript titled *"Impact of chromium (VI) as a co-contaminant on the sorption and co-precipitation of uranium (VI) in sediments under mildly alkaline oxic conditions"* authored by Mariah S. Doughman (PhD student, DOE Fellow), Kevin E. O'Shea, Nikolla P. Qafoku, Hilary P. Emerson, James E. Szecsody, Kenneth C. Carroll, and Yelena P. Katsenovich in the Journal of Environmental Management, Vol. 349 (2024) 119463.

Subtask 1.4:

- Completed Milestone 2023-P2-M6 *"Complete baseline testing at pH 12 and Al concentration 0.3-30 ppm at 90ºC"*. FIU conducted a series of static corrosion tests to investigate the influence of aluminum (Al) concentrations in the leachate on glass dissolution rates. The results showed a very defined trend: the increase in Al concentrations up to 30 mg/L contributed to the decrease in boron (B) and rhenium (Re) normalized mass loss due to leaching.
- Completed product consistency tests (PCTs) at 70ºC and 40ºC with an Al-amended solution at pH 12.0 amended with 1, 5, 15 and 30 mg/L Al3+.
- Submitted a manuscript titled *"The corrosion behavior of borosilicate glass in the presence of cementitious waste forms"* authored by Yelena Katsenovich, Vadym Drozd, Shambhu Kandel, Leonel Lagos, and Matthew Asmussen, which was accepted for publication by Dalton Transactions, the International Journal of the Royal Society of Chemistry.
- Completed product consistency tests (PCTs) at 70ºC and 40ºC with an Al-amended solution at pH 12.0 amended with 1, 5, 15 and 30 mg/L Al^{3+}.
- Presented project results at the Goldschmidt conference (invited talk), Chicago, 18-23 August 2024. The presentation was titled "Borosilicate glass dissolution in the presence of cementitious waste forms" by V. Drozd, Y. Katsenovich, L. Lagos. M. Asmussen.
- Completed product consistency test (PCT) for glass waste forms dissolution experiments at 90, 70, 40 and 25ºC using Al-amended solutions at pH 8.

Subtask 1.5:

- Prepared an experimental test plan (Milestone 2023-P2-M5) and commenced experimental work for Phase 1, which involves working with the samples under anaerobic conditions.

- Completed Phase 1 experiments under anaerobic conditions and experimental work is now being conducted under aerobic conditions following the addition of ammonia hydroxide.
- Completed Phase 2 experiments under aerobic conditions following the addition of ammonium hydroxide.
- Completed processing of all collected samples for the various metal and anion concentrations. The work is now focused on analyzing the data from the collected samples.
- Completed all liquid phase analyses for collected samples with ICP-MS, ICP-OES and IC instruments.
- DOE Fellow Melissa Dieguez has transitioned to a new position at PNNL as an Undergraduate Technical Intern – Level IV.

Task 2. Remediation Research and Technical Support for Savannah River Site

Subtask 2.1:

- Completed sorption kinetics experiments with SRS wetland sediment and organoclays (MRM/PM-199).
- Completed Milestone 2023-P2-M9 entitled *"Complete batch experiments study on the sorption of iodine in the presence of organoclays and SRS wetland sediment"*.
- Completed Deliverable 2023-P2-D3 entitled, *"Draft report on sorption of Iodine in the presence of organoclays and SRS wetland sediment"*. The adsorption kinetics of iodide and iodate by wetland soils at 0-2 feet depth, with added organoclays PM-199 and MRM, were investigated. Iodide was more effectively removed than iodate, with approximately 77% removed by PM-199 and 55% by MRM. Iodate removal was about 30% with PM-199 and 45% with MRM. Initial uptake was faster for PM-199 treated samples and for iodide in both treatments, indicating iodide is more readily adsorbed, consistent with previous research. The effect of pH (4-8) was studied, showing little impact on sorption capacity from pH 4-7 and only a small effect at pH 8, likely due to a negative charge on organoclays inhibiting adsorption. PM-199 was overall more effective at removing iodine species.
- Completed kinetics experiments to study the attenuation of iodide and iodate to organoclays MRM and PM-199 in the presence of SRS wetland topsoil.
- Conducted batch sorption experiments to determine the effect of pH on the sorption of iodide to the minerals (kaolinite, illite, MX-80 bentonite, quartz, and goethite) that represent the SRS F-Area aquifer sediment.

Subtask 2.2:

- Completed experiments to study the sorption of iodine species onto SRS sediment. Samples will be analyzed via ICP-MS for aqueous iodine concentrations to estimate the sorption of iodine species.
- Completed sorption experiment to study the sorption of KW-30 onto SRS sediment in deionized water (DIW) and synthetic groundwater (SGW). DIW samples had an average sorption of 1,750 mg/kg (36% KW-30 removal) while SGW samples had an average of 1,250 mg/kg (25% KW-30 removal).

- Performed UV-Vis spectrometer analysis of the different concentrated solutions from both DIW and SGW calibrations ranging from 5 ppm-25 ppm in range of 190 nm-1000 nm.
- Completed experiments to study the sorption of co-contaminants in the presence of uncoated and KW-30-coated sediments. A set of control samples were also prepared to observe any precipitation.

Task 3: Contaminant Fate and Transport Modeling for the Savannah River Site

Subtask 3.1:

- ***(FIU Year 3 Carryover Scope)*** Completed Milestone 2023-P2-M7, which involved simulations and evaluation of event-based uranium transport in Tims Branch. Former DOE Fellow, Juan Morales, included this research as a component of his PhD dissertation titled *"Long-Term Monitoring of Heavy Metals Using Numerical Modeling and Molecular Indices"* which he defended and passed in March 2024.
- Milestone 2023-P2-M13, Complete draft manuscript on uranium transport model for Tims Branch (Subtask 3.1) due 9/1/2024 will be reforecast to FIU Year 5.
- Continued adjusting input parameters and running simulations to achieve better results and identify the best MIKE ECO Lab model parameters to simulate long-term uranium transport within the river network of Tims Branch.

Subtask 3.2.1:

- Successfully completed Milestone 2023-P2-M4 entitled*: "Finalize calibration of MIKE model for Fourmile Branch using upstream observations"*.
- Completed Milestone 2023-P2-M10 entitled *"Complete long-term simulations of Fourmile Branch watershed using MIKE model for current and future climate"* on May 31, 2024. Climate data used to force the MIKE model was downloaded from the latest version of the NASA Earth Exchange Global Daily Downscaled Projections (NEX-GDDP-CMIP6) which contains downscaled historical data and future projections for 1950–2100. Thirteen (13) simulations were run for the periods 1950 – 1980, 1980 – 2015, 2015 – 2050, 2050 – 2080, and 2080 – 2100. For each time period between 2015 – 2100, four different scenarios based on the climate model projections were simulated. For the time periods between 1950 – 2015, simulations were based on the climate model's historical data.
- Ran simulations of 4 scenarios to examine long term changes in discharge using current and future climate data derived from the NASA Earth Exchange Global Daily Downscaled Projections for CMIP6 to force the MIKE model, SSP1-2.6: Sustainability (Taking the Green Road), SSP2-4.5: Middle of the Road, SSP3-7.0: Regional rivalry (A Rocky Road) and SSP5-8.5: Fossil-Fueled Development (Taking the Highway), which each have different projections for future greenhouse gas emissions and temperature variability.

Subtask 3.2.2:

- Completed Milestone 2023-P2-M2, which involved enhancement of the ATS model by inclusion of upstream channel flow in the F-Area hillslope domain, by integrating time series data for inflow at two strategic points within the watershed. This allows the model to represent more realistic scenarios by considering how water movement at these points affects the overall system behavior.

- Extended the Python package, Watershed Workflow, to automate the download of NASA Earth Exchange Global Daily Downscaled Projections for CMIP6 and its conversion to an ATS readable format. Multi-year ATS simulations of the F-Area hillslope were then performed for current and future climate (Milestone 2023-P2-M11) and a report on model long-term simulations of hydrological response of F-Area hillslope and Fourmile Branch watershed (Deliverable 2023-P2-D5) was submitted to DOE-EM collaborators.

Task 5: Research and Technical Support for WIPP

- This task was put on hold during FIU year 4 due to the loss of personnel but will resume in FIU Year 5.

Task 6: Hydrology Modeling for Basin 6 of the Nash Draw near the WIPP

Subtask 6.2:

- Completed enhancements to the ATS model for Basin 6, which included the incorporation of known sinkhole locations into the mesh (Milestone 2023-P2-M3) to permit the analysis of the impact of sinkholes and karst features on groundwater recharge.
- Developed two ATS model simulations, one with sinkholes explicitly represented and the other in which sinkholes were not accounted for. This methodology enabled a comparative analysis between the two model scenarios to assess the potential impact of sinkholes on the hydrology of Basin 6.
- Ran 8-year simulations of Basin 6 with sinkholes incorporated in the mesh using the NERSC supercomputer, thus completing Milestone 2023-P2-M8 *"Long-term simulations of Basin 6 explicitly representing sinkholes and river network infiltration variations"*, which revealed the most significant runoff on September 20, 2014. Preliminary data analysis indicated that the precipitation event on this day caused a substantial increase in water table height and potential ponding in sinkholes, consistent with excessive runoff and ponding water in Basin 6 recorded around this date by Goodbar et al. 2020.
- Completed a second round of 8-year ATS model simulations of Basin 6, this time excluding sinkholes in the mesh to generate results that would allow a comparative analysis to be performed with the results of the previous simulation in which sinkholes were included, to quantify the impact of sinkholes on runoff and water table dynamics.
- Analyzed the ‘Sinkhole’ and ‘No-Sinkhole’ ATS simulations to define the wet seasons for the years 2012 – 2018, then calculated and graphed the significant differences between the ‘Sinkhole’ and the ‘No-Sinkhole’ simulations for evapotranspiration (ET), runoff (Q), and infiltration (I).
- Provided Basin 6 model results in the form of a draft manuscript titled *“The Role of Sinkholes on the hydrology of Basin 6 of the Nash Draw in New Mexico using Amanzi-ATS”* (Deliverable 2023-P2-D6) which provides insight on the role of sinkholes and the river network on local and regional scale groundwater recharge. It describes the incorporation of sinkholes into the simulations and the forecasting of groundwater recharge under various climate scenarios.

Subtask 6.3

- Completed soil texture analysis on the 48 soil samples collected in Basin 6, NM west of the WIPP during the summer of 2023. The values derived provide valuable site-specific information regarding the physical properties of the Basin 6 soils within the study area.
- Completed report titled, *"Soil Parameter Variability in Basin 6"* (Deliverable 2023-P2-D2), which contains site-specific soil texture information (i.e., bulk density, porosity, and percentage composition) derived from soil samples collected within the Basin 6 study domain.
- Completed field work in Basin 6 just west of the WIPP. Routine maintenance on the existing piezometers was conducted and the water level and temperature data were downloaded prior to their redeployment. Three additional units were installed in strategic locations within the study area, e.g., further west closer to the brine lakes, and additional soil samples were collected in locations other than where previously collected to determine the soil physical properties in a broader geographic range.
- Completed the analysis of porosity (Phase 1 of the Soil Analysis procedure) for all 32 soil samples that were collected in Basin 6 during the fieldwork conducted by FIU at the end of May 2024. The remaining soil analyses (i.e., bulk density, organic content and soil texture) will be completed in FIU Year 5.

Note: The field and laboratory work plan developed by FIU during Year 3, "In-Situ Data Collection in Basin 6, NM to Support Development of a Hydrological Model using the Advanced Terrestrial Simulator (ATS)", was used to execute the field and laboratory procedures for Subtask 6.3 in Year 4.

TASK 1: REMEDIATION RESEARCH AND TECHNICAL SUPPORT FOR THE HANFORD SITE

Subtask 1.2: Re-oxidation of Redox Sensitive Contaminants Immobilized by Strong Reductants

Subtask 1.2 was completed in FIU Year 3.

Subtask 1.3: Evaluation of Competing Attenuation Processes for Mobile Contaminants in Hanford Sediments

Subtask 1.3 was completed in FIU Year 3.

Subtask 1.4: Experimental Support of Lysimeter Testing

Subtask 1.4: Introduction

Vitrification has been established as a highly effective method for immobilizing radioactive waste. This process involves melting waste materials along with glass-forming additives, encapsulating contaminants within the glass structure. Among the different types of glasses studied for this purpose, borosilicate glasses have emerged as the most extensively researched and implemented. These glasses can accommodate large quantities of actinides, demonstrate lower corrosiveness to melters compared to molten phosphate glasses, and are expected to exhibit high durability during long-term disposal (Grambow, 2006; Ojovan and Lee, 2011).

One configuration at Hanford's Field Lysimeter-testing units involves the co-disposal of grout waste forms above glass waste forms. The placement of grout waste forms above the glass is anticipated to significantly influence both the mechanisms and rate of glass corrosion. It is assumed that the alkaline water resulting from contact with the grout waste forms may enhance the dissolution rate of the glass waste forms beneath, and pre-experimental modeling has suggested such behavior. The grout-contacted water, characterized by elevated pH (~12), contains dissolved species from the grout (e.g., Si, Al, Ca, K) that might impact the rate of glass dissolution through common ion effects or precipitation reactions. If the composition of the pore water contacting the glass is predominantly influenced by the grout, the formation of calcium-silicate-hydrates is anticipated due to the strong affinity between calcium and silica gels in alkaline media (Armelao et al., 2000).

A field lysimeter test is currently ongoing at the Hanford site in which glass and cementitious waste forms are placed within disposal backfill near the planned disposal facility (Bacon et al., 2018). In FIU Year 4, research efforts have been dedicated to examining the impact of aluminum ions within solutions of varying pH levels on the corrosion behavior of borosilicate glass.

Subtask 1.4: Objectives

This study aims to determine the influence of temperature, pH, and dissolved components on the dissolution rate of borosilicate glass in the presence of a grout-contacted solution. The objective is to examine the effect of aluminum ions on the dissolution behavior of the glass.

Subtask 1.4: Methodology

Further details on the methodology can be found in the full version of Subtask 1.4 included in APPENDIX B.

Subtask 1.4: Results and Discussion

Further details on the experimental results can be found in the full version of Subtask 1.4 included in APPENDIX B.

Subtask 1.4: Conclusion

The corrosion behavior of ORLEC 28 borosilicate glass in Al-amended solutions was studied using the Product Consistency Test under varying pH and temperature conditions. Results show that the presence of aluminum in the solution decreases the dissolution rate of borosilicate glass. However, this effect is significantly weaker—approximately six times less—than the influence of calcium under similar conditions.

Glass powders treated in Al-amended solutions were extensively characterized using powder X-ray diffraction, scanning electron microscopy coupled with energy-dispersive spectroscopy, and BET specific surface area measurements.

The achievement of this task also includes a manuscript titled "The corrosion behavior of borosilicate glass in the presence of cementitious waste forms" authored by Yelena Katsenovich, Vadym Drozd, Shambhu Kandel, Leonel Lagos, R. Matthew Asmussen" published in *Dalton Transactions*, 53, 12740 DOI: 10.1039/D4DT00855C

Subtask 1.4: References

ASTM (2018). Standard practice for measurement of the glass dissolution rate using the single-pass flow-through test method (Designation: C1662-18). Philadelphia, PA: ASTM

Frugier, P., Chave, T., Gin, S., and Lartigue, J.-E., 2009, Application of the GRAAL model to leaching experiments with SON68 nuclear glass in initially pure water: Journal of Nuclear Materials, v. 392, no. 3, p. 552-567.

Gin, S., 2001, Protective effect of the alteration gel: a key mechanism in the long-term behaviour of nuclear waste glass.

Gin, S., Abdelouas, A., Criscenti, L. J., Ebert, W. L., Ferrand, K., Geisler, T., Harrison, M. T., Inagaki, Y., Mitsui, S., and Mueller, K. T., 2013a, An international initiative on long-term behavior of high-level nuclear waste glass: Materials Today, v. 16, no. 6, p. 243-248.

Grambow, B., 2006, Nuclear waste glasses-How durable?: Elements, v. 2, no. 6, p. 357-364.

Jantzen, C. M., Brown, K. G., and Pickett, J. B., 2010, Durable glass for thousands of years: International Journal of Applied Glass Science, v. 1, no. 1, p. 38-62.

Jégou, C., Gin, S., and Larché, F., 2000, Alteration kinetics of a simplified nuclear glass in an aqueous medium: effects of solution chemistry and of protective gel properties on diminishing the alteration rate: Journal of Nuclear Materials, v. 280, no. 2, p. 216-229.

Neeway, j.j., et al., 2018, FY2017 ILAW Glass Corrosion Testing with the Single-Pass Flow-Through Method: Pacific Northwest National Lab. (PNNL), Richland, WA (United States).

Ojovan, M. I., and Lee, W. E., 2011, Glassy wasteforms for nuclear waste immobilization: Metallurgical and Materials Transactions A, v. 42, no. 4, p. 837-851.

Okhrimenko, D., Nielsen, C., Lakshtanov, L., Dalby, K., Johansson, D., Solvang, M., Deubener, J., and Stipp, S., 2020, Surface Reactivity and Dissolution Properties of Alumina–Silica Glasses and Fibers: ACS applied materials & interfaces, v. 12, no. 32, p. 36740-36754.

Paul, A., 1989, Chemistry of glasses, Springer Science & Business Media.

Ribet, S., and Gin, S., 2004, Role of neoformed phases on the mechanisms controlling the resumption of SON68 glass alteration in alkaline media: Journal of Nuclear Materials, v. 324, no. 2-3, p. 152-164.

Sjöberg, S., 1996, Silica in aqueous environments: Journal of Non-Crystalline Solids, v. 196, p. 51-57.

Standard, A., 2014, C1285-14, Standard Test Methods for Determining Chemical Durability of Nuclear, Hazardous, and Mixed Waste Glasses and Multiphase Glass Ceramics: The Product Consistency Test (PCT): ASTM International, West conshohocken, PA.

D. Strachan, 2017, Glass dissolution as a function of pH and its implications for understanding mechanisms and future experiments: Geochimica et Cosmochimica Acta, v. 219, p. 111-123.

Vienna, J. D., Ryan, J. V., Gin, S., and Inagaki, Y., 2013, Current understanding and remaining challenges in modeling long-term degradation of borosilicate nuclear waste glasses: International Journal of Applied Glass Science, v. 4, no. 4, p. 283-294.

Subtask 1.5: Remediation Research of Ammonia Gas Coupled with Strong Reductants for Vadose Zone Treatment

Subtask 1.5: Introduction

Recent bench-scale tests have provided insights into the reduction of pertechnetate ($Tc^{VII}O_4^-$) in the presence of uranyl ions ($U^{VI}O_2^{2+}$) using strong reductants such as zero-valent iron (ZVI) and sulfur-modified iron (SMI) (Katsenovich et al., 2024). These reductants can decrease the mobility of Tc^{VII} and U^{VI} by reducing them to lower oxidation states, Tc^{IV} and U^{IV}, respectively, which have decreased solubility. However, the observed limitation of using only ZVI/SMI technology is the reoxidation and remobilization of U^{VI} and Tc^{VII} to the aqueous phase when aerobic conditions are restored. To address this challenge, additional strategies are being explored that involve incorporating Tc and U into other low solubility phases or coating them to prolong the immobilization of these contaminants.

Among the technologies being considered is the *in-situ* injection of ammonia gas, designed to temporarily increase the pore water pH to around pH 11. This elevated pH helps dissolve mineral phases present in the contaminated areas of the Hanford Site vadose zone (DOE/RL-2019-28, August 2019). Several simultaneous removal mechanisms occur for the coexisting contaminants, including the co-precipitation of U and Tc reduced phases with Si, Al, and Ca-saturated aqueous phases (Di Pietro et al., 2022; Szecsody et al., 2012). Subsequently, this is followed by the coating of adsorbed and co-precipitated U and Tc phases with low solubility precipitates as the system returns to a neutral pH after the gas dissipates (Szecsody et al., 2015). The addition of ammonia gas may also sustain anaerobic conditions for an extended period by displacing air during injection, keeping U and Tc in their reduced forms at higher pH (Di Pietro et al., 2020). During oxidation of ZVI, U and Tc can be incorporated into iron oxides (Boglaienko et al., 2020), which are subsequently coated with secondary phyllosilicate alteration products (Szecsody et al., 2015). This approach could prevent reoxidation and promote more stable contaminant immobilization.

Recent studies have shown effective removal of Tc^{VII} from alkaline media up to pH 10 under aerobic conditions (Kandel et al., 2021; Katsenovich et al., 2023). However, it remains unclear whether ZVI/SMI reductants are applicable in strongly alkaline media with pH levels up to 11 generated in sediment during ammonia gas injection. The objective of this research is to study re-oxidation behavior of vadose zone pore water contaminants, such as Tc^{VII} collocated with U^{VI} and NO_3^-, that have been initially reduced by strong reductants such ZVI, SMI in batch-scale experiments under anaerobic conditions followed by ammonia gas treatment. This is the first attempt to couple strong reductants with ammonia gas treatment to prolong the effectiveness of contaminant immobilization.

Subtask 1.5: Objectives

The objective for this study is to investigate the reduction of redox sensitive contaminants, Tc, U, NO_3^-, using strong reductants such as SMI and H-ZVI under anaerobic conditions. This will be followed by the application of ammonia gas to maximize contaminant sequestration through the formation of aluminosilicate coatings on the reduced U and Tc phases under aerobic conditions. The study will also investigate potential remobilization of reduced Tc, U and other targeted contaminants throughout the process.

Subtask 1.5: Methodology

Sediment samples that were evaluated in these experiments include $^{99}Tc^{VII}$ collocated with $^{238}U^{VI}$ and NO_3^-.

The study involved batch-scale experiments to evaluate the effectiveness of ZVI or SMI at a concentration of 1.0 wt.% in minimizing the re-oxidation of Tc and U after their initial immobilization through reduction under anaerobic conditions. ZVI (Ferox PRB, 297 µm, 325 mesh, 95+% pure) was obtained from Hepure Technologies Inc. and SMI was a product of SMI, PS Inc. The experiments used Ringold Formation sediments representative of the Hanford Site vadose zone in the Central Plateau. The sediment was dried in an oven at 30˚C for 48 hours and sifted through a 2 mm sieve.

The synthetic pore water (PW) recipe that mimics the composition found in the 200-DV-1 Operable Unit (Serne et al., 2016; Szecsody et al., 2022) is presented in Table 1. The solution was then pH-adjusted by using small quantities of hydrochloric acid (HCl, TraceMetal™ Grade, 0.1 M) to a pH of 7.2 ± 0.1. The initial pH of the new solution was 9.16 and was lowered to 7.10 by adding 1.625 mL of 0.1 M HCl. The pH electrode was calibrated using three buffers (pH: 4.01, 7.00, and 10.01) immediately before measuring the pH of the solutions.

The synthetic porewater solution was then amended with 150 mg/L of uranium and 100 µg/L of Tc(VII) (340 pCi/L) inside the anaerobic glove box. The concentration of nitrate in the PW simulant was measured as 204 mg/L.

Table 1. Chemicals for Simulant PW Solution (Serne et al., 2016; Szecsody et al., 2022)

Order to Dissolve	Concentration (mol/L)	Reagent	Molecular weight (g/mol)	Mass in 1 liter (g)	Mass in 1.5 L (g)
1	0.012	$CaSO_4 \times 2H_2O$	172.1723	2.0661	3.09915
2	0.0017	NaCl	58.4430	0.0994	0.1491
3	0.0004	$NaHCO_3$	84.0068	0.0336	0.0504
4	0.0034	$NaNO_3$	84.9948	0.2890	0.4335
5	0.0026	$MgSO_4$	120.3660	0.3130	0.4695
6	0.0024	$MgCl_2 \times 6H_2O$	203.3034	0.4879	0.73185
7	0.0007	KCl	74.5515	0.0522	0.0783
Adjust pH to 7.0 to 7.2 with sodium hydroxide or sulfuric acid.					

The PW solution was prepared on the ultrapure deionized water (> 18 $M\Omega^{-cm}$, DIW) that was purged with N_2 for 30 minutes and transferred into the anaerobic chamber (Coy Laboratory). An anaerobic CAM-12 meter inside the anaerobic chamber monitored oxygen (ppm) and hydrogen (%) levels. The anaerobic glove box was connected to two cylinders: (i) high purity nitrogen and (ii) nitrogen (95%) mixed with hydrogen (5%). The level of H_2 was kept as ~2% and O_2< 10 ppm. A palladium catalyst in the anaerobic chamber was replaced and regenerated weekly by heating in the oven at 180 ºC for 4-5 h.

The batch experiments with Ringold Formation sediments (silty sand) collected from the Hanford Site were conducted in two phases. Phase 1 focused on the reducing ^{99}Tc comingled with U^{VI} and NO_3^- in the presence of strong reductants under anaerobic conditions for 36 days. Bottles were shaken to ensure mixing about 2-3 times each weekday. Phase 2 involved treating the system with ammonium hydroxide (NH_4OH) under aerobic conditions to investigate the re-oxidation behavior of the reduced Tc and U and changes in NO_3^- and NO_2^- over 50 days, bringing the total experiment duration to 86 days. Capped samples were placed on a shaker (100 rpm, ThermoScientific) with slow aeration to ensure sufficient oxygen in the aqueous phase throughout Phase 2 experiments and for the slow reoxidation of redox-sensitive contaminants.

Sediment samples were prepared in triplicate using 250 mL bottles, with each bottle containing 10 g of sediment and 100 mL of solution, maintaining a solid-to-liquid ratio of 1:10. The samples were also amended with 100 mg of ZVI or SMI. Two sacrificial control samples with 100 mL PW synthetic solutions containing the same concentrations of ^{99}Tc, U, and NO_3^- as those used in the experimental samples amended with ZVI or SMI were prepared inside the glovebox. These samples were sacrificed after Phase 1 for solids characterization. Weekly sampling was performed to track changes in the system. At each sampling point, 0.4 mL of the sample was filtered through a 0.2 µm PTFE syringe filter (Fisher Scientific) and stored at 5 ºC in sealed 1.5 mL tubes until analysis. The total volume loss in the batch reactors remained below 10 % throughout the experiment.

Filtered samples were analyzed using inductively coupled plasma-mass spectrometer (ICP-MS, Thermo Fisher Scientific iCAP RQ) to measure Tc and U concentrations. Each sample was diluted 10-100x with a 2% nitric acid (HNO_3, TraceMetal Grade) solution and stored in a refrigerator until analysis. ^{99}Tc calibration standards ranged from 0.005 µg/L to 50 µg/L were prepared through a serial dilution from 1.0 mg/L stock solution, which was itself prepared from 4.217 mM (417.483 mg/L) stock solution. The accuracy of the 1.0 mg/L stock solution was assessed using a liquid scintillation counter (LSC, Tricarb 2910 TR, Perkin Elmer).

ICP-MS U standards were prepared from 1,000 mg/L commercial uranyl nitrate stock solution purchased from High Purity Standards by the dilution to 1 mg/L stock (0.01 -500 µg/L).

The liquid samples were also analyzed by inductively coupled plasma-optical emission spectrometry (ICP-OES, Optima 7300DV, PerkinElmer) to measure calcium (Ca) and magnesium (Mg) concentrations. Calibration standards were prepared from a High Purity Standards stock solution in the range of 10-5000 µg/L.

Anion concentrations, including nitrate (NO_3^-), nitrite (NO_2^-), and sulfate (SO_4^{2-}), were measured using ion chromatography (IC, Integrion Dionex). Calibration standards were prepared from a stock solution in DIW using special IC vials. The combined stock solution for NO_3^- and NO_2^- had concentrations of 100 mg/L. The concentration ranges for NO_3^- and NO_2^- calibration standards were 50 – 5000 µg/L for a 5 mL sample volume. The analysis utilized the Dionex IonPac AS11 analytical column (2x250 mm) and an Anion Dynamically Regenerated Suppressor (ADRS) (2 mm).

The oxidation-reduction potential (ORP), pH, and dissolved oxygen (DO) levels were monitored weekly throughout the experiment.

The solids characterization of dried sediment samples was conducted using a scanning electron microscope equipped with energy-dispersive X-ray spectroscopy (SEM/EDS) and X-ray diffraction (XRD) measurements. Micrographs and elemental analysis of solids surface morphology and elemental composition were obtained using a JEOL JSM 5900LV SEM/EDS, operating at 25.0 kV. XRD analysis for solid phase identification was performed with a Bruker D2 PHASER X-ray diffractometer, equipped with a LYNXEYEXET detector and a rotating collimator source. Solid phase identification was further analyzed using EVA 5.1 XRD pattern processing software.

Subtask 1.5: Results and Discussion

$Tc^{(VII)}$, $U^{(VI)}$, and NO_3^- are redox sensitive contaminants and the reduction of $Tc^{(VII)}$ to $Tc^{(IV)}$, $U^{(VI)}$ to $U^{(IV)}$ and NO_3^- to NO is described by the following equations 1-3 (Bard, 2017; Milazzo et al., 1978).

$$\boldsymbol{TcO_4^-} + 3e^- + 4H^+ \rightarrow \boldsymbol{TcO_2 \cdot xH_2O}(s) + (2-x)H_2O \qquad E^0 = 0.748\text{ V} \qquad \text{Eq.1}$$

$$\boldsymbol{UO_2^{2+}} + 2e^- + 4H^+ \rightarrow \boldsymbol{UO_2} + H_2O \qquad E^0 = 0.327\text{ V} \qquad \text{Eq.2}$$

$$\boldsymbol{NO_3^-} + 3e^- + 4H^+ \rightarrow \boldsymbol{NO_g} + 2H_2O \qquad E^0 = 0.96\text{ V} \qquad \text{Eq.3}$$

During Phase 1, the pH was increased to approximately 8.0 in the SMI samples and 7.5 in ZVI-amended samples. In Phase 2, after the injection of NH_4OH, the pH was measured ~ 10.6-10.7 for both iron materials (Figure 1). In Phase 1, conducted under anaerobic conditions, DO levels were around 1.0 mg/L for SMI and between 1.3 to 1.4 mg/L for ZVI. In Phase 2, under aerobic conditions, DO levels quickly increased, reaching 6.0 mg/L (Figure 2). In Phase 1, ORP measured against Ag/AgCl reference ranged from 60 mV to 100 mV. In Phase 2, ORP ranged between -3 and 23 mV (Figure 3).

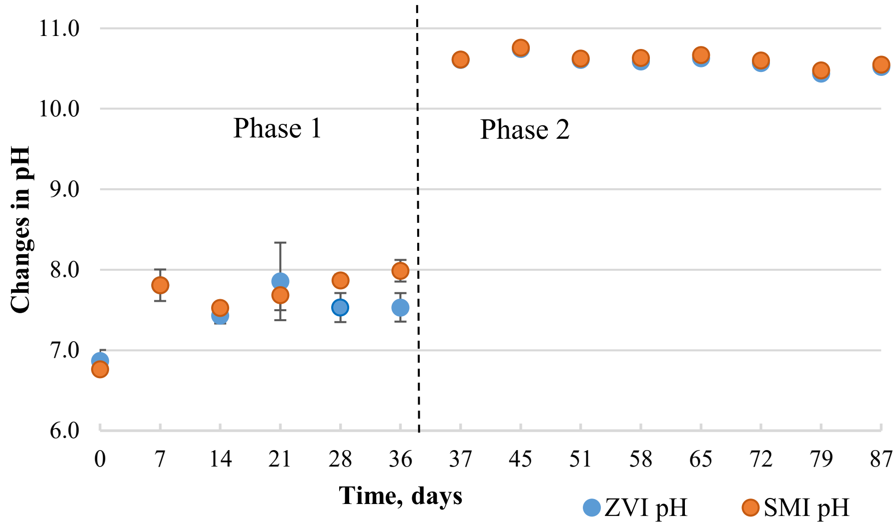

Figure 1. Changes in pH over time in synthetic PW amended with 1.0 wt.% H-ZVI or SMI where Phase 1 was conducted under analerobic confitions and Phase 2 after the addition of NH_4OH in the aerobic condition. A dash line separates Phase 1 and Phase 2 on day 36.

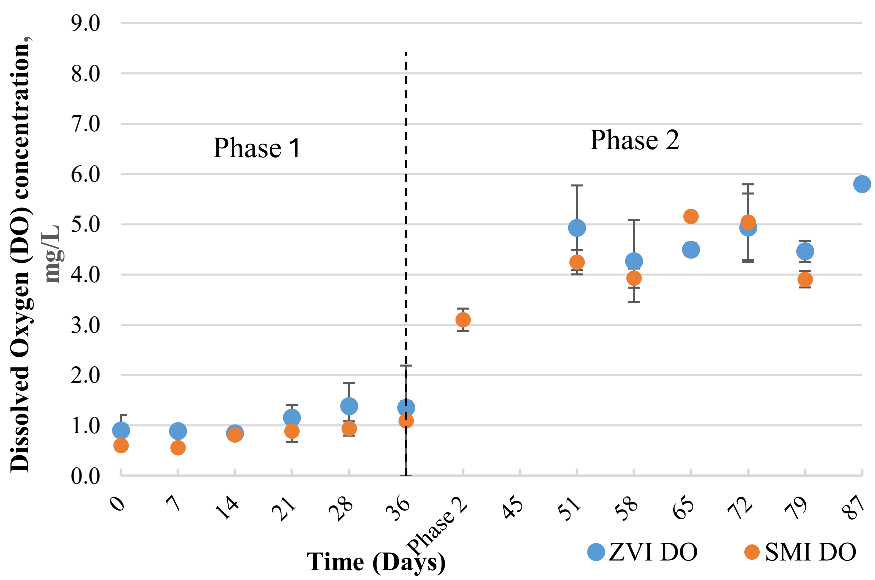

Figure 2. Dissolved oxigen changes over time in synthetic PW amended with 1.0 wt.% H-ZVI or SMI where Phase 1 was conducted under analerobic confitions and Phase 2 after the addition of NH_4OH in the aerobic conditions. A dash line separates Phase 1 and Phase 2 on day 36.

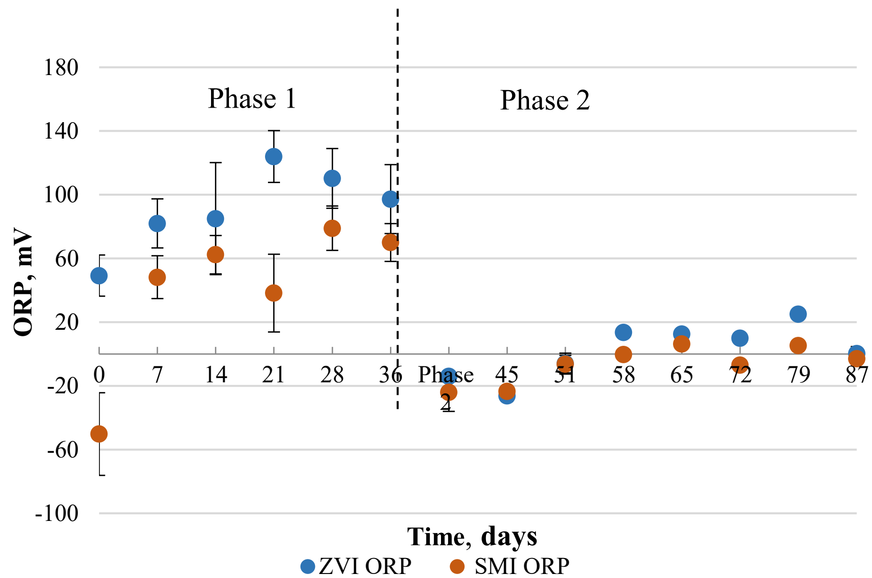

Figure 3. Oxidation-reduction potential (ORP) changes over time in synthetic PW amended with 1.0 wt.% H-ZVI or SMI where Phase 1 was conducted under analerobic confitions and Phase 2 after the addition of NH_4OH in the aerobic conditions. A dash line separates Phase 1 and Phase 2 on day 36.

SMI at 1 wt.% was more effective at reducing U under the anaerobic conditions of Phase 1 compared to ZVI. The remaining U fraction in the SMI treatments was measured at 0.42 ± 0.1, compared to 0.71 ± 0.08 for ZVI (Figure 4). However, the remaining U fraction significantly decreased to 0.001±0.0007 after the addition of NH_4OH under aerobic conditions, likely due to the formation of U hydroxide at a pH of approximately 11 (Figure 4). In the ZVI-free control, no changes in the remaining U fraction were observed during the anaerobic conditions of Phase 1, but the fraction dropped to less than 0.03 following the addition of NH_4OH in Phase 2 (Figure 4).

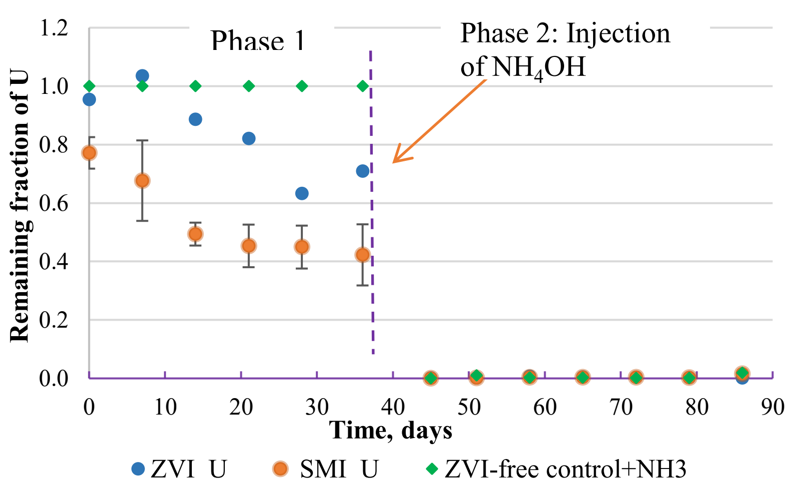

Figure 4. Changes in aqueous U remaining fraction in samples amended with 1.0wt.% ZVI or 1.0 wt.% SMI.

SMI was also more effective than ZVI in reducing Tc under the anaerobic conditions of Phase 1 with a remaining aqueous fraction of 0.05±0.03 compared to 0.61±0.05 for ZVI. However, after the addition of NH_4OH and the shift to aerobic conditions in Phase 2, the concentration of Tc rebounded. Despite this, SMI showed greater resistance to reoxidation, with a remaining fraction of 0.65±0.01, compared to ZVI's remaining fraction of 0.88±0.03 (Figure 5). No Tc reduction was observed in the iron-free control samples (Figure 5). The rapid reoxidation of Tc may be due to the relatively short duration in which the samples remained under anaerobic conditions. This limited time likely prevented the formation of protective coatings on the precipitates' surfaces, which may have hindered the slow incorporation of Tc into the iron oxide structure or the development of coatings from non-radioactive minerals, such as goethite. These coatings would have helped stabilize the reduced Tc, thus reducing the likelihood of reoxidation. Additionally, vigorous shaking on the bench likely caused a fast increase in dissolved oxygen levels, further accelerating the Tc reoxidation process.

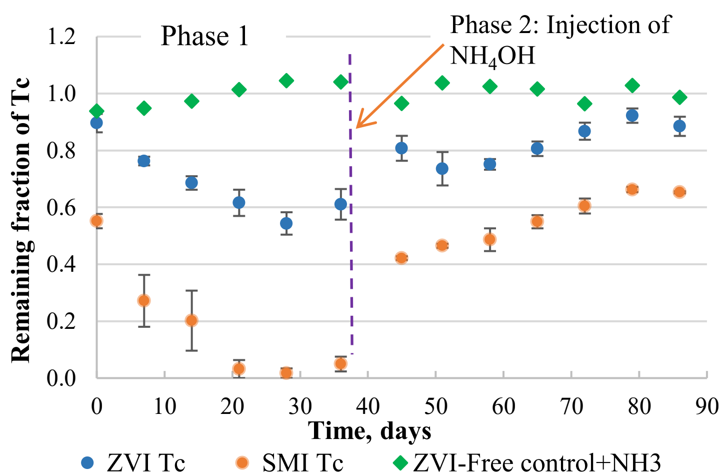

Figure 5. Changes in aqueous Tc remaining fraction in samples amended with 1.0 wt.% ZVI or 1.0 wt.% SMI.

SMI was also more effective than ZVI in removing NO_3^- (Figure 6). This increased removal efficiency led to higher concentrations of NO_2 being measured in the presence of SMI. During Phase 1, the NO_3 concentration was reduced by 39%, dropping from 3.8 mmol/L to 2.3 mmol/L. In Phase 2, it further decreased to 1.3 mmol/L, resulting in a total reduction of 66%. The total removal of NO_3^- in ZVI-amended samples was much lower, achieving only about 15% reduction (Figure 6).

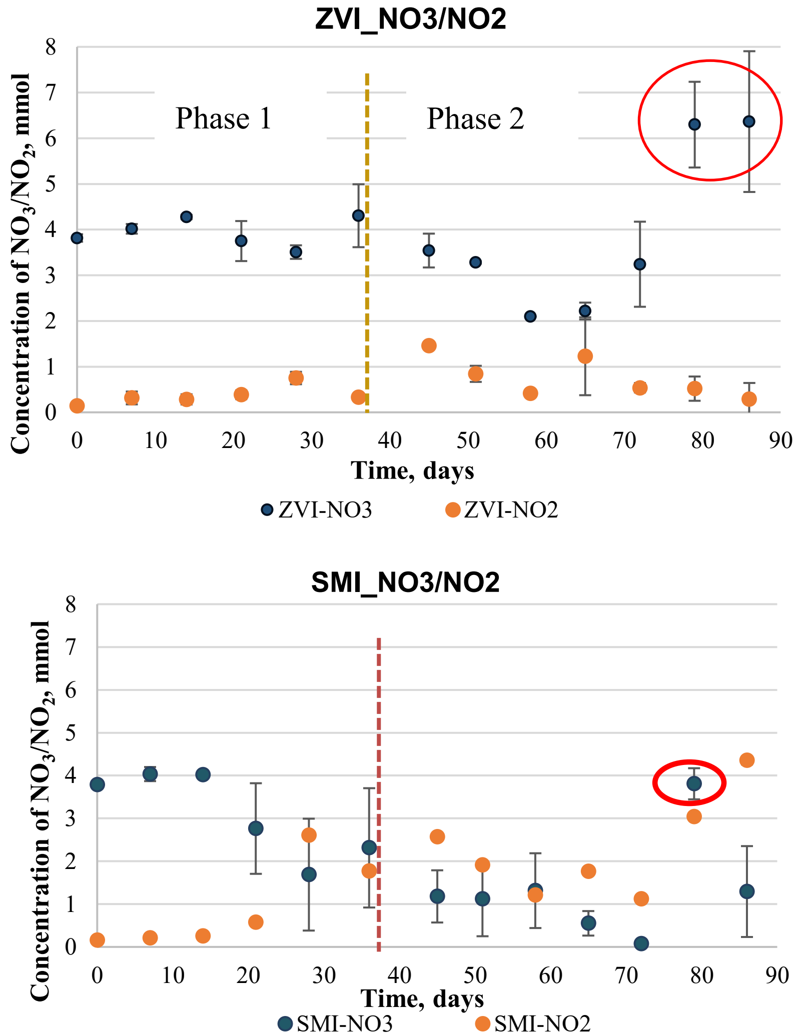

Figure 6. Changes in nitrite and nitrate concentrations in samples amended with 1% Hepure zero valent iron (ZVI) and 1% SMI during the experiments.

In Phase 2, following the addition of NH_4OH, the system traps CO_2, resulting in the precipitation of $CaCO_3$ and $MgCO_3$ under the high pH conditions. This leads to a significant decrease in the aqueous concentrations of Ca and Mg. The behavior of the iron-free control samples with NH_4OH was identical to that of the samples amended with ZVI or SMI, showing similar trends in the reduction of Ca and Mg concentrations (Figure 7). The newly formed carbonate phases, such as $CaCO_3$ and $MgCO_3$, can form precipitate coatings on the reduced U and Tc phases as a result of the pH manipulation from the NH_4OH treatment.

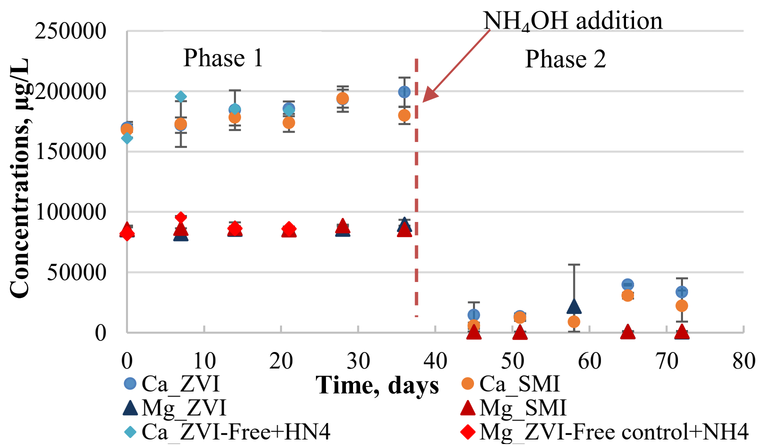

Figure 7. Changes in Ca and Mg concentrations in samples amended with 1.0 wt.% ZVI or 1.0 wt.% SMI.

Solids characterization

Solids characterization was performed on sacrificial samples collected after Phase 1 and at the end of Phase 2 experiments.

Measurements from the scanning electron microscope (SEM) were used to evaluate the elemental composition in each of the dried solid samples. SEM provides an accurate assessment, which helps with mineralogical analysis using other methods like X-ray diffraction (XRD). SEM/EDS provided maps of elements such as S, Tc, Fe, and U, enabling the visualization of elements for comparing their associations on the sample surface.

In sacrificial samples after Phase one amended with 1 wt.% SMI, Tc and U showed good alignment with Fe, S and K. Despite very low initial concentration of 100 µg/L, the normalized mass of Tc was measured at 0.6 % - 1.6 % in selected points on the sample surface. The same points showed the normalized mass values ranging from 44 % to 66 % for U (Figure 8).

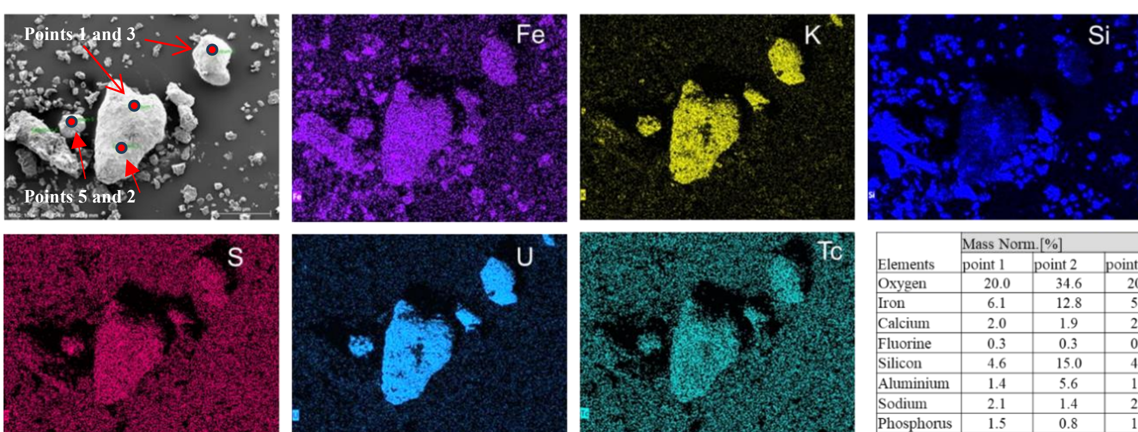

	Mass Norm.[%]			
Elements	point 1	point 2	point 3	point 5
Oxygen	20.0	34.6	20.1	40.0
Iron	6.1	12.8	5.5	25.5
Calcium	2.0	1.9	2.6	1.0
Fluorine	0.3	0.3	0.4	
Silicon	4.6	15.0	4.6	22.9
Aluminium	1.4	5.6	1.3	4.0
Sodium	2.1	1.4	2.3	
Phosphorus	1.5	0.8	1.6	
Magnesium	0.2	5.3	0.3	2.8
Uranium	60.8	22.3	60.1	1.4
Technetium	1.1	0.0	1.2	
Potassium				1.4

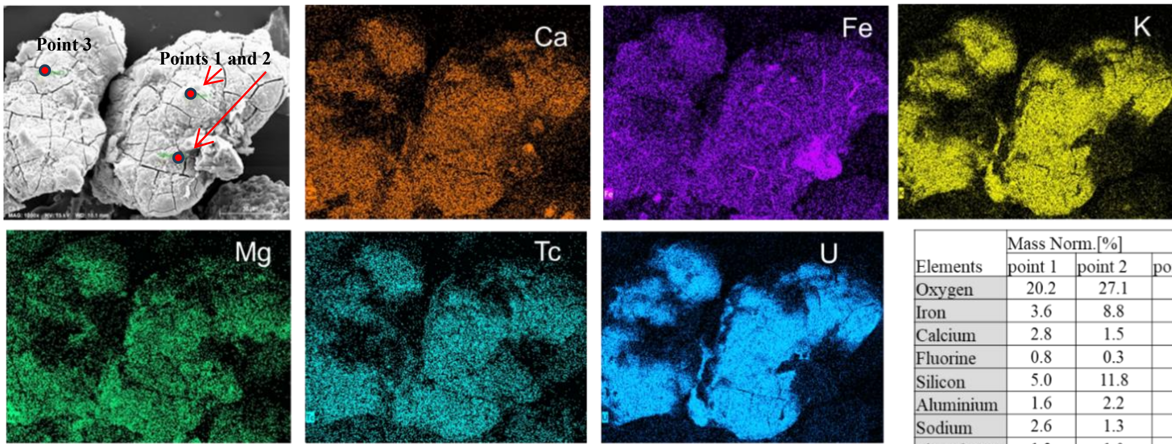

Elements	Mass Norm.[%] point 1	point 2	point 3
Oxygen	20.2	27.1	19.0
Iron	3.6	8.8	4.1
Calcium	2.8	1.5	2.7
Fluorine	0.8	0.3	
Silicon	5.0	11.8	5.1
Aluminium	1.6	2.2	0.4
Sodium	2.6	1.3	
Phosphorus	1.3	1.0	1.1
Magnesium	0.4	1.5	0.4
Uranium	60.1	43.7	66.5
Technetium	1.6	0.9	0.6

Figure 8. Elemental maps for sacrificial samples amended with 1wt.% SMI collected after Phase 1.

In the sacrificial samples amended with ZVI, the normalized mass of U was approximately 0.9%, and no Tc was detected on the surface (Figure 9). This correlated with a lower removal of U and Tc observed in the aqueous samples.

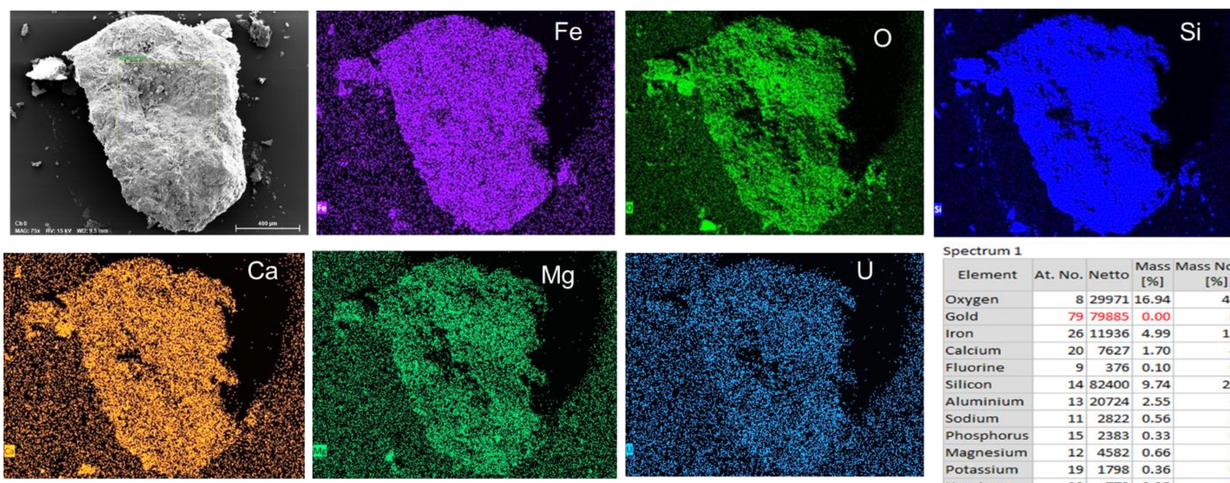

Spectrum 1

Element	At. No.	Netto	Mass [%]	Mass Norm. [%]
Oxygen	8	29971	16.94	43.77
Gold	79	79885	0.00	0.00
Iron	26	11936	4.99	12.89
Calcium	20	7627	1.70	4.40
Fluorine	9	376	0.10	0.25
Silicon	14	82400	9.74	25.18
Aluminium	13	20724	2.55	6.58
Sodium	11	2822	0.56	1.46
Phosphorus	15	2383	0.33	0.86
Magnesium	12	4582	0.66	1.70
Potassium	19	1798	0.36	0.92
Uranium	92	779	0.35	0.90
Titanium	22	1829	0.42	1.09
Technetium	43	0	0.00	0.00
		Sum	38.70	100.00

Figure 9. Elemental maps for sacrificial samples amended with 1% Hepure zero valent iron (ZVI) collected after Phase 1.

In SMI-amended samples collected after Phase 2, U showed a strong alignment with Fe. The U appeared to concentrate in areas where Fe oxides had precipitated on the surface, suggesting that it was either adsorbed on the surface or covered by these precipitates. Tc levels on the surface were below the detection limit, indicating its reoxidation, as measured in aqueous samples. The normalized mass percentage of U ranged from 0.16 % to 2.2 % (indicated by the red dot), which was higher than in the ZVI-amended samples but much lower than in the Phase 1 samples. Additionally, alignment was observed among Al, Si, Na, K, and O (Figure 10). XRD measurements suggested that sediment samples are composed of quartz, albite, anorthite, laumonite (Ca-Al-Si), cancrinite Na-Al-Si-$CaCO_3$, calcite and $MgCO_3$, which correlate with results of EDS maps.

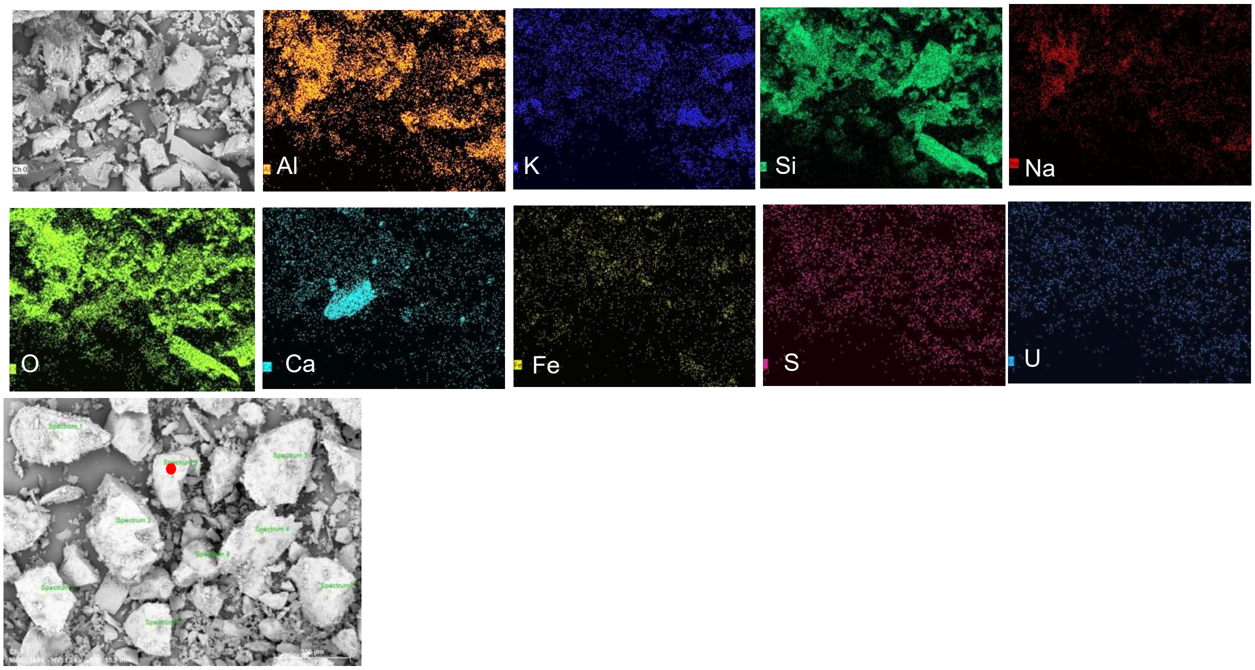

Figure 10. Elemental maps for sediment samples amended with 1wt.% SMI collected after Phase 2.

In the ZVI-amended samples, higher Fe content correlated with higher U wt.%. Elemental maps showed alignment between Al, K, Na, Si, and O. Single-point measurements indicated a normalized mass of U ranging from 0.17 % to 1.0 %. The single point marked in red had the highest measured U levels, ranging from 0.6 % to 1.0 % normalized mass (Figure 11.).

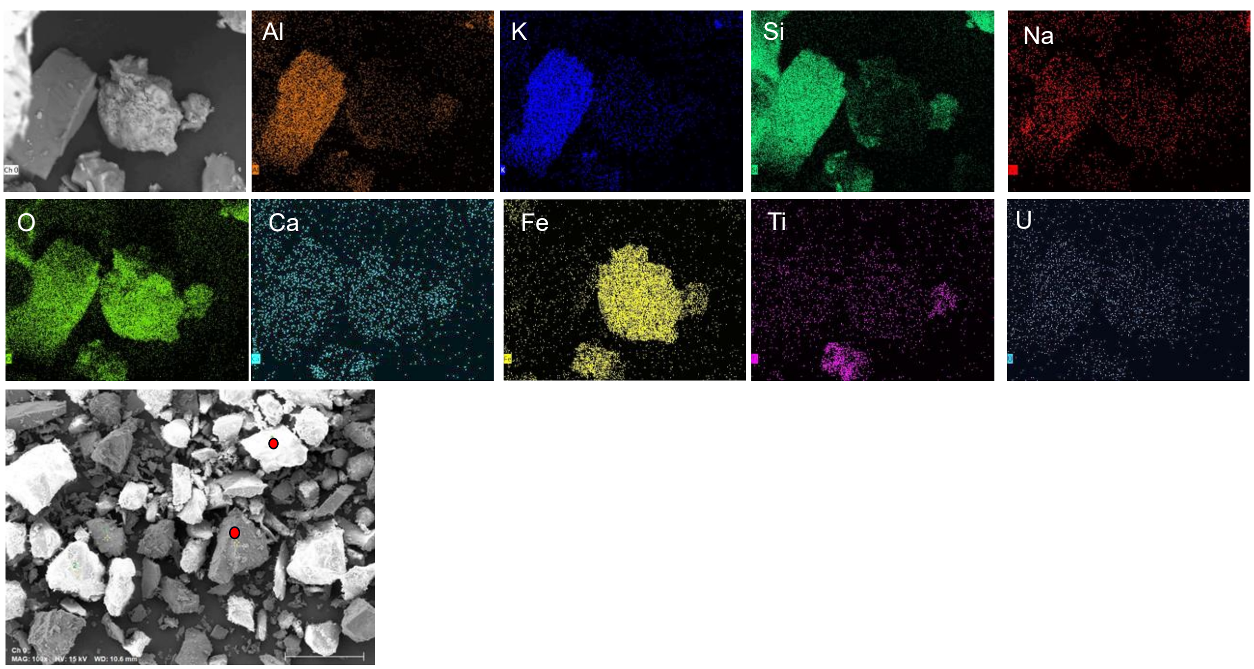

Figure 11. Elemental maps for samples amended with 1 wt.% ZVI at x2000 collected after Phase 2.

The solids and supernatant solutions were separated from nine experimental samples at the end of Phase 2. The supernatant solutions from sediment-removed samples were centrifuged and dried at 35-40°C in a vacuum oven. The dried clay-like material collected from the top of the centrifuged tube was ground and run through X-ray diffraction analysis to identify mineralogical composition (Figure 12).

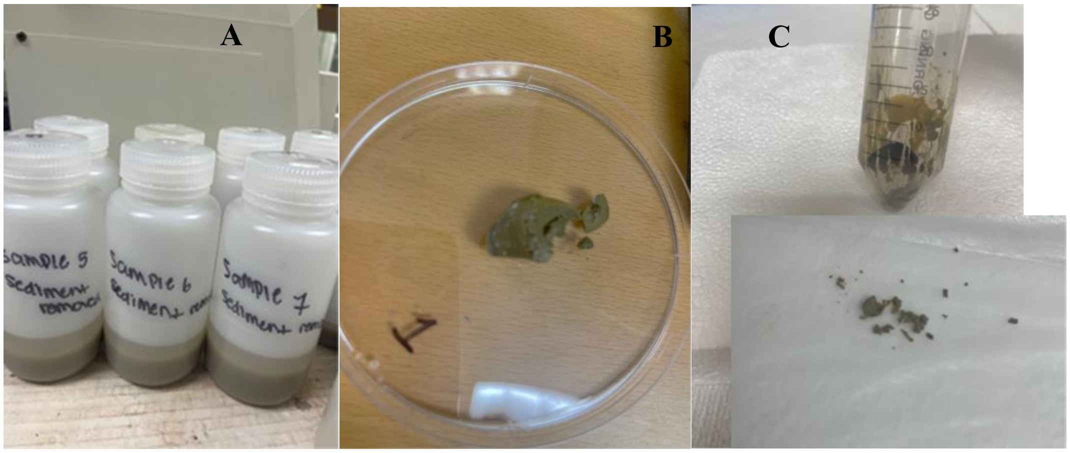

Figure 12. A) Sediment-removed samples collected after Phase 2; B) Centrifuged and dried samples with sediment removed showing clay-like material collected from the top of the tube; C) Dried precipitates collected from the bottom of the tube.

XRD measurements suggested that sediment samples are composed of Quartz, Albite, Anorthite, Laumonite (Ca-Al-Si), Cancrinite Na-Al-Si-$CaCO_3$, Calcite and $MgCO_3$. There are also traces of Metaschoepite. In the sediment-removed samples, the clay-like precipitates are composed of Montmorillonite, Silicon oxide, Aragonite- $CaCO_3$ and iron oxides such as Goethite/Lepidocrocite. Heavier precipitates collected from the bottom of the tube were similar to sediment in composition and composed of Quartz, Albite, Goethite, Laumontite (Ca-Al-Si), Aragonite-$CaCO_3$, and Cancrinite- Na-Al-Si-$CaCO_3$.

EDS maps of clay-like sediment in SMI amended samples suggest an alignment between Al, Si, Na, K, and O, which correlates with the clay-like phases identified by XRD. Similar to other sediment samples, U aligns with Fe, and the clay-like phases are enriched in U. For example, U was measured at 0.4 -1.7 Norm mass % (indicated by red dot) and Fe ranged from 3.2 to 15.6 normalized mass %. A higher Fe normalized mass % correlates with a higher U normalized mass % (Figure 13).

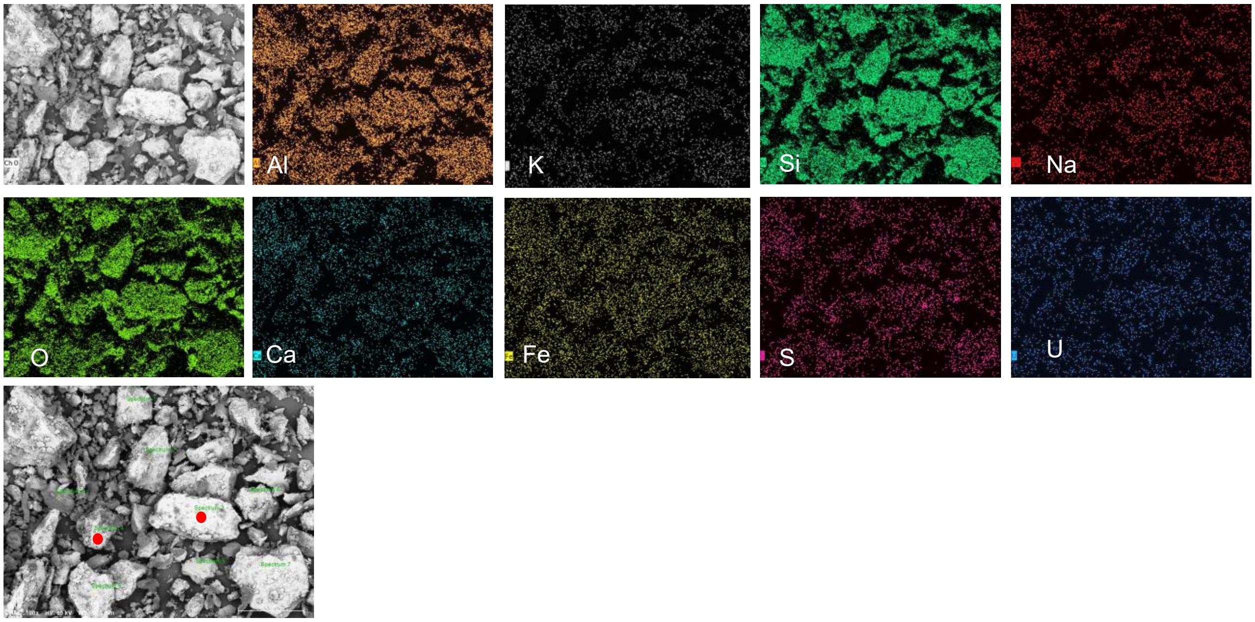

Figure 13. Elemental maps for SMI amended clay-like sample at x100 after Phase 2.

Subtask 1.5: Conclusions

These experiments investigated the re-oxidation behavior of immobilized Tc and U after reduction using 1.0 wt.% ZVI or SMI under anaerobic conditions in Phase 1 and then reoxidation following addition of NH_4OH in aerobic conditions of Phase 2. SMI appeared to be a stronger reductant for U(VI), Tc(VII) and NO_3 than ZVI during Phase 1. The primary limitation of ZVI/SMI technologies observed was the reoxidation and remobilization of Tc back into the aqueous phase when conditions returned to natural aerobic conditions. The reoxidation behavior of uranium when conditions return to neutral pH remains an open question and requires further investigation. The pH manipulation caused by NH_4OH treatment leads to the formation of carbonate phases, such as $CaCO_3$ and $MgCO_3$, which can form precipitate coatings on the reduced U and Tc phases. Future work will focus on coupling ZVI/SMI and ammonia in Phase one under anaerobic conditions and Phase two under aerobic conditions, with pH set at 8, 9, and 10, to test reduction and precipitation processes at variable pH. These studies complement ongoing DOE and PNNL technology treatability studies for a multitude of Operable Units (e.g., DV-1, WA-1, and EA-1).

In Year 4, an abstract titled *"The Reoxidation Behavior of Tc(IV) and U(IV) in Perched Water of the Hanford Site Vadose Zone after Treatment with Strong Reductants"* and authored by Yelena Katsenovich, Hilary Emerson, Jim Szecsody, Nik Qafoku, Leonel Lagos was submitted to the Waste Management Symposia, Phoenix, Arizona. The WM2024 abstract was accepted as an oral presentation.

Subtask 1.5: References

Bard, A., 2017, Standard potentials in aqueous solution, Routledge.

Boglaienko, D., Soltis, J. A., Kukkadapu, R. K., Du, Y., Sweet, L. E., Holfeltz, V. E., Hall, G. B., Buck, E. C., Segre, C. U., and Emerson, H. P., 2020, Spontaneous redox continuum reveals sequestered technetium clusters and retarded mineral transformation of iron: Communications Chemistry, v. 3, no. 1, p. 1-11.

Di Pietro, S. A., Emerson, H. P., Katsenovich, Y., Qafoku, N. P., and Szecsody, J. E., 2020, Phyllosilicate mineral dissolution upon alkaline treatment under aerobic and anaerobic conditions: Applied Clay Science, v. 189, p. 105520.

Di Pietro, S. A., Emerson, H. P., Katsenovich, Y. P., Johnson, T. J., Francis, R. M., Mason, H. E., Marple, M. A., Sawvel, A. M., and Szecsody, J. E., 2022, Solid phase characterization and transformation of illite mineral with gas-phase ammonia treatment: Journal of Hazardous Materials, v. 424, p. 127657.

Kandel, S., Katsenovich, Y., Boglaienko, D., Emerson, H. P., and Levitskaia, T., 2021, Time dependent zero valent iron oxidation and the reductive removal of pertechnetate at variable pH: Journal of Hazardous Materials, p. 127400.

Katsenovich, Y., Emerson, H., Szecsody, J., Qafoku, N., ,, and Lagos, L., 2024, The Reoxidation Behavior of Tc(IV) and U(IV) in Perched Water of the Hanford Site Vadose Zone after Treatment with Strong Reductants, Waste Managment Symposia: Phoenix, Arisona.

Katsenovich, Y. P., Maria, A. A., Williams, J., Kandel, S., Boglaienko, D., Emerson, H. P., and Levitskaia, T. G., 2023, Reductive removal of pertechnetate and chromate by zero valent iron under variable ionic strength conditions: Journal of Hazardous Materials, v. 445, p. 130546.

Milazzo, G., Caroli, S., and Braun, R. D., 1978, Tables of standard electrode potentials: Journal of The Electrochemical Society, v. 125, no. 6, p. 261C.

Serne, R. J., Lanigan, D. C., Westsik, J. H., Williams, B. D., Jung, H., and Wang, G., 2016, Extended leach testing of simulated LAW cast stone monoliths: Pacific Northwest National Lab.(PNNL), Richland, WA (United States).

Szecsody, J. E., Emerson, H. P., Mackley, R. D., Snyder, M., Resch, C. T., and Baum, S. R., 2022, Characterization of Contaminants and Mobility in WMA A-AX Boreholes D0006 and D0008: Pacific Northwest National Laboratory (PNNL), Richland, WA (United States).

Szecsody, J. E., Truex, M. J., Zhong, L., Johnson, T. C., Qafoku, N., Williams, M. D., Greenwood, W. J., Wallin, E. L., Bargar, J., and Faurie, D. K., 2012, Geochemical and geophysical changes during ammonia gas treatment of vadose zone sediments for uranium remediation: Vadose Zone Journal, v. 11, no. 4.

Szecsody, J. E., Truex, M. J., Zhong, L., McKinley, J. P., Qafoku, N. P., Lee, B. D., and Saurey, S. D., 2015, Remediation of technetium in vadose zone sediments using ammonia and hydrogen sulfide gases: Vadose Zone Journal, v. 14, no. 7, p. 1-12.

TASK 2: REMEDIATION RESEARCH AND TECHNICAL SUPPORT FOR THE SAVANNAH RIVER SITE

Subtask 2.1: Environmental Factors Controlling the Attenuation and Release of Contaminants in the Wetland Sediments at Savannah River Site

Subtask 2.1: Introduction

The Department of Energy's Savannah River Site (SRS) produced radionuclides, including tritium (^{3}H) and plutonium-239 (^{239}Pu), from 1955 to 1988. The F-Area Hazardous Waste Management Facility is composed of three unlined seepage basins, which were designed to absorb radionuclide waste from this production in the sediments without contaminating the groundwater[1]. However, nitric acid-containing influent caused acidic conditions, which resulted in radionuclides escaping into the groundwater, and further spreading to F-Area wetlands[2]. Contaminants included cesium-137 (Cs-137), strontium-90 (Sr-90), uranium isotopes, and iodine-129 (I-129), as well as other radioactive and nonradioactive materials. Multiple remediation strategies have been implemented in the F-Area, including the pump-and-treat method and the funnel and gate method. However, in recent years, increased levels of radioiodine were found in the groundwater of the Fourmile Branch wetland, mostly as ^{129}I with multiple anionic species (iodide, iodate, and organoiodide)[3]. Speciation is the primary controlling factor in the availability of iodine species, with I^{-} being the dominant species near the basin while IO_3^{-} and organo-iodine are the major species near the wetland[4]. One of the geochemical processes affecting the transport of the iodine species includes the adsorption onto clay minerals and organic matter, which is influenced primarily by redox potential and pH[5].

Subtask 2.1: Objectives

This study aims to investigate the adsorption mechanisms of iodine species (I^{-} and IO_3^{-}) onto SRS wetland soils, particularly when treated with organoclay amendments, PM-199 and MRM. The primary objective is to evaluate the effectiveness of these organoclay amendments in removing iodine species from contaminated soils. The research specifically addresses three areas: the kinetics of iodine adsorption, the influence of pH on adsorption, and the comparative efficacy of PM-199 and MRM organoclays in removing iodine from SRS wetland soil. To achieve this, the study involved experiments with wetland topsoil collected from an uncontaminated area along the Fourmile Branch stream.

Subtask 2.1: Results

Further details on the experimental results can be found in the draft manuscript included in Appendix C.

Organoclay Isotherms

For adsorption isotherms, iodine solutions (I^{-} and IO_3^{-}) were introduced to PM-199 and MRM in varying concentrations. The aqueous solution at the end of the equilibration period was analyzed using inductively coupled plasma mass spectrometry (ICP-MS) to determine the iodine retention capacity of each organoclay.

In the adsorption isotherms, the results showed that PM-199 exhibited an adsorption capacity of approximately 16 mg of iodide per gram of organoclay. However, neither PM-199 nor MRM reached equilibrium with iodate, even at concentrations far exceeding environmentally relevant levels, indicating that both organoclays are highly efficient at removing iodate. MRM had a slightly lower adsorption capacity (~13 mg iodide per gram of organoclay) compared to PM-199, but it followed the same trend of not reaching equilibrium with iodate. These results suggest that both organoclays are effective and efficient at removing both iodide and iodate from solution.

Kinetics

The kinetic experiments assessed the time-dependent adsorption of iodine species onto SRS wetland topsoil treated with organoclays. The study found that iodide was removed more efficiently than iodate. Specifically, PM-199-treated soil removed approximately 77% of iodide from solution, while MRM-treated soil removed around 55%. In contrast, iodate removal was lower: PM-199-treated soil removed about 30%, while MRM-treated soil removed 45%. Initial adsorption was faster for PM-199-treated soil for both iodine species, which aligns with the observation that iodide is more readily adsorbed than iodate. The faster initial uptake of iodide in both organoclay treatments suggests that the presence of PM-199 and MRM enhances the removal of iodide at a quicker rate compared to iodate.

Effect of pH

The effect of pH on iodine adsorption was also evaluated by varying the pH from 4 to 8. The study found that pH had minimal impact on the adsorption of iodine species, with little difference observed in adsorption capacity between pH values of 4 and 7. At pH 8, however, there was a slight reduction in adsorption capacity. This is likely due to the development of a negative charge on the organoclays at higher pH levels, which inhibits adsorption[6]. PM-199 was consistently more effective at removing iodine than MRM across the entire pH range. For iodide, PM-199 removed around 94% of the iodine at pH 4-6, 91% at pH 7, and 87% at pH 8. MRM was more effective at removing iodate than iodide across all pH values, but its overall iodine removal capacity was lower than PM-199's.

Subtask 2.1: Conclusion

In conclusion, this study demonstrates that both PM-199 and MRM organoclays are effective at adsorbing iodine species from SRS wetland soils, with PM-199 showing slightly better performance overall. Both organoclays exhibited high removal capacities for iodide, while iodate was less effectively removed, with neither organoclay reaching equilibrium for iodate even at high concentrations. The kinetics of iodine adsorption revealed that iodide was more readily adsorbed than iodate, with PM-199 showing the fastest initial uptake. The effect of pH was found to be minimal across the pH range of 4-7, with a slight reduction in adsorption capacity at pH 8 due to changes in the charge of the organoclays. These findings suggest that organoclay amendments, particularly PM-199, could serve as an effective remediation strategy for mitigating iodine contamination in the F-Area wetlands of the SRS site. By improving the removal of iodine species, this approach offers a promising solution for reducing environmental risks associated with radioactive contamination in wetland ecosystems.

Subtask 2.1: References

1. F-Area Hazardous Waste Management Facility Corrective Action Report, Third and Fourth Quarter 1997. Volume 1. https://doi.org/10.2172/626399

2. Looney, B. B.; Grant, M. W.; King, C. M. Estimation of Geochemical Parameters for Assessing Subsurface Transport at the Savavannah River Site, DPST-85-904; E.I. Du Pont de Nemours & Co.: Wilmington, DE, 1987.

3. Zhang, S., Ho, Y.-F., Creeley, D., Roberts, K. A., Xu, C., Li, H.-P., Schwehr, K. A., Kaplan, D. I., Yeager, C. M., & Santschi, P. H. (2014). Temporal variation of iodine concentration and speciation (127I and129I) in wetland groundwater from the Savannah River Site, USA. *Environmental Science & Technology*, *48*(19), 11218–11226. https://doi.org/10.1021/es502003q

4. Otosaka, S., Schwehr, K. A., Kaplan, D. I., Roberts, K. A., Zhang, S., Xu, C., Li, H.-P., Ho, Y.-F., Brinkmeyer, R., Yeager, C. M., & Santschi, P. H. (2011). Factors controlling mobility of 127i and 129i species in an acidic groundwater plume at the Savannah River Site. Science of The Total Environment, 409(19), 3857–3865. https://doi.org/10.1016/j.scitotenv.2011.05.018

5. Emerson, H. P., Xu, C., Ho, Y.-F., Zhang, S., Schwehr, K. A., Lilley, M., Kaplan, D. I., Santschi, P. H., & Powell, B. A. (2014). Geochemical controls of iodine uptake and transport in Savannah River Site Subsurface sediments. *Applied Geochemistry*, *45*, 105–113. https://doi.org/10.1016/j.apgeochem.2014.03.002

6. Pham, P. (2023). Remediation of Heavy Metals And Radionuclides From The Environment Using Environmentally Friendly Sorbents (dissertation).

Subtask 2.2: Humic Acid Batch Sorption Experiments with SRS Soil

Subtask 2.2: Introduction

The Savannah River Site (SRS), located in South Carolina, was a pivotal nuclear facility during the Cold War, from 1953 to 1988, producing nuclear weapons and nuclear energy programs, involving the manufacturing of materials such as plutonium and tritium for nuclear weaponry (Evans, et al., 1992). These operations generated radioactive waste and environmental contamination, which pose complex challenges requiring ongoing remediation efforts and environmental management at the site. The F-Area Seepage Basins received approximately 1.8 billion gallons of low acidic waste solutions containing nitrate, metals, and several radionuclides. At that time, it was believed that most of the radionuclides present in the waste solution would bind to the soil, precluding the migration of the radionuclides. Throughout the years, radionuclides, including uranium isotopes, strontium-90, and iodine-129, have gradually permeated from the vadose zone into the saturated zone. As these contaminants infiltrated the groundwater, they found their way through the Fourmile Branch watershed. The uranium contamination further intensified the situation by its properties that increase the pH of the groundwater, which poses an additional challenge. The groundwater remains acidic, with uranium concentrations surpassing the Environmental Protection Agency (EPA) maximum contaminant levels (Dong et. al., 2012). Efforts such as pump-and-treat systems were deployed in an attempt to mitigate the contamination. However, these approaches were costly and generated additional radioactive waste. In 2004, the pump-and-treat system was replaced with a funnel and gate system that created a treatment zone by injecting a solution of sodium hydroxide and carbonate. The injections were done directly into the gates of the F-Area groundwater to raise pH levels. The purpose of the treatment zone was to reverse the acidic nature of the contaminated sediments, thereby producing a more negative net charge on the surface of sediment particles and enhancing the adsorption of cationic contaminants. This increased the adsorption of cationic contaminants onto the sediment, leading to reduced concentrations of Sr-90 and U-238, but had no impact on iodine treatment. Systemic injections were necessary to preserve the pH neutrality within the treatment zone. Carbonate forms strong complexes with uranium and could remobilize uranium that was already adsorbed within the treatment zone (Gudavalli et al., 2013).

Humic substances (HS) are polyfunctional organic macromolecules found in soil organic matter, formed from the decomposition of biomass or dead organic matter (Trevisan et al., 2010). Humic substances can be divided into three main fractions: humin, which is insoluble at all pHs; humic acid (HA), soluble at pHs greater than 3.5; and fulvic acids, which are soluble at all pHs (Choppin et. al., 1992). Humic acid is a key ligand for ion exchange and metal complexing, with a high capacity to bind metals and affect their migration behavior (Davis et al., 2002). Previous studies suggest that the sorption of U(VI) in the presence of humic acid is a complex process (Perminova et al., 2002). Ivanov et al (2012) studied U(VI) sorption onto bentonite with and without humic acid and proved enhanced uranium sorption at pHs lower than 3.8, while it was reduced at pHs above 3.8. In another study, U(VI) sorption proved to be influenced by pH, the U(VI) concentration, humic acid, and inorganic carbon species (Krepelova et al., 2007).

Chemically modified humate materials, commercially known as KW-30, is being tested for its use in remediation techniques to reduce the mobility of uranium, strontium, and iodine in the subsurface at SRS.

Subtask 2.2: Objectives

The objective of this research is to investigate the effect of sorbed modified humic acid (KW-30) on the sequestration of commingled contaminants, specifically uranium, strontium, and iodine, within the Savannah River Site (SRS) F-Area. This investigation takes place under varying site-specific conditions, aiming to identify a feasible remediation technology for deployment. The study evaluates the potential for in-situ contaminant remediation at SRS Fourmile Branch using humic acid and suggests its future applicability to other sites with different conditions.

Subtask 2.2: Methodology

Materials:

This study utilized sediment samples collected from the F-Area at SRS (FAW1 70-90 ft) and sieved through a 2mm sieve. The fraction ≤ 2 mm was used in the experiments. This sediment was chosen due to its comparability to the soil composition in the uranium-contaminated aquifer layer. For U(VI), a commercial 1,000 ppm uranyl stock solution in 2% nitric acid was used. A humate stock solution (KW-30) consisting of 1,000 mg in 1,000 mL of deionized water (DIW) was prepared for use in the experiments. Iodide and iodate solutions were prepared using 1000ppm stock solutions, with a commercial iodide standard (I^-, 1000 ug/mL) obtained from SPEC CeroPrep, and an Iodate standard (IO_3^-, 1000 mg/L) obtained from VeriSpec. To maintain ionic strength, 0.2M sodium perchlorate was used, and the sample's pH was adjusted using 0.1M HCl/NaOH. Synthetic groundwater was prepared using the SRS monitoring wells FOB20 and FOB21 elemental data and recreated in the laboratory.

A synthetic groundwater recipe was formulated, replicating conditions in SRS F-Area wells (FOB20 and FOB21). The synthetic groundwater was prepared by combining salts with deionized water at 1,000 times concentration in one liter. The amount of salt needed for each element can be found in Table 2, where the amount of each salt needed was calculated by multiplying the molecular weight (mg/mmol) by the concentration (mol/L) found from the previous procedure in the groundwater recipe.

Table 2. Calculations for the Amount of Each Salt Needed in One Liter of DIW

Salts	Molecular Weight (mg/mmol)	Concentration (mmol/L)	Concentration (mol/L)	Concentration Calculations [x1000] (mg/L)	g/L
$CaCl_2*2H_20$	147.02	0.04	40.83	6002.45	6.00
$NaSO_4$	142.04	0.13	132.79	18861.80	18.86
$MgCl_2$	95.21	0.08	77.40	7369.64	7.37
NaCl	58.44	0.31	312.59	18267.56	18.27
KCl	74.55	0.03	25.00	1863.78	1.86
$NaNO_3$	84.99	1.84	1844.86	156803.64	156.80

Experimental Procedures:

Humate Sorption

200 mg of dried SRS sediment was combined with 50 ppm modified humic acid (KW-30) in 20 mL of deionized water (DIW) and synthetic groundwater (SGW) solutions. The samples' pH was adjusted to 4.0 daily using 0.1 M HCl/NaOH during the sorption period. After this period samples were placed on a platform shaker at 100 rpm for 7 days to equilibrate. Following this, samples were centrifuged at 2,700 rpm for 30 minutes, and the supernatant was analyzed via UV-Vis spectrophotometer to calculate the amount of KW-30 sorption onto the sediment.

Contaminant Sorption

Triplicate samples were prepared with iodide (I^-), iodate (IO_3^-), and uranium (U) in synthetic groundwater (SGW) and deionized water (DIW). 200 mg of coated and uncoated sediment along with control samples (no sediment) were prepared with 700 ppb of U and 150 ppb of I^-/IO_3^- in DIW/SGW. 0.01M of perchloric acid was added to adjust and maintain ionic strength, and sample pH was adjusted to 4 and placed on platform shaker at 100 rpm for two weeks. At the end of the sorption period, samples will be analyzed via ICP-MS for aqueous U and I concentrations to calculate sorption (removal).

Subtask 2.2: Results and Discussion

Sorption of KW-30

As shown in Figure 14 and Figure 15, DIW samples had an average sorption of 1,750 mg/kg (36% KW-30 removal) while SGW samples had an average of 1,250 mg/kg (25% KW-30 removal).

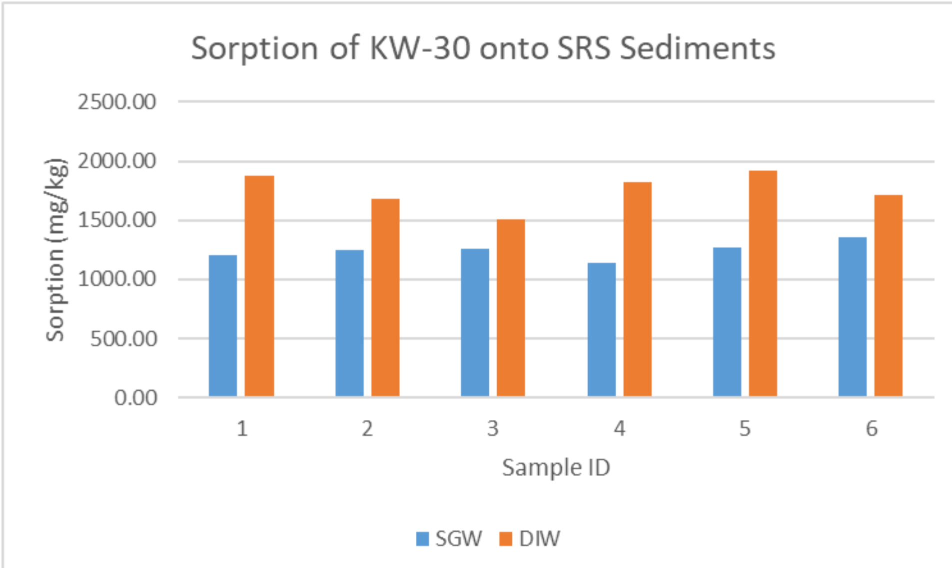

Figure 14. Sorption of KW-30 onto SRS sediment in the presence of DIW and SGW.

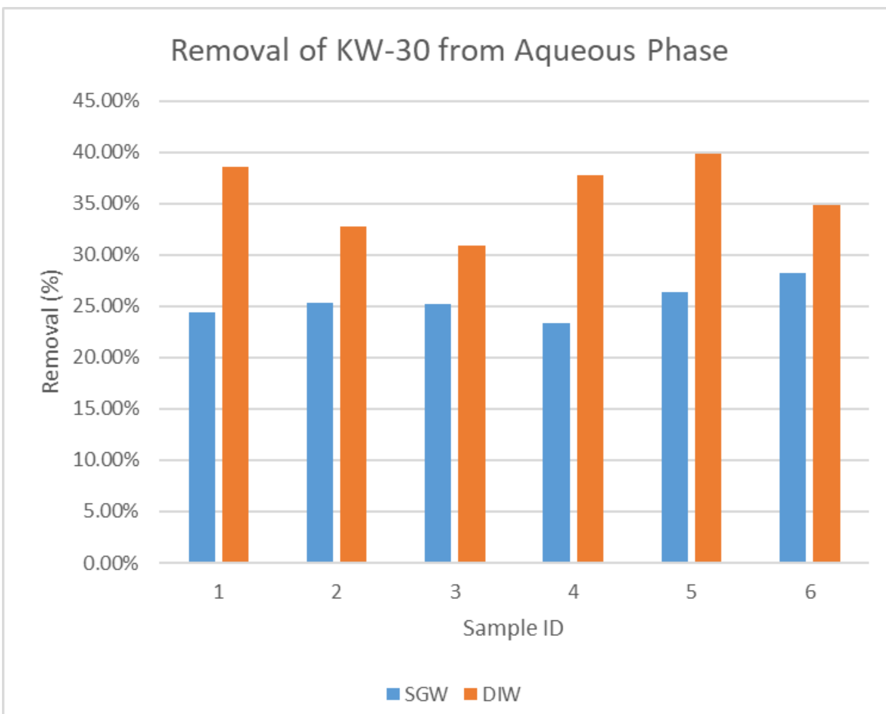

Figure 15. Percent Removal of KW-30 in the presence of DIW and SGW.

DIW and SGW samples were analyzed via VU-Vis using a DIW-based calibration. To accurately measure the sorption/removal of KW-30 in SGW samples, a new calibration curve was built to analyze SGW samples. The sorption and removal of KW-30 for SGW samples were 859-1457 mg/kg and 17%-29% (Figure 16 and Figure 17). DIW samples had an average sorption of 1,750 mg/kg and 36% while SGW samples had an average of 1,060 mg/kg and 22%.

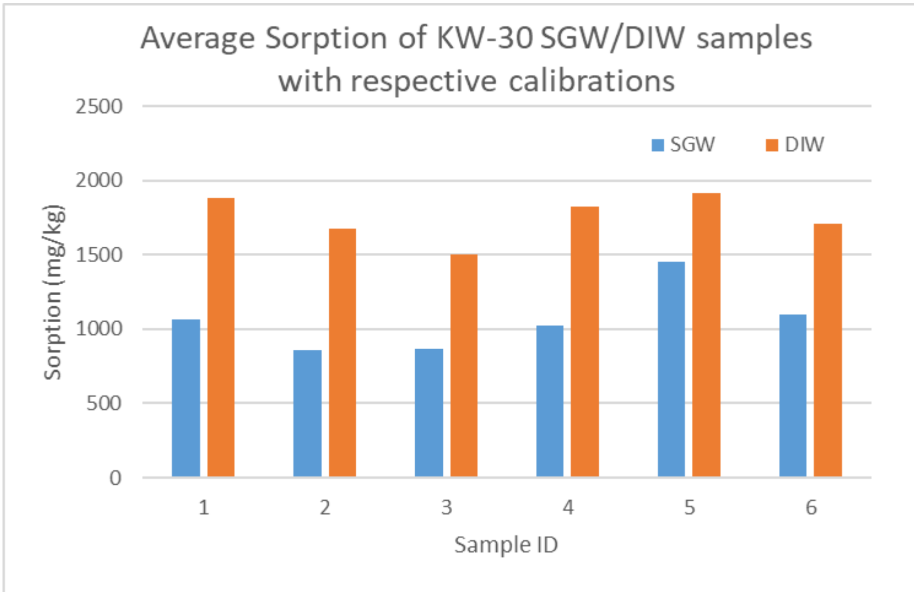

Figure 16. Sorption of KW-30 onto SRS sediment in the presence of DIW and SGW with their respective calibrations.

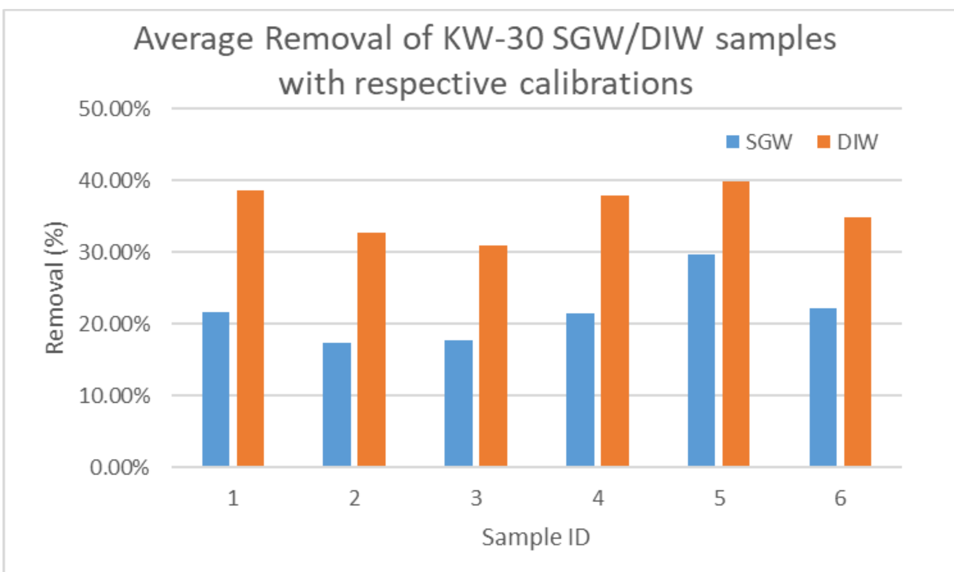

Figure 17. Percent removal of KW-30 in the presence of DIW and SGW with their respective calibrations.

A spectrometer analysis of the different concentrated solutions from both DIW and SGW calibrations ranging from 5 - 25 ppm was conducted in the range of 190 – 1,000 nm (Figure 18 and Figure 19). The DIW blank is causing a large absorbance for SGW samples, hence a new spectrum analysis will be conducted with DIW blank for DIW standards and SGW blank for SGW standards.

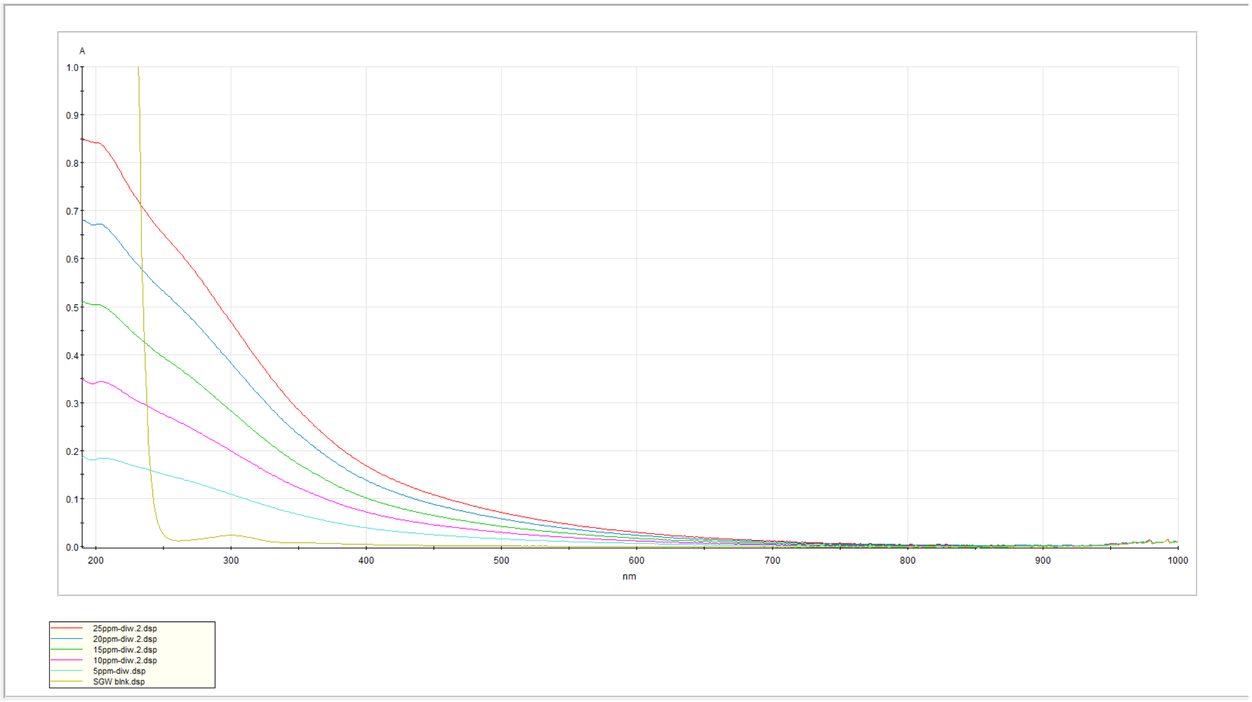

Figure 18. UV-Vis spectrum analysis of DIW standards.

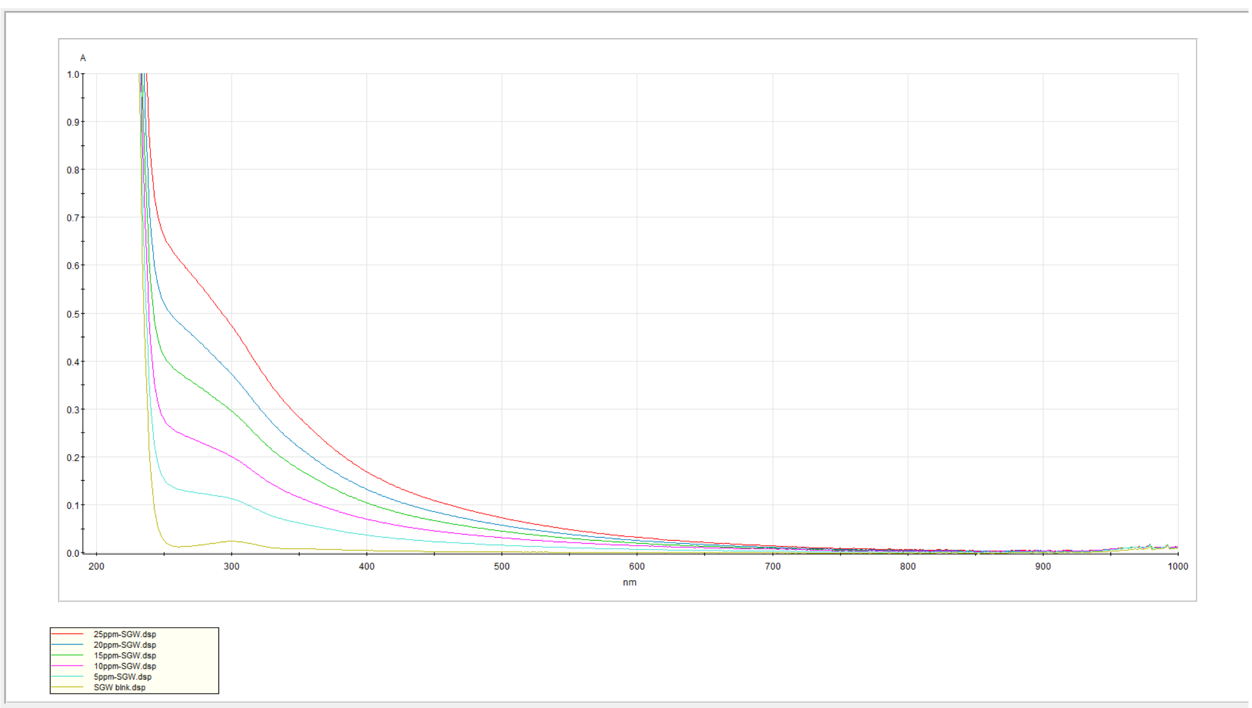

Figure 19. UV-Vis spectrum analysis of SGW standards.

Sorption of Contaminants

Contaminant (uranium and iodine) sorption experiments were conducted with coated and uncoated sediment. 200 mg of coated and uncoated sediment along with control samples (no sediment) were prepared with 700 ppb of U and 150 ppb of I^-/IO_3^- in DIW/SGW. 0.01M of perchloric acid was added to adjust and maintain ionic strength, and the sample pH was adjusted to 4 and placed on a platform shaker at 100 rpm for two weeks. At the end of the sorption period, samples were analyzed via ICP-MS for aqueous U and I concentrations to calculate sorption (removal). Data analysis is currently in progress.

Subtask 2.2: Conclusions

The sorption of KW-30 onto SRS sediment was evaluated in both deionized water (DIW) and synthetic groundwater (SGW) solutions. The results demonstrated that KW-30 removal was significantly higher in DIW samples, with an average sorption of 1,750 mg/kg (36% removal), compared to 1,060 mg/kg (22% removal) in SGW samples. These findings suggest that the presence of SGW may reduce the sorption capacity of KW-30, potentially due to the complex interactions between the sediment, humic acid, and the ions present in SGW.

Subtask 2.2: References

Choppin, G.R., 1992. The role of natural organics in radionuclide migration in natural aquifer systems. *Radiochim. Acta* 58/59, 113.

Davis. J.A., Adsorption of natural dissolved organic matter at the oxide/water interface, 1982, 2002. Geochim. Cosmochim. Acta 46, 2381-2393.

Dong, W., Tokuanga, T. K., Davis, J. A., Wan, J., (2012). Uranium(VI) Adsorption and Surface Complexation Modeling onto Background Sediments from the F-Area Savannah River Site. Environ. Sci. Technol. 46, 1565-1571.

Evans, A.G., Bauer, L.R., Haselow, J.S., Hayes, D.W., Martin, H.L., McDowell, W.L., Pickett, J.B., 1992. Uranium in the Savannah River Site environment. Westinghouse Savannah River Co., Aiken, SC (United States), p. 95.

Gonzalez-Raymat, H., Anagnostopoulos, V.; Denham, M.; Cai, Y.; Katsenovich, Y. P., Unrefined humic substances as a potential low-cost amendment for the management of acidic groundwater contamination. Journal of Environmental Management 2018, 212, 210-218.

Gudavalli, R., Katsenovich, Y., Wellman, D., Idarraga, M., Lagos, L., Tansel, B., 2013. Comparison of the kinetic rate law parameters for the dissolution of natural and synthetic autunite in the presence of aqueous bicarbonate ions

Hay, M. B., Myneni, S. C. B., Structural environments of carboxyl groups in natural organic molecules from terrestrial systems. Part 1: Infrared spectroscopy. Geochimica et Cosmochimica Acta 2007, 71 (14), 3518-3532.

Ivanov, P., Griffiths, T., Bryan, N.D., Bozhikov, G. and S. Dmitriev, 2012. The effect of humic acid on uranyl sorption onto bentonite at trace uranium levels. *J. Environ. Monit.,* 14, 2968 - 2975.

Jiang, W., Cai, Q., Xu, W., Yang, M., Cai, Y., Dionysiou, D. D., O'Shea, K. E., Cr (VI) adsorption and reduction by humic acid coated on magnetite. Environmental science & technology 2014, 48 (14), 8078-8085.

Kimmig, S. R., C. Thompson, S. Baum and C. F. Brown (2021). "Evaluation of iodine speciation and 129I/127I ratios at low concentrations in environmental samples using IC-ICP-MS." Journal of Radioanalytical and Nuclear Chemistry 327(2): 929-937.

Köhler, F., B. Riebe, A. C. Scheinost, C. König, A. Hölzer and C. Walther (2019). "Sorption of iodine in soils: insight from selective sequential extractions and X-ray absorption spectroscopy." Environmental Science and Pollution Research 26(23): 23850-23860.

Krepelova. A., 2007. Influence of Humic Acid on the Sorption of Uranium(VI) and Americium(III) onto Kaolinite (Dissertation).

Largitte, L. and R. Pasquier (2016). "A review of the kinetics adsorption models and their application to the adsorption of lead by an activated carbon." Chemical Engineering Research and Design 109: 495-504.

Perminova, I.V, Hatfield, K., Hertkorn, N., 2002. Use of humic substances to remediate polluted environments: from theory to practice. In the proceedings of the NATO Advance Research Workshop, Springer, P.O Box 17, 3300 AA Dordrech, The Netherland.

Trevisan, Sara, et al. "Humic Substances Biological Activity at the Plant-Soil Interface." *Plant Signaling & Behavior*, vol. 5, no. 6, 2010, pp. 635–643., doi:10.4161/psb.5.6.11211.

Wang, W. and J. Wang (2018). "Comparative evaluation of sorption kinetics and isotherms of pyrene onto microplastics." Chemosphere 193: 567-573.

Zhou, T., S. Huang, D. Niu, L. Su, G. Zhen and Y. Zhao (2018). "Efficient Separation of Water-Soluble Humic Acid Using (3-Aminopropyl)triethoxysilane (APTES) for Carbon Resource Recovery from Wastewater." ACS Sustainable Chemistry & Engineering 6(5): 5981-5989.

TASK 3: CONTAMINANT FATE AND TRANSPORT MODELING FOR THE SAVANNAH RIVER SITE

This task involves the development and application of integrated hydrology and contaminant transport models for studying the impact of extreme atmospheric events and climate change on hydrology and the fate and transport of priority pollutants at DOE sites, with an emphasis on sedimentation and particle transport processes in the stream systems at SRS. The aim is to examine the response of these streams to historical discharges and environmental management remediation actions. The knowledge gained through these studies will provide a means of assessment, evaluation and post-closure long-term monitoring of water quality and environmental conditions following remedial activities. The models provide information needed for informed decision-making in existing DOE-EM soil and groundwater remediation programs. Results obtained will provide DOE-EM suggestion of key locations for contaminant monitoring. Furthermore, the models can be utilized as forecasting tools to predict suspended sediment loads and the extent of remobilization regimes under different scenarios of extreme storm events and erosion conditions. This research will assist in developing cost-effective remediation plans integrated into the SRS Area Completion Project (ACP) and accelerate progress of the DOE EM environmental restoration mission.

Subtask 3.1: Calibration of the Tims Branch Watershed Model and Scenario Analysis

Subtask 3.1: Introduction

FIU has developed a MIKE SHE/MIKE 11 integrated hydrology and contaminant transport model to simulate the impact of extreme storm events on the hydrological response and the transport of uranium in the Tims Branch watershed, and to assess the anticipated role of climate change on flow and contaminant transport in Tims Branch. Tims Branch represents an important applied science opportunity due to significant past research by Savannah River National Laboratory (SRNL) and Savannah River Ecology Laboratory (SREL). Tims Branch has served as an ideal test bed for the development of a modeling approach to examine the response of a braided stream system at SRS to historical and future discharge events, for simulation of heavy metal transport, and assessment of environmental management remediation actions. The current version of the model simulates surface water flow (velocity, depth, and discharge), sediment and uranium fluxes throughout Tims Branch during extreme precipitation events ranging from 5-year to 500-year return periods, with storm durations ranging from 6-hour to 96-hour. In addition, in FIU Year 3, longer-term simulations were performed to assess the long-term impact of storm events and base flow conditions on the fate and transport of major contaminants of concern. The research under this task will directly support interpretation of historical data on the trends of contaminant concentration and distribution in Tims Branch, and support planning and execution of future biota sampling in this important ecosystem, particularly considering the effect of extreme hydrological events on the stream flow and pollutant transport. In addition, this research fosters collaboration between the students and scientists at FIU, the Savannah River National Laboratory (SRNL) and the Savannah River Ecology Laboratory (SREL).

Subtask 3.1: Objectives

In FIU Year 4, the principal objective was to finalize existing work originally scheduled for Year 3 of the project. In Year 3 event-based and long-term simulations of the hydrological and sediment transport response of Tims Branch watershed were simulated. This provided important information concerning the stability and fate of known existing locations within the Tims Branch river network contaminated with uranium. However, due to software license issues with the DHI MIKE model, it was not possible to finalize the event-based and long-term simulations of uranium. Therefore, in FIU Year 4, the aim as to use the previously calibrated MIKE SHE/MIKE 11 model together with the MIKE11-ECO Lab library to simulate the event-based and long-term response of uranium within the basin, with specific focus on the simulated response of the locations contaminated with uranium, locations where deposition is anticipated to occur, as well as maximum uranium concentrations in the water column as simulated during heavy flow events. Finally, these simulations would be used to evaluate how changes in extreme precipitation events and prolonged periods of drought impact the mobilization of adsorbed heavy metals in sediment, and accumulation of priority contaminants of concern due to sedimentation.

Subtask 3.1: Methodology

In FIU Year 3, during the calibration process of the MIKE11 ECO Lab contaminant transport module of the Tims Branch watershed model, simulation results showed insensitivity to changes in certain model parameters, specifically the critical velocity for resuspension of suspended solids. This led to the suspicion of a potential bug in the model as the MIKE AD (advection-dispersion) simulation results showed the suspended solid simulations to be highly dependent on the chosen critical velocity values. FIU therefore transitioned from the 2014 to the 2021 version of MIKE in the hope that the issue would be resolved by upgrading the software license to a more recent version, particularly as technical support by the software company, DHI, is no longer provided for the 2014 version. This resulted in a delay in completing simulations that would aid in the evaluation of event-based uranium transport in Tims Branch and a further subsequent delay in completing a draft manuscript based on this research. As such, the following milestones, originally scheduled to be completed in FIU Year 3, were reforecast to FIU Year 4:

- 2022-P2-M11: Complete simulations and evaluation of event-based uranium transport model for Tims Branch.
- 2022-P2-M14: Complete draft manuscript on uranium transport model for Tims Branch

Additionally, in Year 4 FIU's plans included completion of the analysis of results from the long-term U transport simulations performed in Year 3 that were aimed at evaluating the potential impact of event-based, seasonal, and annual variations on the transport of uranium in the Tims Branch watershed. The results from this study will be used to develop a manuscript in conjunction with DOE-EM collaborators to be published in a relevant peer reviewed journal. FIU anticipates this subtask to be closed out in Year 5. Discussions will be held with collaborators at SRNL, SRS and DOE-EM HQ to determine the method of transfer of the model and its results to DOE and/or whether there is a need to perform additional scenario analyses utilizing the model in its current state.

Subtask 3.1: Results and Discussion

During the first 6 months of Year 4 of the DOE-FIU Cooperative Agreement, FIU experienced a delay in trying to resolve a licensing issue with the MIKE software, which was finally resolved at the end of March 2024. Work on this subtask was therefore only reinitiated in April 2024. Although attempts were made to get this task back on track, the significant delay required Milestone 2023-P2-M7 titled *"Complete simulations and evaluation of event-based uranium transport model for Tims Branch"* to be reforecast from March 29, 2024, to September 1, 2024.

FIU Year 3 Carryover Scope

The uranium transport simulations within Year 4 have been delayed due to issues with the MIKE ECO Lab software. These were resolved by the end of Spring. The MIKE uranium transport simulations were split into two components. Part one focused on identifying effect model parameters for long-term simulations. A number of simulations were performed, however the process of identifying the optimal parameters is still ongoing. The second aspect focused on uranium transport for short duration flow events. This work was part of the PhD research of Juan Morales, a former DOE Fellow. Using the previously calibrated MIKE model for Tims Branch, he performed a sensitivity analysis to determine controlling variables and optimum values of parameters affecting U geochemical processes in Tims Branch. The parameters Koc and foc were identified as controlling variables and used as the primary focus of the model calibration process. It was observed that for baseflow simulations, uranium concentrations are negligible. However, during the peak flow events, which result in erosion of the channel bed, concentrations increase. This is in alignment with observed data in published literature (Hayes 1986).

Event-Based U Transport in Tims Branch Watershed

At the end of FIU Year 4, Milestone 2023-P2-M7 was completed, which involved simulations and evaluation of event-based uranium transport in Tims Branch. Former DOE Fellow, Juan Morales, included this research as a component of his PhD dissertation titled *"Long-Term Monitoring of Heavy Metals Using Numerical Modeling and Molecular Indices",* which he defended and passed in March 2024 (Abstract in APPENDIX E). Milestone 2023-P2-M13, Complete draft manuscript on uranium transport model for Tims Branch (Subtask 3.1) due 9/1/2024, will be reforecast to FIU Year 5.

Year 4 accomplishments included:

- Sensitivity analysis - to determine controlling variables and optimum values of parameters affecting U geochemical processes in TB.
- Koc and foc identified as controlling variables – primary focus of model calibration process.
- Simulation results highlight Koc to be driver of U flux at TB outlet, thus optimum Koc values determined.
- Simulated U flux in alignment with observed data in published literature (Hayes 1986).

The figures below show the simulated breakthrough curves representing dissolved U concentration in TB outlet.

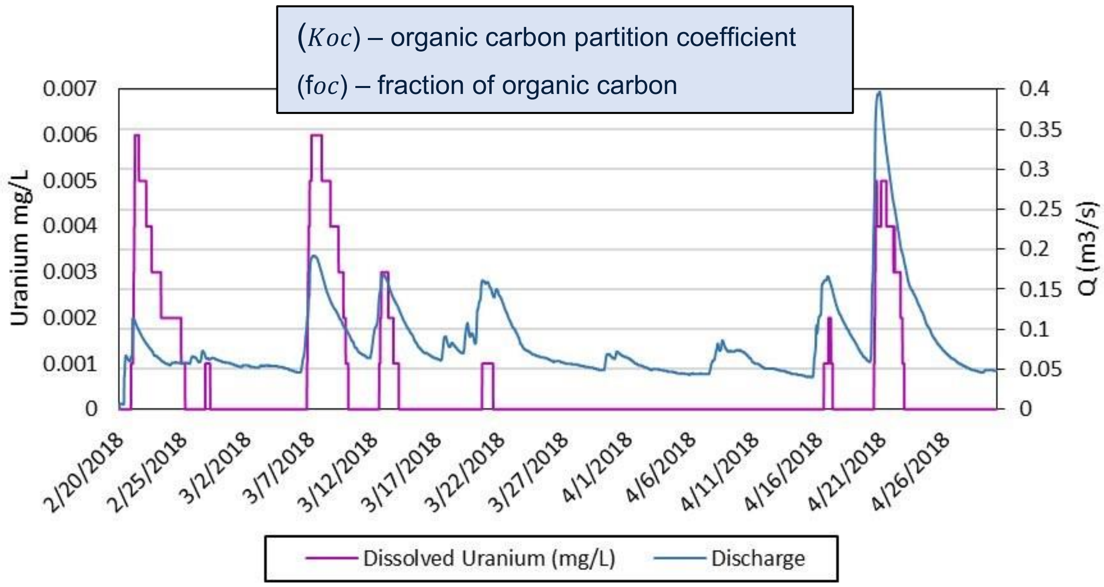

Figure 20. Simulated breakthrough curves of dissolved U and discharge in response to increased discharge scenarios caused by episodic precipitation in TB outlet for the evaluation calibration period.

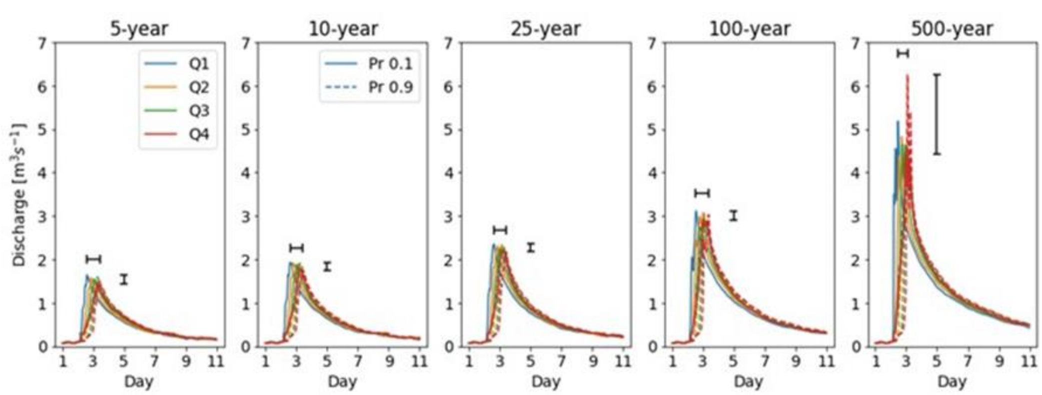

Figure 21. Simulated breakthrough curves of dissolved U and discharge in response to increased discharge scenarios caused by episodic precipitation in TB outlet for the evaluation calibration period.

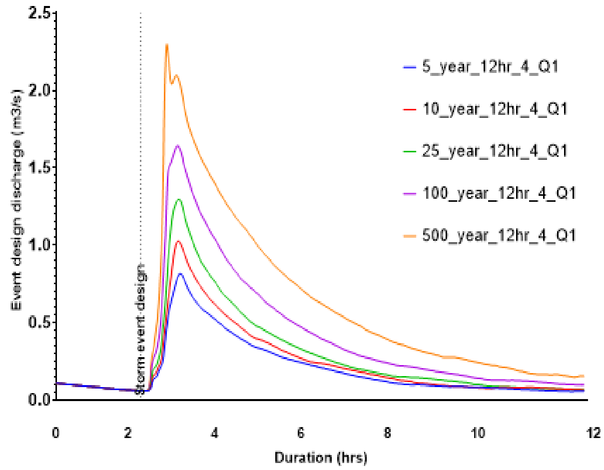

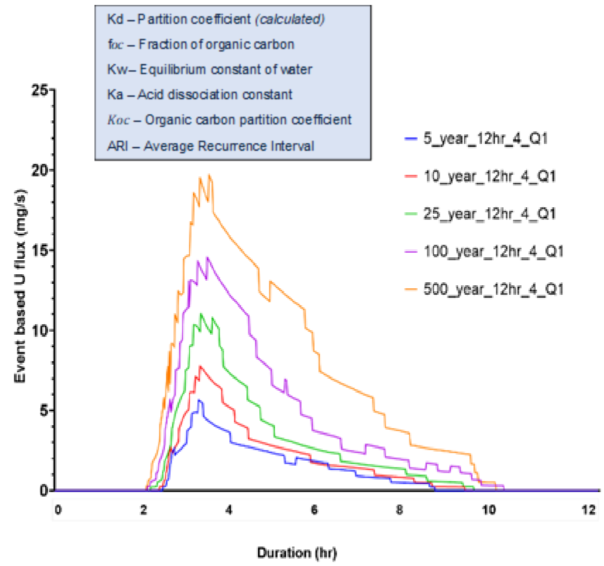

Figure 22. Event-based scenario results: Increased discharge after episodic storm events (left); U flux due to increased precipitation and discharge at Tims Branch outlet (right).

The next step is to use the calibrated MIKE11 ECO Lab parameters for the transport of uranium in Tims Branch. For this, focus will be on extreme events for various return periods, such as those presented in the figure above as well as focusing on long-term variation to also include the impact of joint erosion and deposition processes occurring throughout the basin. Due to significant delays in getting the latest version of the MIKE 11 software in Year 4, these analyses will be carried over and form the scope for Year 5.

Subtask 3.1: References

Batson, V. L, Bertsch, P. M., & Herbert, B. E. (1996). Transport of anthropogenic uranium from sediments to surface waters during episodic storm events. *Journal of Environmental Quality*, *25*(5), 1129–1137.

Batson, V. L. (1994). *Surface water transport and distribution of uranium in contaminated sediments near a nuclear weapons processing facility*. Texas A&M University.

Evans, A. G., Bauer, L. R., Haselow, J. S., Hayes, D. W., Martin, H. L., McDowell, W. L., & Pickett, J. B. (1992). *Uranium in the Savannah River Site Environment*. Westinghouse Savannah River Co., Aiken, SC (United States).

Hayes, D.W. (1986). *Sediment transport studies in Tims Branch*. Rep. DPST-86- 468. E.I. du Pont de Nemours & Co, Savannah River Laboratory, Aiken, SC.

Kaplan, D. I., Smith, R., Parker, C. J., Baker, M., Cabrera, T., Ferguson, B. O., Kemner, K. M., Laird, M., Logan, C., & Lott, J. (2020). Uranium Attenuated by a Wetland 50 Years after Release into a Stream. *ACS Earth and Space Chemistry*, *4*(8), 1360–1366.

Kaplan, D. I., Smith, R. J., Parker, C. J., Roberts, K. A., Hazenberg, P., Morales, J., O'Loughlin, E. J., Boyanov, M. I., Weisenhorn, P., Kemner, K. M., and Powell, B. A. (2023). Natural Attenuation of Uranium in a Fluvial Wetland: Importance of Hydrology and Speciation, *Applied Geochemistry*, 155, 105718. Doi: 10.1016/j.apgeochem.2023.105718

Subtask 3.2: Model Development for Fourmile Branch with Specific Focus on the F-Area Wetlands

Subtask 3.2: Introduction

The Fourmile Branch watershed at the U.S. Department of Energy's (DOE's) Savannah River Site (SRS) is a highly braided wetland stream system that has been contaminated by the historical release of 1.8 billion gallons of acidic, low-level radioactive waste from 1955 to 1988 to unlined underground seepage basins in the F-Area (Figure 23), resulting in the downward migration of radiological contaminants through the vadose zone to the uppermost aquifer, creating a large groundwater contaminant plume which is slowly traveling downstream and anticipated to eventually resurface at outcrops (seep line) in the adjacent F-Area wetlands before entering the Fourmile Branch stream.

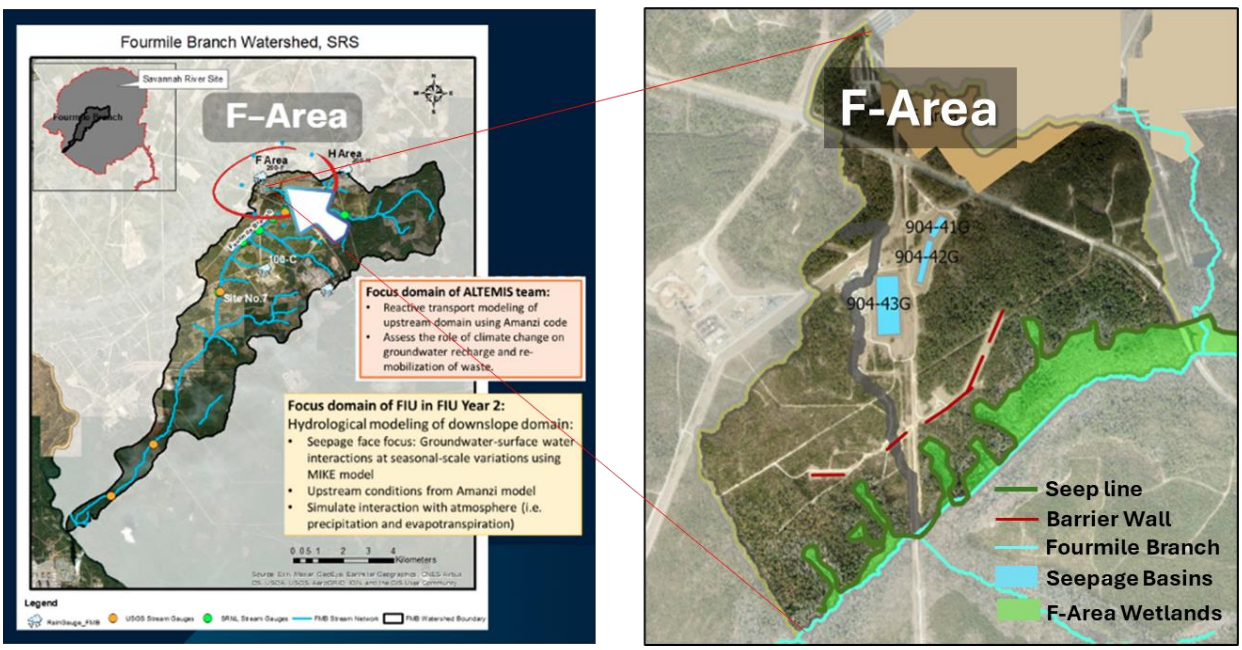

Figure 23. Fourmile Branch watershed (left) and F-Area study domain (right).

The F-Area wetlands have thus been a primary area of concern due to the presence of low-level radiological contamination in the groundwater. Currently, the main risk drivers for the groundwater in the F-Area are Sr-90, uranium isotopes, I-129, Tc-99, tritium, and nitrate (Denham and Vangelas, 2008). The geochemical complexity of the affected area and the comingled plume constituents pose significant challenges for effective remediation efforts. In addition, the high acidity of the contaminated groundwater greatly enhances the mobility of metals and radionuclides. The variety of radiological, cationic, and anionic species in the plume therefore necessitates a range of remedial strategies to effectively treat all the contaminants involved (ITRC, 2017).

Several groundwater remedial technologies (e.g., subsurface barriers and water capture with irrigation) have been implemented by SRS, successfully reducing the contaminant flux to Fourmile Branch. Many of these technologies have since remained in place to control the rate of contaminant movement and minimize the risk of radiological exposure to human and ecological receptors. It remains unclear, however, whether their effectiveness will be impacted by the increasing intensity of storms due to climate change, limiting their ability to prevent contaminant migration from the groundwater into other environmental compartments.

Currently, remediation in the F-Area focuses on an enhanced monitored natural attenuation (MNA) approach, with periodic injections of a base solution to increase the sorption of cationic contaminants, making them less bioavailable. While these strategies are successful in sequestering the contaminants of concern, a long-term monitoring strategy is necessary as there is potential for contaminant remobilization. Zones of potential vulnerability exist as there is uncertainty regarding the conditions influencing contaminant flux to the braided wetland system of the SRS F-Area. Furthermore, it is also unclear how wet and dry moisture variations between extreme storm events and at seasonal timescales impact the release of contaminants into the FMB stream.

Subtask 3.2: Objectives

To gain a better understanding of the Fourmile Branch watershed hydrology, FIU has developed a modeling approach that involves the development of two separate models which examine hydrological behavior in the Fourmile Branch watershed at the basin scale as well as at the sub-catchment scale. A detailed high-resolution model was developed using the open-source Advanced Terrestrial Simulator (ATS) that focuses on the hillslope and braided river network system of a small sub-catchment within the SRS F-Area where there is known radiological contamination in the groundwater. The model will be used to simulate the hydrological response of the F-Area hillslope in current and future climate, as well as the flow through the groundwater downslope and the interaction between the groundwater and river network system to determine the sub-catchment's contribution with respect to discharge into the main Fourmile Branch stream channel when exposed to extreme weather conditions. In addition, the ATS model incorporates the F-Area seepage basins in the mesh as well as man-made engineering structures, such as the upstream barrier wall used as part of DOE-EM's remediation strategy, to simulate their impact on the hydrology. Model simulation results are anticipated to provide information on the groundwater-surface water interaction, as well as seasonal and long-term variations along the seep line/riparian zone interface.

A second model was simultaneously developed at lower resolution using the MIKE SHE/MIKE 11 software developed by the Danish Hydraulic Institute (DHI) that includes the entire Fourmile Branch watershed to improve our understanding and evaluate the overall basin-scale response with respect to discharge under extreme meteorological conditions occurring as individual events, between various seasons, as well as across longer-term timescales. It is expected that the developed model will enable evaluation of the anticipated role of climate change on the basin's moisture and flow variability and will enable FIU to hypothesize how this can potentially impact contaminant transport and redistribution.

The implementation of hydrological modeling approaches at two different spatial extents will enable simulation of surface-subsurface hydrology and estimation of the flow components which are essential to understand contaminant fate and transport dynamics. Understanding the groundwater flow processes and its interaction with the seepline interface as it migrates upslope, moving from unsaturated to saturated conditions, is key to understanding the hydrological behavior of this natural system under various environmental conditions. Results from this study will also assist SRS in refinement of the site conceptual model by contributing to a better watershed-scale understanding of contaminant fate and transport in SRS streams.

Subtask 3.2: Methodology

Fourmile Branch MIKE SHE/MIKE 11 Model Development

Hydrological models are standard tools used for investigating surface/subsurface flow behavior. They provide uncertainty quantification, risk and decision support for water resource management, and evaluation of water quality, erosion, deposition, and transport. The MIKE SHE/MIKE 11 model is a fully integrated hydrological modeling software created to simulate interactions between surface water and groundwater in complex systems, with a toolset that takes into account all the significant hydrological compartments including surface, subsurface, precipitation and evapotranspiration. An integrated Python module also facilitates tailored simulations and automation of model workflows. MIKE SHE employs advanced algorithms to model rainfall-runoff processes, groundwater flow, soil moisture dynamics, and surface water routing, while MIKE 11 simulates channel flow, water level, and sediment transport, making the MIKE software suite appropriate for studying the various surface and subsurface hydrologic processes and the fate and transport of sediment bound radiological contaminants in the Fourmile Branch watershed. This will assist DOE-EM in ensuring the achievement and maintenance of regulatory compliance goals for water quality in this contaminated SRS stream system.

MIKE Model Inputs

Geospatial Data

The MIKE SHE/MIKE 11 hydrological modeling package has a built-in GIS user interface that can directly use geospatial data for model input parameters, which is significant not just for the spatial representation of hydrologic features, but particularly because of its integration with timeseries data attributes such as flow rates and directions, contaminant concentrations, water levels, precipitation, etc. Geospatial data for the MIKE Fourmile Branch model was downloaded from online state/federal databases and converted to a MIKE-compatible format (.dfs2). Data layers included a 1-m high-resolution lidar-based (3DEP) digital elevation model (DEM) from the United States Geological Survey (USGS). Using this DEM, the D8 flow method was used to delineate the stream network and upstream basin boundary. Furthermore, the DEM was used to derive cross-section elevation information for numerous locations along the river network. The DEM was subsequently averaged to a 250 m model resolution (Figure 24 top left). Land surface information, used by MIKE to calculate interception and actual evaporation, was derived from the Multi-Resolution Land Characteristics Consortium (MRLC) national land cover dataset (NLCD) for 2016 (Figure 24 top right). This product was aggregated to a 250 m MIKE SHE model resolution. For each land surface class, Leaf Area Index (LAI) information, used for evapotranspiration calculations, was obtained from long-term (2002-2020) satellite-based MODIS observations (Figure 24 bottom).

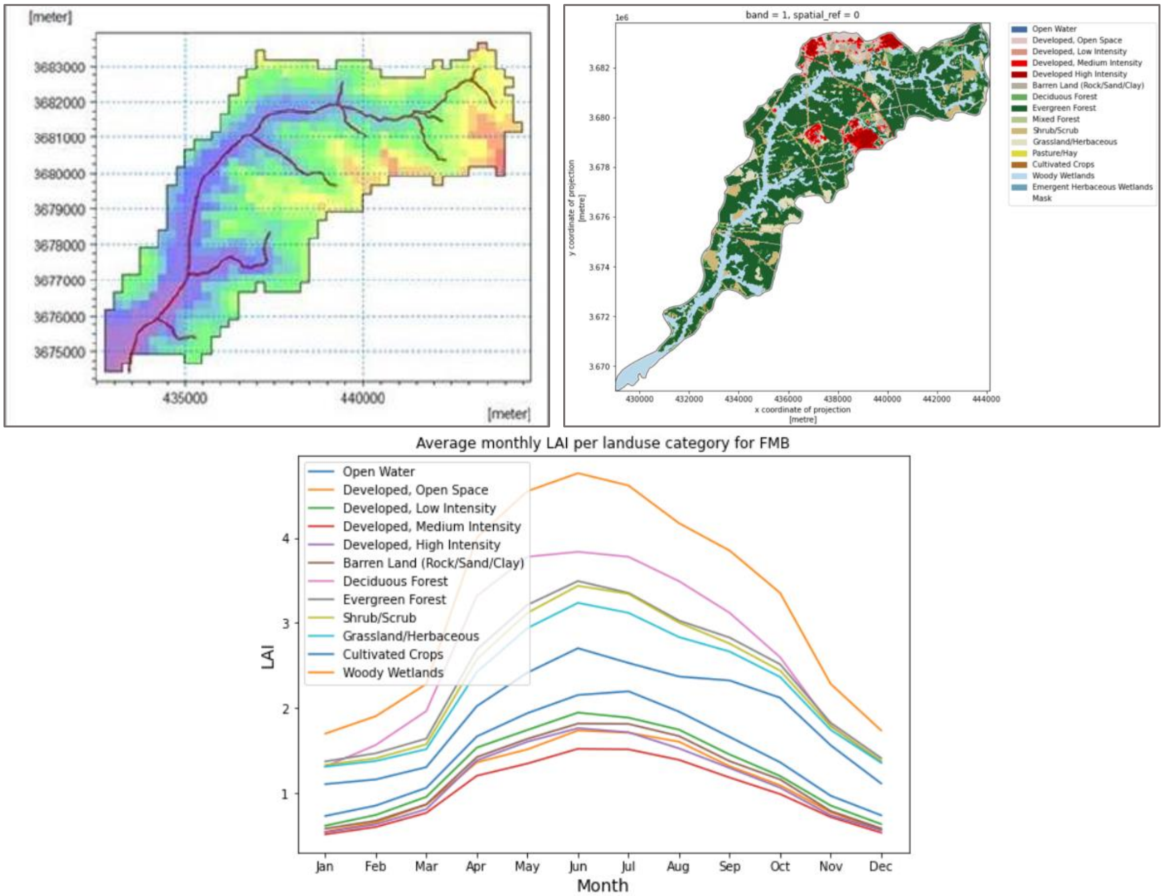

Figure 24. Geospatial input data for Fourmile Branch MIKE model: elevation topography grid derived from DEM and MIKE 11 river network (*top left*); NLCD 2016 land cover classification (*top right*); MODIS satellite-derived Leaf Area Index (LAI) per land use class (*bottom)*.

To simulate flow through the unsaturated zone, MIKE SHE uses the van Genuchten parametrization. For each model grid pixel, the soil physical parameters of this parameterization were obtained from the SoilGrids™ 2.0 database, a global digital soil mapping system that maps the spatial distribution of soil properties across the globe using state-of-the-art machine learning methods. Figure 25 shows the parameter values used.

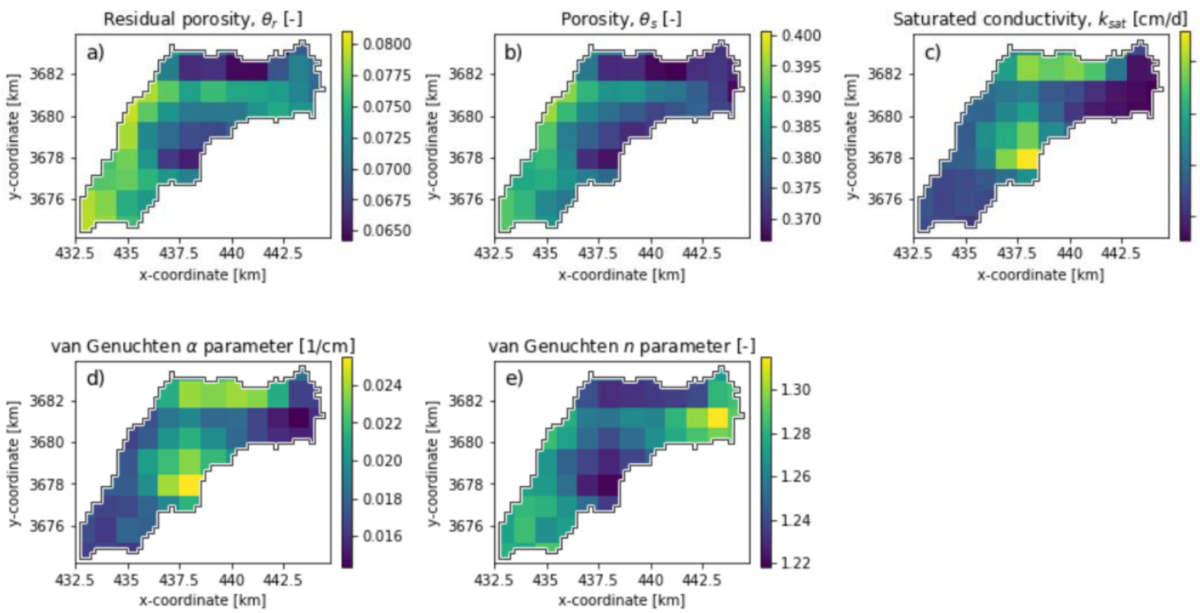

Figure 25. Soil parameter values for each 250x250m pixel used within MIKE SHE as derived from the SoilGrids™ 2.0 dataset.

Timeseries Data

As sub-daily precipitation variability can have a considerable impact on the simulated runoff, it was decided to force the MIKE Fourmile Branch model with timeseries data such as hourly precipitation, temperature and potential evapotranspiration data. For the first two model forcings, precipitation and temperature data available within the Analysis of Record for Calibration (AORC) was used. The AORC is a gridded record of near-surface weather conditions covering the continental United States and Alaska and their hydrologically contributing areas. This long-term dataset was specifically created to contain continuous data to be used for model simulation and calibration and covers the period 1979-2021 [1]. The MIKE model also uses hourly potential evapotranspiration as model forcing. It was decided to use the global hourly PET database as estimated from historical ERA5-Land data, recently developed by [2]. Hourly average values for Fourmile Branch were extracted from this global database with a grid resolution of 0.1 x 0.1 degrees for the period 1982-2020.

To automate the generation of model forcing, using the basin shapefile as input, a Python script was written to generate the hourly precipitation, temperature and potential evapotranspiration data using the procedure described above. Final results are being stored as (.dfs0) files to allow for immediate adoption by the MIKE model.

Climate Forecasting Model Data

To understand how climate change will impact the hydrological response of both Fourmile Branch watershed and the F-Area domain, FIU downloaded and processed climate model data of the current and future climate. This data is used to force both the MIKE and ATS models. Specifically, the latest version of the NASA Earth Exchange Global Daily Downscaled Projections (NEX-GDDP-CMIP6) was chosen. This archive contains downscaled historical and future projections for 1950–2100 based on climate model simulations from Phase 6 of the Climate Model

Intercomparison Project (CMIP6), the most recent level of climate model data. The NEX-GDDP-CMIP6 dataset contains information from 35 global climate models for five CMIP6 experiments (historical, SSP126, SSP245, SSP370, and SSP585). These represent the historical climate (1950-2015) as well as 4 different assumptions of shared socio-economic pathways (2015-2100) to represent global development within the (near) future.

The 4 SSPs include SSP1-2.6, SSP2-4.5, SSP3-7.0, and SSP5-8.5. Each SSP is a unique pathway which is summarized in Table 3 below.

Table 3. Socio-Economic Pathways (2015-2100) and Different Assumptions of Shared Socio-Economic Pathways (2015-2100) to Represent Global Development within the (Near) Future [0]

SSP1-2.6	Low GHG emissions: CO_2 emissions cut to net zero around 2075	Likely climate range 1.3-2.4°C
SSP2-4.5	Intermediate GHG emissions: CO_2 emissions around current levels until 2050, then falling but not reaching net zero by 2100.	Likely climate range: 2.1-3.5°C
SSP3-7.0	High GHG emissions: CO_2 double by 2100	Likely climate range: 2.8-4.6°C
SSP5-8.5	Very High GHG emissions: CO_2 emissions triple by 2075	Likely climate range: 3.3-5.7°C

A benefit of using the NEX-GDDP-CMIP6 dataset as compared to the original CMIP6 modeling archive is that this is a downscaled product, containing daily simulated values for 8 atmospheric variables (e.g., precipitation, temperature, humidity, and wind) which have been bias corrected and spatially disaggregated using monthly historical observations to a 1/4-degree horizontal resolution.

FIU has chosen to work with the climate data produced by a single climate model, Version 2 of the Community Earth System Model (CESM2), which was developed by the National Center for Atmospheric Research (NCAR) in Boulder, CO, USA.

F-Area ATS Model Development

The Advanced Terrestrial Simulator (ATS) was used to develop a detailed hydrological model for the hillslope surrounding the braided river network in the F-Area domain of Fourmile Branch. ATS, developed by the Department of Energy's Office of Biological and Environmental Research (DOE BER), is a fully integrated surface/subsurface hydrological model that analyzes surface and groundwater flows. ATS is an ecosystem-based, integrated, distributed hydrology simulator that is built upon the underlying multi-physics framework provided by Amanzi [0], the high-performance computing simulator, and naturally integrates with the Advanced Simulation and Capability for Environmental Management (ASCEM) Program. ATS is supported by the DOE BER program through the Environmental System Science (ESS) Science Focus Area (SFA) projects, IDEAS-Watersheds, and ExaSheds. Compared to MIKE, which uses a regular grid, ATS uses a triangular network that allows the simulation of more detail (i.e., using a finer mesh) for locations of interest. For the F-Area, these locations exist along the braided river network, where interaction between the contaminated groundwater and the channel occurs.

ATS Model Inputs

The mesh of the F-Area domain was created with the Python module, Watershed Workflow [0]. Watershed Workflow allows for the incorporation of publicly available data into the mesh, such as digital elevation maps (DEMs), spatial variations in National Land Cover Dataset (NLCD) land cover types, Soil Survey Geographic Database (SURRGO) soil texture, and GLobal HYdrogeology MaPS (GLHYMPS) subsurface information. The F-Area surface mesh with the location of the seepage basins, river network, inflow and outflow points, and the barrier wall is shown in Figure 26 below.

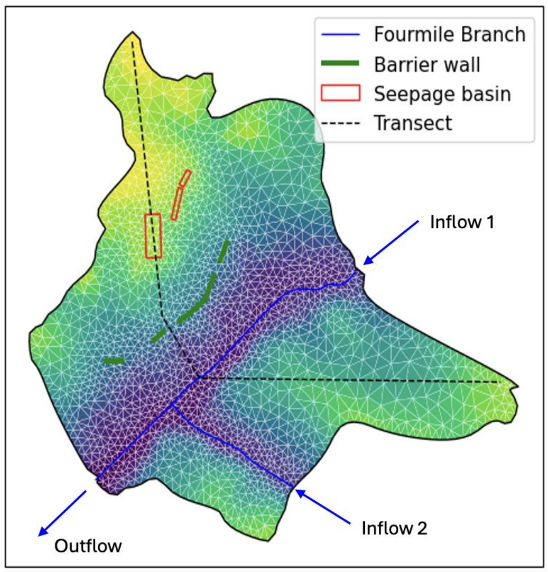

Figure 26. Plot of the F-Area mesh as used by ATS with the seepage basins (red), river network (blue), inflow and outflow points, and the barrier wall (green) displayed

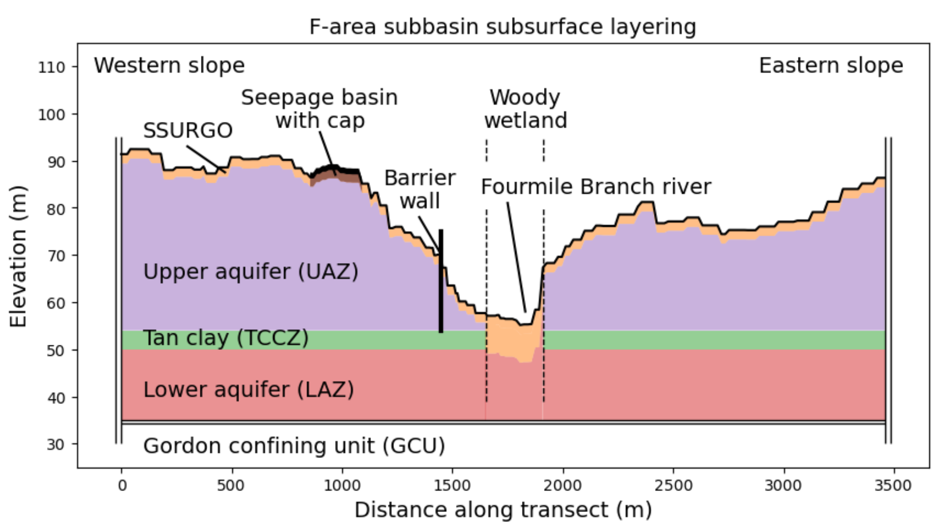

Figure 27. Plot of the subsurface layers along the transect in Figure 26, which were implemented in the F-Area ATS model.

Figure 27 shows the subsurface layers along the transect in Figure 26 that were used in the volume mesh and ATS model of the F-Area. These subsurface layers include the upper and lower aquifers and the tan clay confining zone.

For the historical ATS simulations of the F-Area, 33 years of daily atmospheric forcing (precipitation, temperature, and radiation) for the period 1/1/1982-12/31/2014 were derived from the DayMet reanalysis dataset provided by National Aeronautics and Space Administration's (NASA's) Distributed Active Archive Center (DAAC) at ORNL. To simulate future climate scenarios, the NEX-GDDP-CMIP6 dataset was used, as described earlier. Since ATS simulations are time consuming due to their detailed high-resolution meshes, the future climate simulations were broken into three 13-year periods: 2017 – 2030, 2047 – 2060, and 2077 – 2090.

The output of Watershed Workflow (the mesh, surface soils, and subsurface layers) was then used within an ATS input file. This input file is written in XML format and configures the set of coupled processes for the simulation at run time. The input file also defines all aspects of the hydrological model, such as meteorological data, geometric regions and mesh information, model parameter values, mathematical equations, and visualization output. FIU previously developed a Python script that enables automatic generation of the input file within Watershed Workflow. The ATS input file developed for the F-Area includes two different boundary conditions. A seepage face boundary condition was added to the surface boundary, not including inflow areas, to allow water (e.g., runoff) to leave the F-Area domain when saturation is present. At the inflow points, upstream channel flow was included by applying Neumann boundary conditions. At the two inflow points, extracted simulation data from the MIKE FMB model was used as upstream flow data. Figure 28 shows the upstream inflow used in the ATS model from the MIKE FMB model for both Inflow Point 1 (north) and Inflow Point 2 (east) in m^3/s from 1984 to 2014.

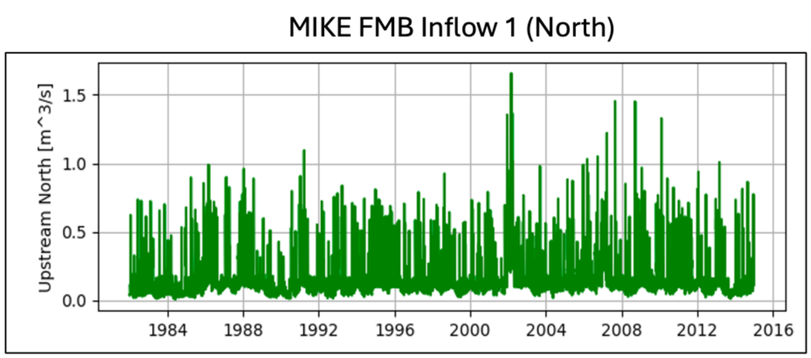

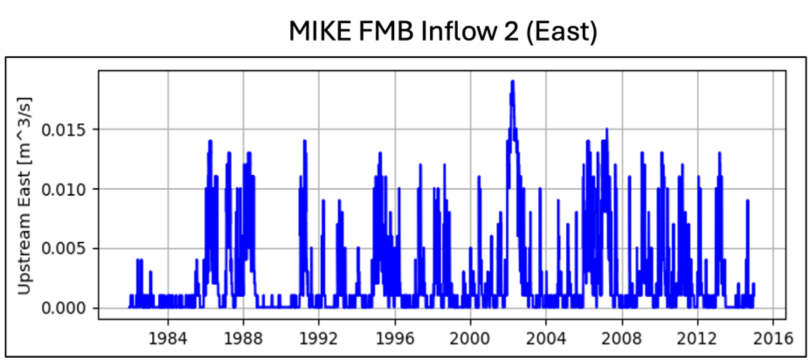

Figure 28. MIKE FMB upstream inflow used in the ATS model for Inflow Point 1 (top) and Inflow Point 2 (bottom) in m^3/s from 1984 to 2014.

Subtask 3.2: Results and Discussion

Long-Term Changes in Atmospheric Forcing

Figure 29 shows the historical and future climate model forcing for the CESM2 climate model. Also shown in this figure are the historically observed temperature and precipitation. For both yearly average temperature and total precipitation, the historical CESM2 dataset shows a good correspondence to the observed values. This is also reflected by the black and blue boxplots in the column. For Fourmile Branch and the DOE Savannah River Site in general, this model shows, for all four climate scenarios, an increase in temperature and potential evapotranspiration on a yearly basis compared to the historical climate. Temperature increases from about 18ºC for the historical climate to about 20ºC for SSP1-2.6 and SSP2-4.5 and about 21ºC for SSP3-7.0 and SSP5-8.5. The increase for the latter two scenarios becomes clearly visible towards the end of the century. Similarly, this also holds for potential evaporation.

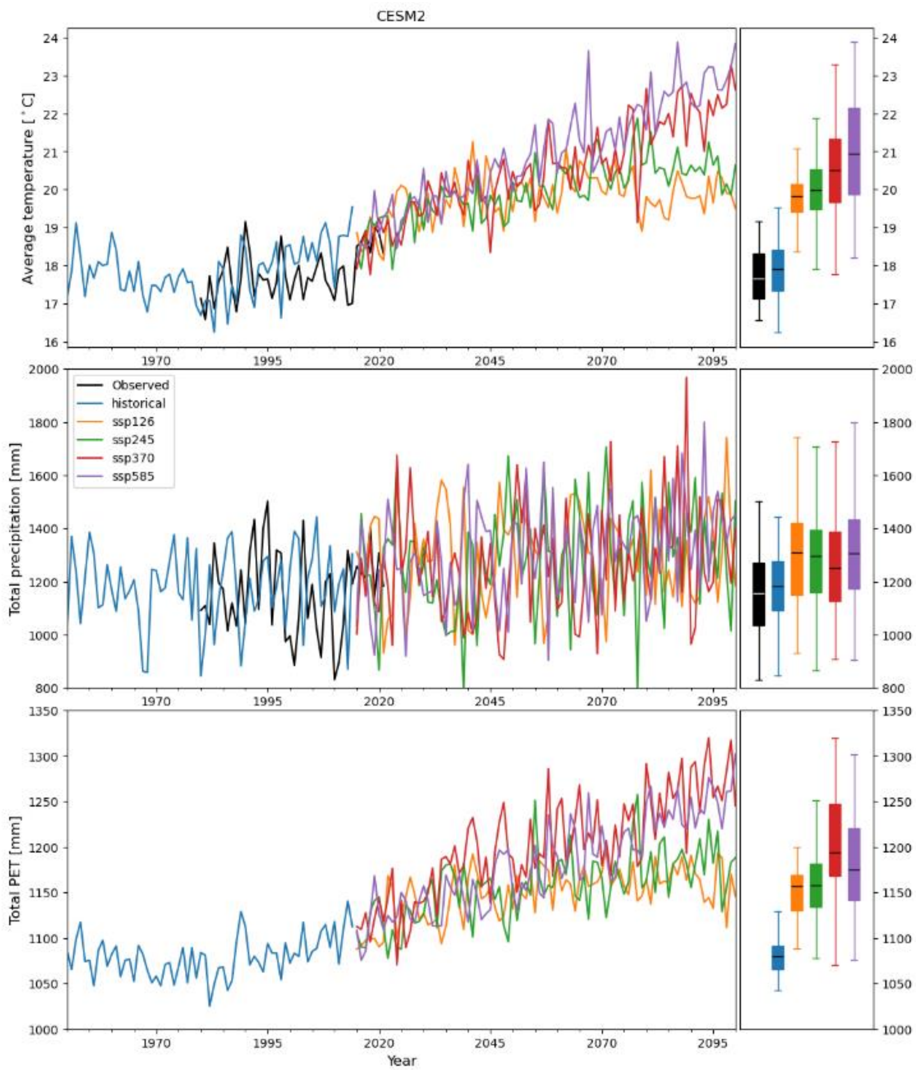

Figure 29. CESM2 model results showing climate variability (temperature, precipitation, and potential evapotranspiration) for the years 1950-2100 for four different climate scenarios. Also shown in these figures are the historical observations (black).

Yearly precipitation shows a larger variability for the future. The median yearly precipitation accumulation is anticipated to increase from about 1200 mm for the historical period, to around 1300 mm for the four climate scenarios. However, given the large inter-yearly variations, the expected changes in yearly accumulations are not significant. These data will be used to force both the MIKE model for Fourmile Branch and the ATS model for the F-Area hillslope in the coming months. Figure 29 above displays the CESM2 model results showing climate variability (temperature, precipitation, and potential evapotranspiration) for the years 1950-2100 for four different climate scenarios.

To obtain additional information on the performance of the CESM2 precipitation product, the figure below shows the maximum one-day precipitation accumulation. These maximum one-day precipitation accumulations are anticipated to result in intense flow events, that can lead to the migration of contaminated soil particles situated within the braided riverbed to downstream locations. Figure 30 shows that the observed one-day event accumulations from the AORC dataset are considerably higher compared to the historical CESM2 climate model precipitation forcing dataset. These event-based underestimations can potentially lead to reduced runoff simulations. For the future scenarios, a slight increase in the maximum one-day accumulation is simulated. This especially holds for the period 2060-2100. The largest increase is expected to occur for SSP3-7.0.

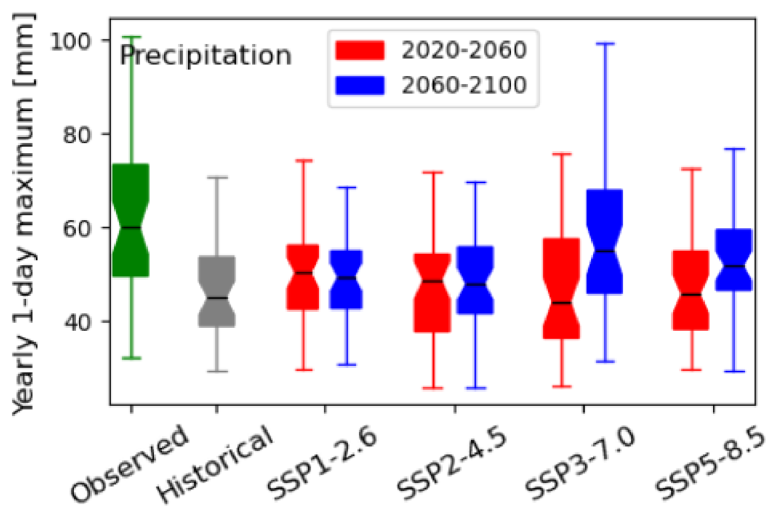

Figure 30. Boxplot of maximum 1-day precipitation accumulations from observed data for period 1980-2000 (green), historical CESM2 climate model forcing for period 1960-2000 (grey) and CESM2 future climate model forcing for the periods 2020-2060 (red) and 2060-2100 (blue) for four scenarios.

Fourmile Branch MIKE Model Results

Long-term Changes in Evapotranspiration

The CESM2 forcing data was used to simulate the hydrological response of Fourmile Branch using the calibrated MIKE model. In Figure 31 the long-term changes in simulated actual evapotranspiration is shown. For the four future socio-economic pathways, the MIKE model simulates an increase in actual evapotranspiration of about 50 mm, as compared to the historical period. The largest increase is expected to occur for SSP3-7.0 and SSP5-8.5, although difference between the four scenarios are small. Therefore, of the almost 100 mm increase in yearly precipitation that is anticipated to happen between the historical and future scenarios (see Figure 29), more than 50% is removed from Fourmile Branch as actual evapotranspiration. The remaining is anticipated to increase discharge and/or groundwater storage.

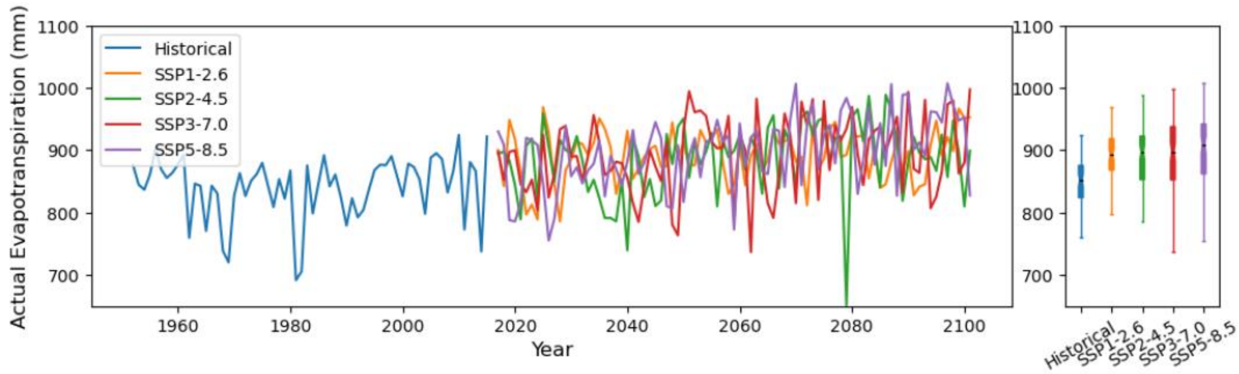

Figure 31. Long-term year changes in actual evaportranspiration rate as simulated by the MIKE model for both the historical period and four socio-economic pathways.

Long-term Changes in Discharge

Figure 32 shows the simulated yearly range in discharge for a location close to the Fourmile Branch outlet for the historical and future simulations. For all climate models, generally a slight increase in both the median as well as the 90th percentile in simulated discharge is shown, although considerable variations between the different years are observed. However, no major changes in low flow conditions can be observed from this figure (10th percentile). Also indicated in the bottom row of Figure 32 is the historically observed discharge. Generally, the observed and simulated historical ranges are very similar on average at the yearly timescale.

In Figure 33, the average seasonal discharge is presented for the different periods. For the historical period, the range in observational and simulated data corresponds very well for the winter (DJF) and spring (MAM) season. However, for the summer (JJA) and fall (SON) the simulated discharge values are slightly higher compared to the observed data. For the future simulations, for scenarios SSP1-2.6, SSP2-4.5 and SSP5-8, for all seasons, an increase in the future discharge compared to the historical period is simulated. However, for SSP3-7.0 different signals are observed between the seasons. For this scenario, the winter and spring discharge is anticipated to increase, while for the summer and fall period, no change or even a small reduction in discharge is anticipated.

To gain an improved understanding of how extreme flow events are represented by the model, in Figure 34 a boxplot of the maximum one-day discharge is presented. Similar to Figure 30, it can be seen from this figure that the simulated one-day maximum discharge for the historical period is considerably lower compared to observed values from a nearby USGS station. As such, maximum peak events are underestimated using the CMIP6 CESM2 climate model data to force the MIKE model. This is caused by an underestimation in the one-day maximum precipitation intensities. Comparing the historical with the future simulations shows that the maximum discharge rates increase in the future, with the largest increases occurring for SSP3-7.0. However, for climate scenario SSP1-2.6 that assumes the maximum reduction in greenhouse gas emissions and the lowest increase in temperature, a considerable increase in maximum one-day discharges is also observed.

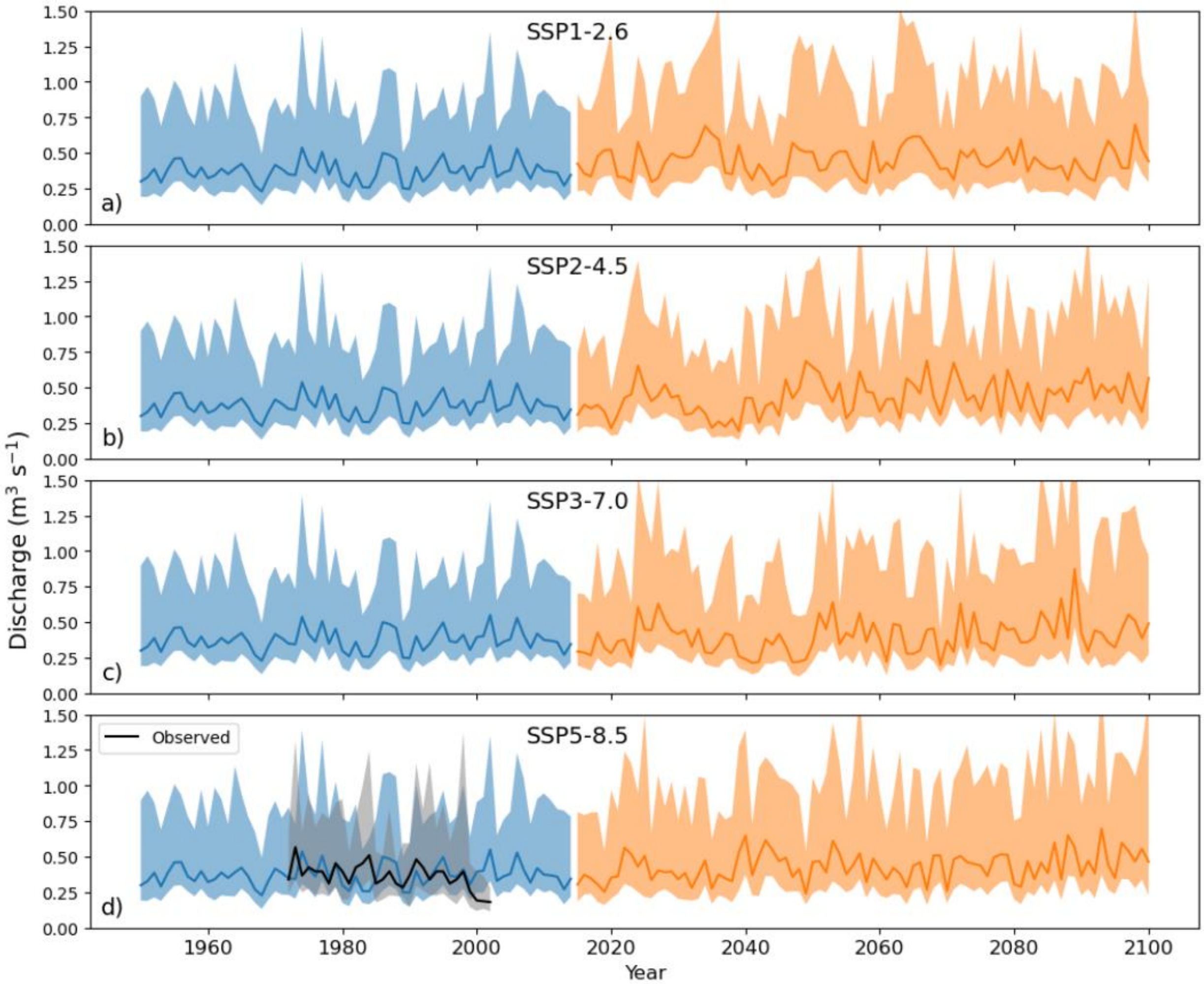

Figure 32. The median (line) and 10th-90th percentile in discharge for location close to outlet for given year as simulated by MIKE model. Historical simulations (blue): each row indicates a different socio-economic pathway. Also shown in the bottom panel are historical observational discharge data.

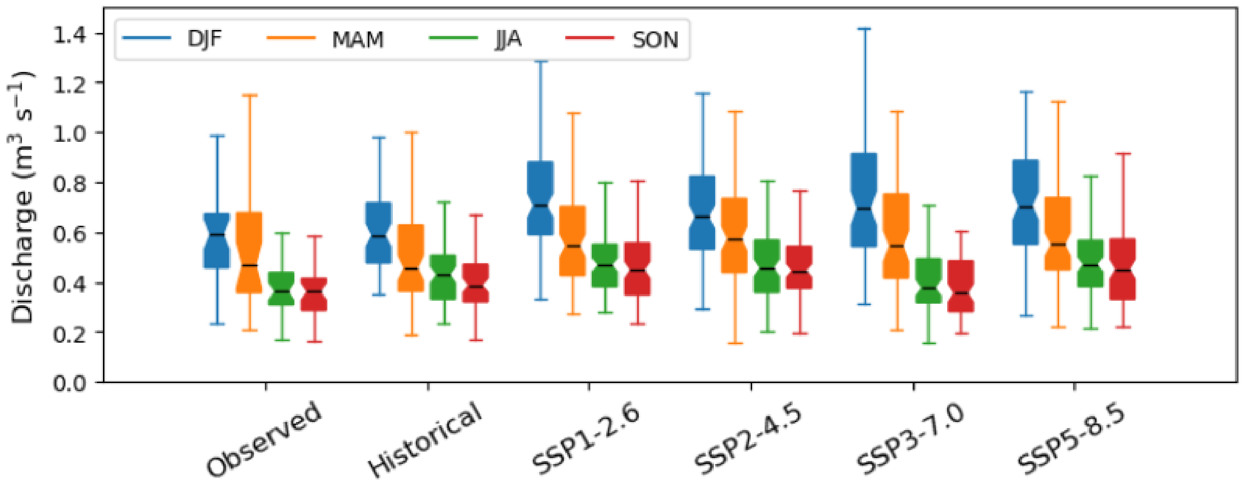

Figure 33. Boxplot of mean seasonal discharge for observational data as well as simulated MIKE model values using CMIP6 CESM2 climate model forcing.

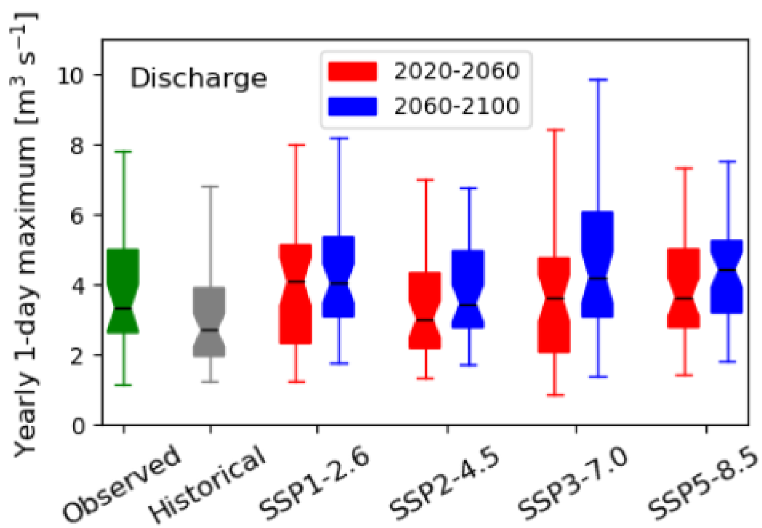

Figure 34. Boxplot of maximum 1-day precipitation accumulations from observed data for period 1980-2000 (green), historical CESM2 climate model forcing for period 1960-2000 (grey) and CESM2 future climate model forcing for the periods 2020-2060 (red) and 2060-2100 (blue) for four scenarios.

Long-Term Changes in Hydrological Extremes

Besides evaluation of the anticipated impact in atmospheric forcing and discharge, the CMIP6 CESM2 forcing and simulated MIKE discharge values were used to identify atmospheric and hydrological drought and wet spells. For both series using the data of the historical period, a given day of the 20th and 80th percentile was calculated. In case the value of a given day lies below the 20th percentile, the day is assumed to be in drought. When the value lies above the 80th percentile, a wet spell is assumed. Atmospheric drought and wet spell occurrence were calculated using the CMIP6 CESM2 forcing data taking the difference between precipitation and potential evaporation. For the hydrological drought and wet spell identification, the simulated discharge values near the outlet of Fourmile Branch were used. In order to mitigate the impact of day-to-day variations, a 30-day moving average was applied to the daily data.

Figure 35 shows the occurrence of drought and wet spell dynamics. For the historical climate, various wet and dry years can be observed. Furthermore, larger yearly fractions in atmospheric drought or wet spells show a strong correlation with hydrological drought and wet spells. However, for some years the maximum in the hydrological extreme is observed one or two years after the maximum in atmospheric extreme.

The percentile statistical threshold derived for the historical climate was also used to identify drought and wet spell occurrences for the future climate, to enable direct comparison between the historical and future period. For SSP1-2.6, for the future, no clear changes in atmospheric drought are observed; however, the fraction in hydrological drought decreases. This reduction is due to the anticipated wetter climate (see Figure 29), which results in a strong increase in the fraction period in which both an atmospheric and hydrological wet spell occur. This wetter climate is also observed for SSP2-4.5, SSP3-7.0 and SSP5-8.5. However, for SSP2-4.5, SSP3-7.0 and SSP5-8.5, for the period 2015-2050, an increase in drought fraction can be observed. However, for SSP2-4.5, the drought occurrence reduces considerably for the second part of the 21st century. This especially holds for hydrological drought. For SSP3-7.0, both an increase in wet spell and drought fraction is simulated, indicating that the simulated flow data are expected to be more skewed towards both lower and higher values. This wetter when wet and drier when dry behavior is anticipated to occur in many regions in the future.

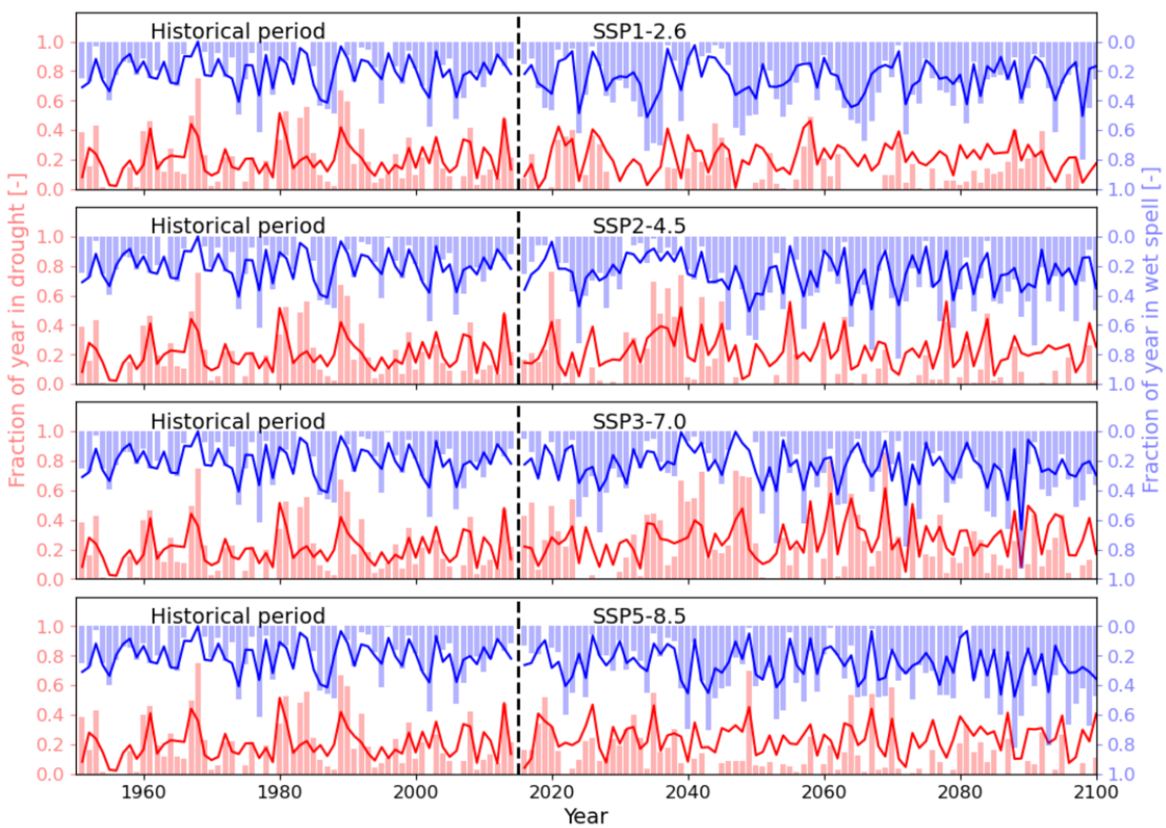

Figure 35. Year fraction of atmospheric (lines) and hydrological (vertical bar) drought (red) and wet spell (blue) variation for historical and future climate scenarios.

The duration of a given drought and wet spell period was also calculated. In Figure 36 the distribution of the hydrological drought and wet spell duration for the historical (1960-2000) and future climate (2020-2060 and 2060-2100) periods is shown. For SSP1-2.6, no major changes in the drought duration distribution are expected. However, a considerable increase in the longest duration wet spells is expected. The longer duration wet spells are also observed for SSP3.7-0 for both future periods and SSP5.8-5 for the period 2020-2060. The largest increase in the drought duration is observed for SSP3-7.0 for the period 2060-2100 and for SSP5-8.5 for the period 2020-2060. Although from Figure 35 no clear increases in the drought fraction were observed, these results indicate that for these models, the occurrence of hydrological drought for Fourmile Branch is expected to cluster more together, resulting in increases in total duration.

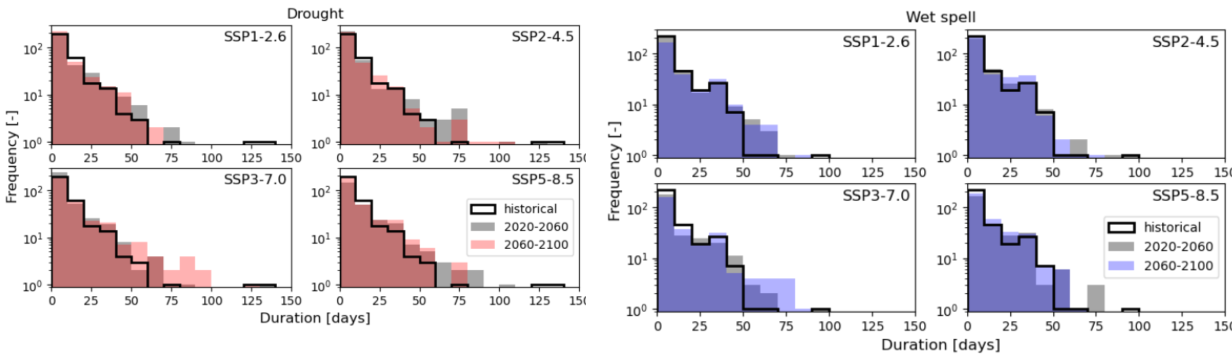

Figure 36. Distributions of total duration of hydrological drought (left) and wet spell (right) for the historical (1960-2000) and future climate (2020-2060 and 2060-2100) periods.

F-Area ATS Model Results

The figures presented below show the results for the first 1,300 days of the simulation, covering the time period from January 1, 1982, through May 26, 1985. Although the simulation was designed to run for a 33-year historical period, the results presented here only represent a portion of that timeframe as the simulation is still in progress on the NERSC (National Energy Research Scientific Computing Center) HPC. Delays were encountered due to limited high-performance computing resources, the computational intensity of the model, queue wait times in the SLURM scheduler, the fact that NERSC resources are shared among other projects, and the limitation of only being able to run one simulation at a time, making progress incremental. As such, for this report, analyses are based solely on the currently available simulation results.

In addition to simulating the hydrological response of the F-Area domain using historical climate data, simulations of future climate scenarios will also be performed. The input meteorological files for the future climate data previously described in this report have already been successfully tested using ATS, so once the historical simulations for the F-Area model are completed, the climate forecasting simulations will be initiated. The final results from the fully completed simulations of both the historical and future climate scenarios will be discussed in the year-end report, providing a comprehensive understanding of both past and future hydrological behavior in the environment surrounding the SRS F-Area.

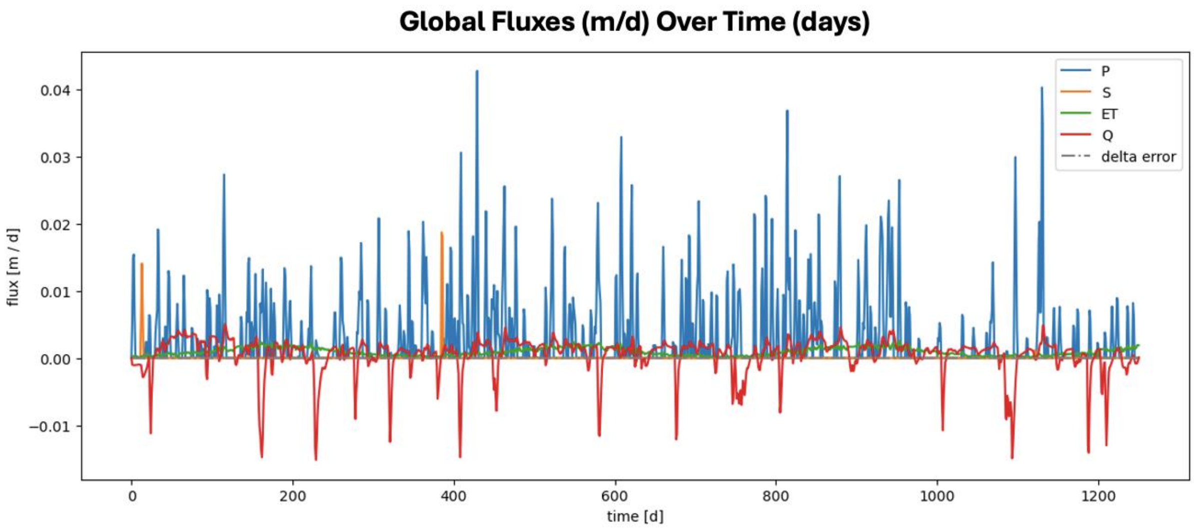

Figure 37. Global fluxes (in m/d) of precipitation (P), snow (S), evapotranspiration (ET), and runoff (Q) over a 1,300-day period.

Figure 37 displays the variation of hydrological fluxes, including precipitation (P), snow (S), evapotranspiration (ET), and runoff (Q), over time, measured in meters per day (m/d) across a period of approximately 1,300 days. Runoff is defined as the flux at the outlet minus the two inflows from upstream, meaning that positive runoff occurs when more water is leaving the system through the outlet, while negative runoff indicates that more inflow is entering from upstream sources than is leaving. Precipitation, represented by the blue line, shows significant variability with prominent peaks, indicating frequent intense precipitation events. These precipitation peaks often correspond with an increase in runoff, represented by the red line, where negative values suggest that more inflow is entering the system upstream than is leaving through the outlet. This negative runoff suggests that water is likely infiltrating into the subsurface or being lost through processes such as evapotranspiration. The consistent presence of negative runoff values throughout time implies that infiltration into the subsurface might be a significant process in this system, potentially aided by porous soils. These periods of negative runoff could also reflect scenarios where water is temporarily stored or diverted, only to later re-enter the system after subsurface movement.

Snow (S), represented by the orange line, exhibits occasional spikes, showing periods where snow accumulation occurs. However, compared to precipitation and runoff, snow has less frequent and smaller variations, implying that snowmelt may not be a significant contributor to the overall water flux in the system during most of the observed period.

Actual Evapotranspiration (ET), depicted by the green line, remains relatively stable over time, with minor fluctuations. In this simulation analysis, actual evapotranspiration (ET) is used rather than potential ET, which is reflected in the results shown in Figure 37. The actual ET is noticeably low, averaging around 1 mm per day, which constitutes only about 30% of the total precipitation during the historical period. This value is lower than what would be expected based on MIKE simulations and historical data, where the simulated 900 mm in total actual ET corresponds to about 2.5 mm per day. The reasons for this discrepancy are being investigated and simulations are in the process of being re-run with varying parameters for evaporation and transpiration to better understand the factors affecting actual ET in this system. These adjustments may help to align the simulated ET with the expected historical patterns and provide more accurate insights into the system's water balance.

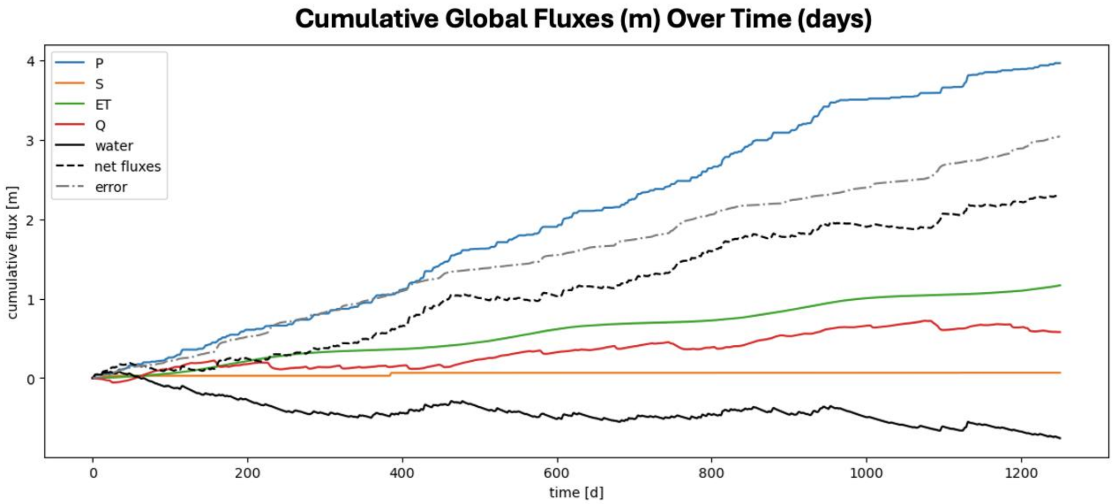

Figure 38. Cumulative global fluxes (in meters) of precipitation (P), snow (S), evapotranspiration (ET), and runoff (Q) over a 1,300-day period.

Figure 38 shows the cumulative global fluxes over time, expressed in meters, for precipitation (P), snow (S), evapotranspiration (ET), and runoff (Q) over the same 1,300-day period. The blue line representing cumulative precipitation steadily increases, showing a total accumulation of over 4 meters, which aligns with the consistent precipitation events seen in the earlier flux analysis. The cumulative evapotranspiration (ET), shown in green, demonstrates a slow, steady increase, with a final value just below 1 meter, reflecting the low actual ET discussed earlier. Cumulative runoff (Q), represented by the red line, remains relatively stable with minor fluctuations, indicating that while runoff occurs frequently, it does not accumulate at a significant rate. Snow (S), in orange, stays flat throughout the period, reinforcing that snowmelt is not a major contributor to water fluxes in this system.

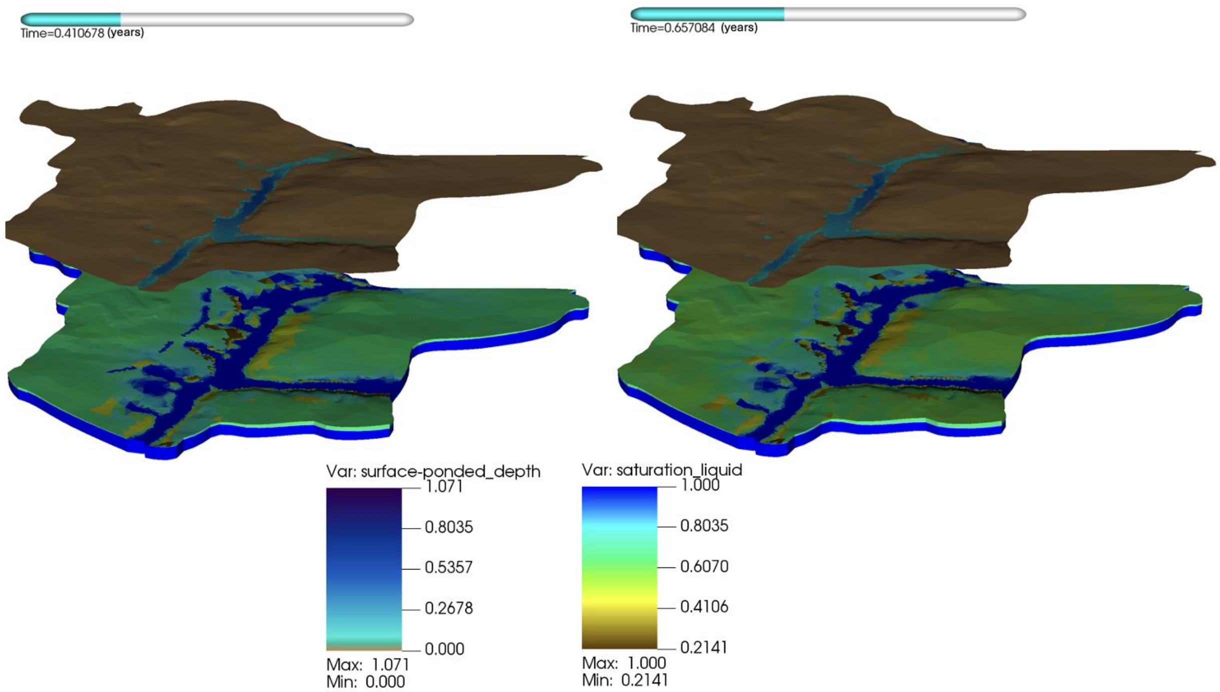

Figure 39. Image from a video simulation of the F-Area model at 0.41 years (left) and 0.66 years (right) in which the surface ponded water depths and subsurface saturation are shown with color tables.

Figure 39 shows the surface ponded depth and subsurface liquid saturation at two different times in the simulation, at 0.41 years (150 days) and at 0.66 years (240 days). The surface layer was given a customized color scheme that shows the ponded depth of water along the surface after precipitation. The brown represents no ponded water at the surface, while the darker blue colors indicate ponding. The surface layer elevation was also transformed upward in the z-direction to better show the subsurface infiltration and the presence of the river network in the domain. The subsurface saturation was also given a customized color scheme, with brown representing low subsurface water saturation and dark blue representing high subsurface water saturation. At 150 days, the ponded surface water and subsurface saturation is much higher than at 240 days. The river basin contains ponded water in the stream and the subsurface is saturated in certain areas where more permeability soil types are present. In both scenarios, throughout the ATS model results, there is water consistently flowing through the wetland. Furthermore, during wet periods, as shown on the left of Figure 39, the extent of the saturated domain surrounding the river network extends a bit more upslope especially in the direction of the barrier wall. On the surface, the ponded water slightly increases, and the river extent expands. These results highlight the importance of accounting for small-scale variations in the groundwater-surface water dynamics and can help us gain an improved understanding of the release, fate and transport of contaminants within these braided wetland systems.

Subtask 3.2: Conclusions

The MIKE model of Fourmile Branch revealed several key findings regarding future discharge from simulated extreme flow events under different climate scenarios. For the future, the CESM2 climate model predicts an increase in both precipitation, temperature and potential evaporation. This increase in precipitation is expected to predominantly lead to increases in actual evaporation, and to a lesser extent to increases in discharge and groundwater storage. Historical simulations closely matched observed discharge patterns, particularly for winter and spring, while summer and fall simulations showed slightly higher discharge than observed. Future projections suggest an overall increase in discharge across most seasons, especially under scenarios SSP1-2.6, SSP2-4.5, and SSP5-8.5, with notable variability in SSP3-7.0. The MIKE model underestimates historical maximum peak events, likely due to an underestimation in precipitation intensities, but future simulations show increases in maximum discharge, particularly under SSP3-7.0. Additionally, while no major changes in drought duration are anticipated under SSP1-2.6, scenarios such as SSP3-7.0 and SSP5-8.5 predict longer and more frequent extreme wet and dry spells, highlighting potential challenges in managing hydrological extremes in the future.

The ATS simulations of F-Area are still on-going due to limited computational resources, but preliminary results show precipitation events exhibit significant variability and correspond with fluctuations in runoff, indicating a strong relationship between these fluxes. Notably, periods of negative runoff suggest substantial infiltration into the subsurface, likely due to porous soils, with evapotranspiration remaining relatively stable but lower than expected. Snowmelt contributes minimally to the water fluxes. The cumulative analysis shows consistent precipitation and modest evapotranspiration over the period, with runoff showing little overall accumulation. Ongoing simulations and parameter adjustments will refine the understanding of these processes, and future climate scenario simulations will begin once historical runs are completed. The completed results, from both the historical and future climate simulations, will be discussed in the year-end report.

Based on the reported results, seasonal changes in the interaction between the groundwater and braided river network strongly impact the release of these contaminants into the river network. Furthermore, sudden and long-term changes in forcing will impact the hydrological exchange between the hillslope, seepage face and braided riparian wetland system, which is projected to impact the release of contaminants both within the F-Area and the Fourmile Branch watershed scale within SRS.

Subtask 3.2: References

Fall, G., D. Kitzmiller, S. Pavlovic, Z. Zhang, N. Patrick, M. St. Laurent, C. Trypaluk, W. Wu and D. Miller. 2023: The Office of Water Prediction's Analysis of Record For Calibration, Version 1.1: Dataset Description and Precipitation Evaluation.” JAWRA Journal of the American Water Resources Association 59 (6): 1246–1272. Doi: 10.1111/1752-1688.13143.

Singer, M.B., Asfaw, D.T., Rosolem, R. et al., 2021: Hourly potential evapotranspiration at 0.1° resolution for the global land surface from 1981-present. Sci Data 8, 224. Doi: 10.1038/s41597-021-01003-9

Amanzi. (2023). GitHub. Retrieved from https://amanzi.github.io/ats/index.html

Coon, E. T., Moulton, J. D., & Painter, S. L. (2016). Managing complexity in simulations of land surface and near-surface processes. Environmental modelling & software, 78, 134-149.

Coon, Ethan T., and Pin Shuai. “Watershed Workflow: A toolset for parameterizing data-intensive, integrated hydrologic models.” Environmental Modelling & Software, 157 (2022): 105502.: https://doi.org/10.1016/j.envsoft.2022.105502

Livingston, D. (2020). TINerator API Reference. Los Alamos National Laboratory.

"Shared Socioeconomic Pathways." Wikipedia, 11 June 2024. Wikipedia, https://en.wikipedia.org/w/index.php?title=Shared_Socioeconomic_Pathways&oldid=1228493012.

"Interstate Technology & Regulatory Council (ITRC). 2017. Remediation Management of Complex Sites. RMCS-1. Washington, D.C.: Interstate Technology & Regulatory Council, Remediation Management of Complex Sites Team. http://rmcs-1.itrcweb.org.

Denham, M., and K.M. Vangelas. 2008. "Biogeochemical Gradients as a Framework for Understanding Waste-Site Evolution." Remediation Journal 19 (1):5-17.

TASK 6: HYDROLOGY MODELING OF BASIN 6 OF THE NASH DRAW NEAR THE WIPP

The Waste Isolation Pilot Plant (WIPP) located in southeastern New Mexico in the city of Carlsbad, is the only deep geologic long-lived radioactive waste repository in the United States. It is situated approximately 2,150 feet below the surface in a thick salt bed, and its effectiveness and success are imperative due to its intended purpose to permanently store and isolate transuranic (TRU) waste generated from the former US nuclear defense program.

The long-term performance and vulnerability of the karst topography surrounding the WIPP is a significant concern of scientists at the U.S. Department of Energy's Environmental Management (DOE-EM) Office, particularly as there is limited knowledge and understanding of how characteristic surface features such as sinkholes, swallets, and karst valleys influence the groundwater recharge. It is hypothesized that these surface depressions create zones where there is potential for increased infiltration and groundwater recharge, and the resultant subsurface flow can subsequently facilitate the transport of radionuclides into the surrounding environment and accelerate dissolution of the geological salt layers in which the TRU waste is being stored. As such, a high-resolution integrated hydrology model that simulates the relationship between groundwater recharge and weather patterns [7] is needed to provide insight into how these features can potentially affect regional groundwater dynamics. This task is therefore focused on the development of an integrated surface water/groundwater hydrological model of Basin 6 (outlined in blue in Figure 40 below) of the Nash Draw which lies just west of the WIPP.

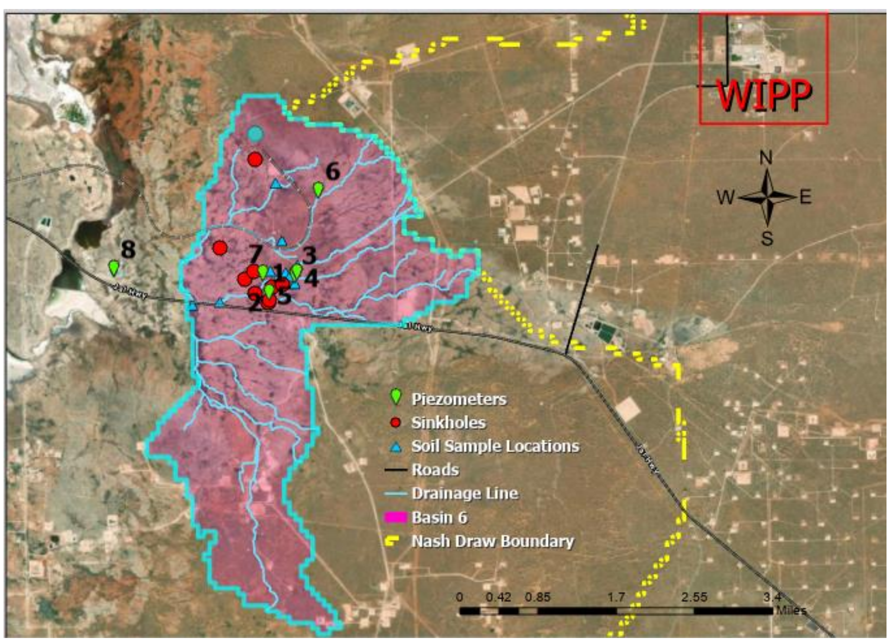

Figure 40. Nash Draw and Basin 6 Study Area West of the WIPP.

The open-source DOE-developed Advanced Terrestrial Simulator (ATS) was used to improve the current understanding of groundwater flow in the vicinity of the WIPP site and the regional water balance, particularly the relationship between the Culebra recharge and the intense, episodic precipitation events typical of the North American monsoon during the summertime. This is essential for understanding the rate of propagation of the shallow dissolution front, and the impact of land-use changes around the WIPP facility on water levels in compliance monitoring wells.

As recharge is anticipated to predominantly occur through localized features, such as along the riparian zone/river network, gullies and through sinkholes and swallets, this task proposes the development of an ATS model for Basin 6. Basin 6 (Figure 40) is situated just west of the WIPP facility and serves as a prototype catchment for hydrological model development to gain an improved understanding of groundwater recharge variability throughout the domain of interest. As the surface features of interest vary over very small spatial scales (within meters), a 1-meter digital elevation model (DEM) was developed for Basin 6 using photogrammetry methods (Subtask 6.1 in FIU Year 1-2). This high-resolution model domain will enable computation of the water balance across multiple scales, simulation of the groundwater recharge and estimation of the propagation rate of the shallow dissolution front.

Long-term changes in climate that are anticipated to occur within the south/southwestern USA are expected to result in more frequent intense precipitation events. It is currently unknown if this will lead to increased groundwater recharge or whether this results in increased surface flow and evapotranspiration. It is unclear whether groundwater recharge would be impacted and how, if impacted, this might affect the dissolution rate of halite within the subsurface. Therefore, once fully developed, the ATS model will be used to evaluate the impact of seasonal and decadal variations in weather (including climate change) on the regional hydrology and groundwater recharge, so DOE-EM scientists can better estimate the rate of halite dissolution and propagation of the shallow dissolution front to predict the potential impact on the WIPP repository performance. For FIU Year 4, there will be two subtasks executed under Task 6, Subtask 6.2, which deals with the ATS model development, and Subtask 6.3, which focuses on obtaining in-situ observations within this data-scarce region.

Subtask 6.2: Model Development

Subtask 6.2: Introduction

This subtask involves the development of a hydrological model for Basin 6 of the Nash Draw just west of the Waste Isolation Pilot Plant (WIPP) site, that includes land surface hydrological processes, subsurface-based recharge, and groundwater flow. Basin 6 serves as a prototype basin representative for the larger area of interest surrounding the WIPP domain. During previous years, after evaluating various open-source surface hydrological models (among others: Community Land Model (CLM) and WRF-Hydro), it was decided to make use of the Advanced Terrestrial Simulator (ATS) to simulate the near-surface hydrological response (i.e., infiltration and evapotranspiration) and how this impacts groundwater recharge. ATS is an ecosystem-based, integrated, distributed hydrology simulator that is built on the underlying multi-physics framework provided by Amanzi, to provide flexible and extensible flow and reactive transport simulation capability. The output of the ATS model includes predictions of infiltration rates over selected regions of interest, such as sinkholes, and groundwater recharge, and hence ensembles of ATS simulations facilitate sensitivity and uncertainty analysis of groundwater and surface water flows. ATS also possesses basic models of evapotranspiration (ET) and is gaining more connections to true land surface models for plants.

An integrated surface/subsurface model of Basin 6 was developed by FIU in Year 3 using the Advanced Terrestrial Simulator (ATS) based on the previously generated high-resolution (1-m)

DEM. The Python package, Watershed Workflow, was implemented to generate the ATS model mesh from publicly available datasets. Successful installation of Watershed Workflow and development of Python scripts to generate the various input files for ATS was achieved. Consistent interaction with DOE-EM scientists assisted with determination of the right setup, including the generation of meshes from the DEM data, setting up of meteorological forcing data and development of input files for the ATS. Input files include a high-resolution mesh for Basin 6 (containing information on spatial variations in NLCD land cover types, SURRGO soil texture and subsurface information), daily atmospheric forcing (precipitation, temperature radiation, etc.) using the DayMet data, as well as a model input XML file containing all the file information, domain and parameter values and simulation requirements. Preliminary simulations were also performed on local and remote systems, including FIU's high performance computer (HPC).

Subtask 6.2: Objectives

The overall objective of this task is to develop an integrated hydrology model for Basin 6 of the Nash Draw near the WIPP site using a high-resolution DEM and the Advanced Terrestrial Simulator (ATS) to evaluate the impact of climate change and surface features (e.g., sinkholes and swallets), soil properties, and vegetation on groundwater recharge. The model will be used to compute the regional water balance and derive more accurate estimates of GW recharge to better predict the propagation rate of the shallow dissolution front and the potential long-term impact on the WIPP repository's performance.

In FIU Year 3, an ATS model for Basin 6 was developed that made use of open-source soil datasets (SSURGO) but did not explicitly represent locations with known sinkholes and changes in surface infiltration conditions along the riparian zone/river network. FIU therefore obtained soil samples throughout Basin 6 and will continue taking additional samples in FIU Year 4 (see Subtask 6.3). The objective for FIU Year 4 is to incorporate local in-situ information on sinkhole locations, as well as integrate the measured soil parameter information into the existing ATS model for Basin 6. The model will then be used to perform longer-term simulations for both current and future climate. These model simulations can subsequently be evaluated to compute the water balance across multiple scales and reduce uncertainties in recharge estimates and the propagation rate of the shallow dissolution front. Furthermore, by explicitly representing sinkholes (through changes in conductivity and porosity) as well as recharge variability along the river network within the model, for the first time, it will be possible to evaluate the impact on local and regional scale recharge. Information on future climate scenarios will be obtained through collaboration with Lawrence Berkeley National Laboratory (LBNL).

Subtask 6.2: Methodology

FIU Year 4 was focused on:

1. Enhancing the ATS Basin 6 model to include known sinkhole locations (Milestone 2023-P2-M3).
2. Completion of long-term simulations of Basin 6 explicitly representing sinkholes and river network infiltration variations (Milestone 2023-P2-M8).
3. Development of a draft manuscript on multi-year simulations of Basin 6 using ATS focusing on the role of sinkholes and the river network on local and regional scale groundwater recharge (Deliverable 2023-P2-D6).

Basin 6 was selected as the study site within Nash Draw. Covering an area of 23 km², it is one of the largest sub-basins in the region. Basin 6 drains toward a central karst valley, which represents the lowest elevation point in the basin. This valley features numerous sinkholes and caves and has a history of flooding during extreme precipitation events. During FIU Year 4, FIU expanded on the ATS model previously developed by incorporating 10 sinkholes in the model, which were derived from Goodbar et al. (2020). Figure 41 shows the 10 sinkholes added, labeled 0-9. In Year 4, FIU also improved evapotranspiration representation in the model based on the Priestley-Taylor formation, which approximates the difference in vapor pressure between the atmosphere and the soil based on available energy. FIU also expanded the mesh into the subsurface, with the volumetric mesh having a depth of 60-meters (196 ft), which is estimated to be at the start of the Dewey Lake formation within the Nash Draw. FIU developed two new transient simulations—one incorporating sinkholes and one excluding them. In this context, "transient" refers to simulations that account for changes over time, reflecting evolving conditions rather than a steady state. All other components of the model remained unchanged, enabling a direct comparison to evaluate the impact of sinkholes on the hydrological response.

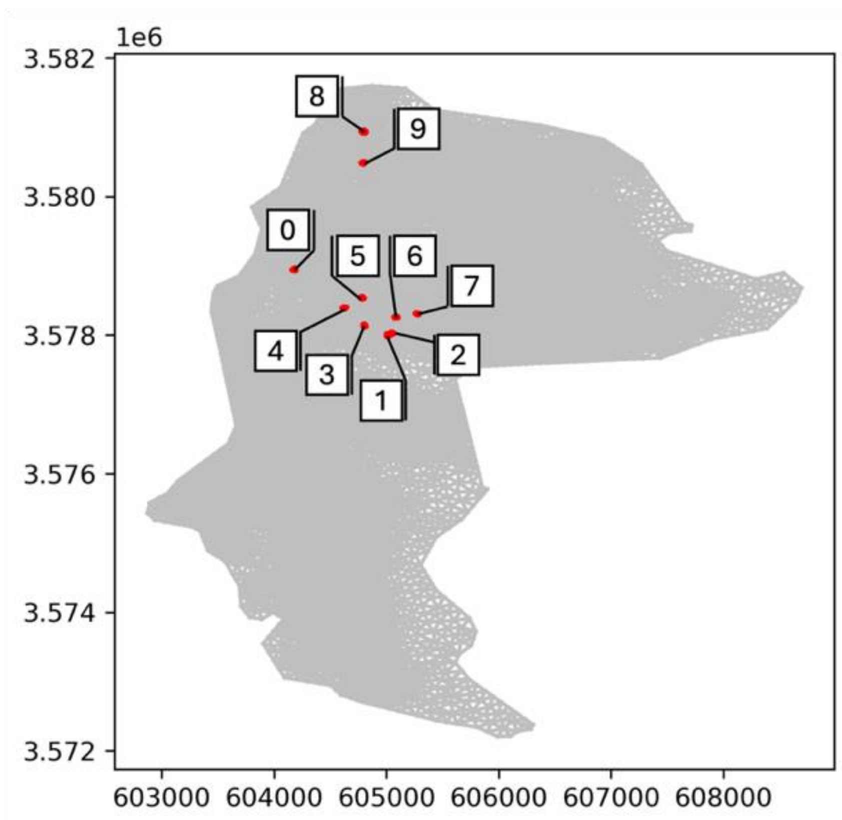

Figure 41. Locations of the 10 sinkholes (#0-9) within Basin 6.

Hydrological, climate and topography datasets were collected from various national database platforms and incorporated in the model mesh using the Python library Watershed Workflow. Watershed Workflow was developed by Oak Ridge National Lab (ORNL) and allows for geometrical and geophysical information about the site to be encoded into the ATS input file. Within the model, spatial variations in NLCD land cover types, SURRGO soil texture, and GLHYMPS subsurface information), were included. Watershed Workflow identified 13 surface soils, four subsurface geologic layers, and eight land cover types within Basin 6. The surface soils were classified using USDA's SSURGO data, labeled by NRCS ID. Figure 42 maps NRCS (SSURGO) surface soils and GLHYMPS subsurface layers in Basin 6. The model used porosity, permeability, and Water Retention Model (WRM) parameters to represent surface soils, with variables like Van Genuchten alpha, Van Genuchten n, residual saturation, and smoothing interval width. Land cover data from the National Land Cover Database (NLCD) was added to the model to account for vegetation and calculate evapotranspiration. Watershed Workflow found eight land cover types, primarily shrub/scrub, within Basin 6. To simplify the model, shrub/scrub was applied across the basin.

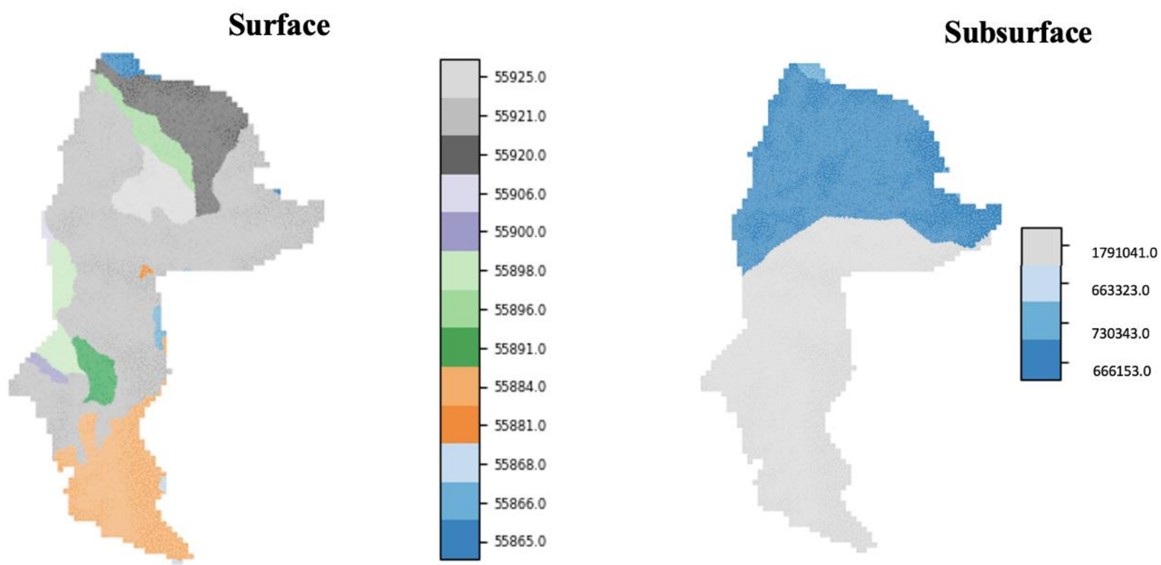

Figure 42. Map of Basin 6 with the NRCS surface soils on the left and GLHYMPS subsurface geologic layers on the right.

The transient model for long-term simulations used meteorological data from January 1, 2012, to December 31, 2018. This period was selected to capture a wide range of precipitation intensities, including both heavy rainfall and drought conditions. Southeastern New Mexico experienced severe drought from June 2011 to July 2013, while Carlsbad, NM, saw multiple extreme precipitation events, particularly during the wet seasons of 2013 and 2014. Key meteorological variables, including air temperature, incoming shortwave radiation, rain and snow precipitation, and air vapor pressure, were sourced from the DayMet archive, which provides historical data with a spatial resolution of approximately 1 kilometer. Also obtained was the Leaf-Area-Index (LAI) for the major land cover types within the region. The LAI is time series-based and directly impacts the evapotranspiration of the model and therefore the entire water balance. The addition of the LAI allows for more accurate evapotranspiration predictions and hydrology modeling (Coon & Shuai, 2022).

In FIU Year 4, the existing spinup model was improved and used for the development of the two transient simulations (with and without sinkholes) for Basin 6. A spinup model is used to establish an equilibrium state so that key hydrological variables, such as soil moisture, groundwater levels, and streamflow, reach a consistent and self-sustaining state. Figure 43 shows the workflow used for model development in FIU Year 4.

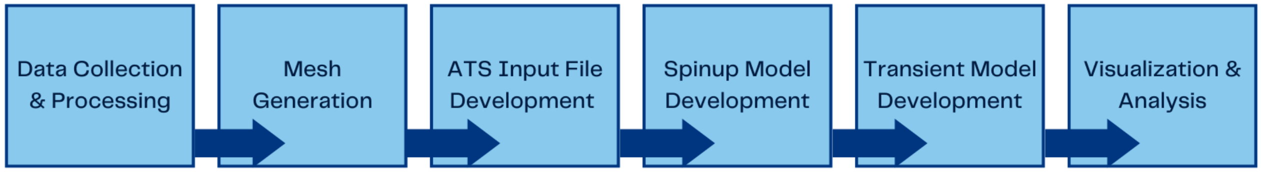

Figure 43. ATS model development workflow.

Subtask 6.2: Results and Discussion

The transient simulation with sinkholes provided insight into the water balance within Basin 6. The total precipitation during the simulation was 108.05 inches. Of this, 32.74 inches contributed to runoff, accounting for 30.30% of the total precipitation, while 73.15 inches was lost to evapotranspiration, representing 67.70% of the total. The combined runoff and evapotranspiration totaled 98.00% of the input precipitation, leaving a 2% discrepancy. This "missing" 2% is likely due to infiltration into the subsurface, which was stored due to the no-flow boundary condition, preventing further drainage. The runoff-to-precipitation ratio was 0.30, and runoff remained lower than total evapotranspiration, characteristic of a semi-arid desert environment.

In the sinkhole simulation, the mean runoff (0.013 in/day) exceeds the median (0.008 in/day), indicating the presence of outliers, likely from extreme precipitation events. The standard deviation of 0.011 in/day suggests moderate variability in runoff. For evapotranspiration, the mean (0.029 in/day) is higher than the median (0.0078 in/day), reflecting seasonal variation—only evaporation was considered in the dry season due to inactive transpiration. Infiltration also shows a higher mean (0.028 in/day) than median (-0.062 in/day), with negative values representing exfiltration, where water exits the subsurface when it reaches capacity.

The sinkhole simulation resulted in slightly lower total runoff (32.74 inches) compared to the non-sinkhole simulation (33.03 inches), indicating that sinkholes enhance infiltration and reduce surface runoff. Infiltration was higher with sinkholes (mean of 0.028 in/day and total of 70.80 inches) compared to the non-sinkhole scenario (mean of 0.027 in/day and total of 70.52 inches), suggesting improved groundwater recharge. Maximum infiltration rates were similar between simulations, implying that sinkholes primarily influence average infiltration rather than extreme events.

To evaluate how sinkholes influence the hydrologic behavior of the system, the differences in simulation outputs were analyzed by subtracting the results of the sinkhole simulation from those without sinkholes. This analysis covered runoff, evapotranspiration, and infiltration from January 1, 2012, to December 31, 2018. Statistical significance was determined using a t-test, which compared the mean differences and calculated a p-value to test the null hypothesis that the datasets differ significantly. Figure 44 shows the runoff without sinkholes minus the runoff with sinkholes in inches per day. On the negative x-axis, the precipitation (in/d) is presented as well. The t-test for runoff yielded a t-statistic of 34.5, with a p-value of 7.76E-214, confirming a statistically significant difference between the two simulations. The positive t-statistic indicates that runoff is generally higher without sinkholes, supporting the hypothesis that sinkholes enhance infiltration, reducing surface runoff.

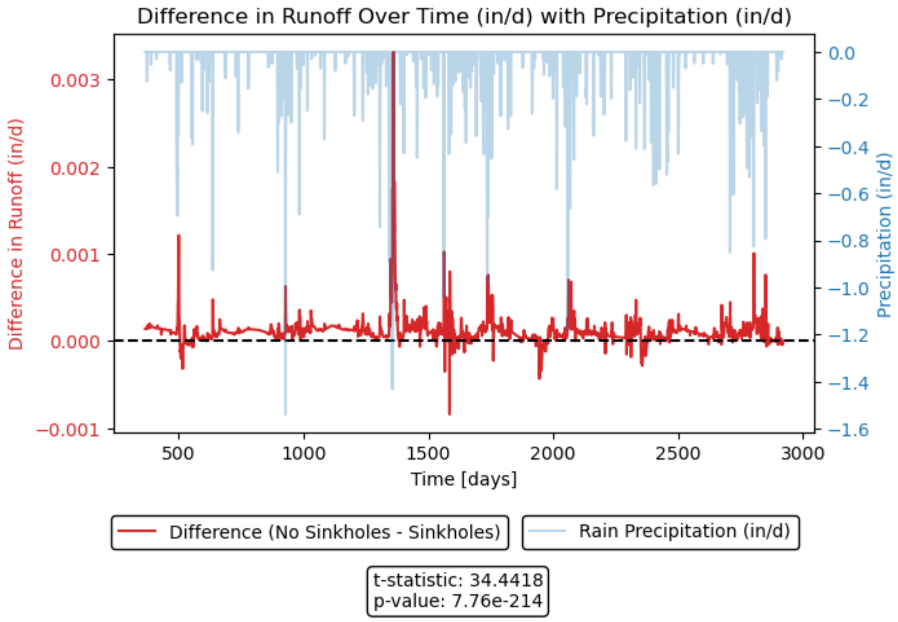

Figure 44. Temporal Analysis of Runoff Differences (in/d) Between No Sinkhole and Sinkhole Simulations with Corresponding Precipitation (in/d) Over Time (Days).

Figure 45 shows the infiltration without sinkholes minus the runoff with sinkholes in inches per day. On the negative x-axis, the precipitation (in/d) is presented as well. For infiltration, the t-statistic was -15.5, with a p-value of 1.06E-51, again indicating a significant difference. The negative t-statistic shows that infiltration is greater with sinkholes, aligning with the hypothesis that sinkholes increase groundwater recharge by acting as infiltration pathways, particularly in low-lying areas where rivers converge. This enhanced infiltration reduces the amount of surface water available for runoff, explaining the observed reduction in runoff when sinkholes are present.

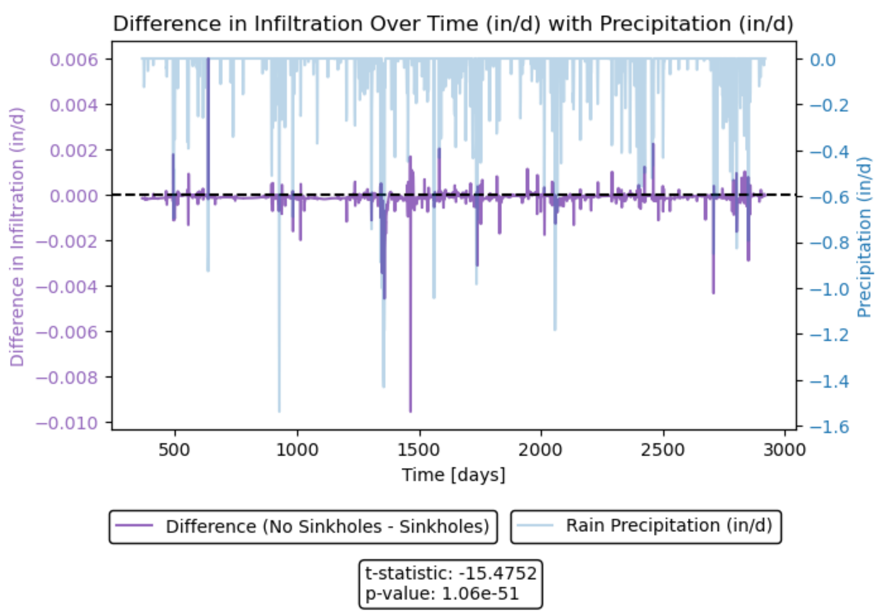

Figure 45. Temporal Analysis of Infiltration Differences (in/d) Between No Sinkhole and Sinkhole Simulations with Corresponding Precipitation (in/d) Over Time (Days).

The groundwater level and water content for Sinkholes 3 and 5 were analyzed for the period from January 1, 2012, to December 31, 2018. These two sinkholes are situated within different subsurface GLHYMPS layers: Sinkhole 5 is in a more porous but less permeable layer, while Sinkhole 3 is in a less porous but more permeable layer. Figure 46 shows the temporal variation of groundwater (white line) and soil water content (color map) across different depths at sinkhole 3 and 5. Both sinkholes showed significant increases in groundwater level and soil water content following the multi-day precipitation event on September 18, 2014 (day 1,356), the largest in the dataset. The response in Sinkhole 3, receiving a significant amount of upstream inflow, featured a large initial spike in groundwater followed by a gradual decline, as it received continuous inflow from upstream. In contrast, Sinkhole 5, showed a slower, rounded response with the groundwater level stabilizing for a few days before descending. The differing subsurface properties influenced the behavior of each sinkhole. Sinkhole 3's higher permeability allowed for quicker conveyance of water, while Sinkhole 5's higher porosity led to greater water retention, resulting in a more gradual decline in groundwater levels after the event. This demonstrates that sinkhole characteristics, along with their subsurface layers, play a significant role in how they respond to precipitation and affect groundwater dynamics in the basin.

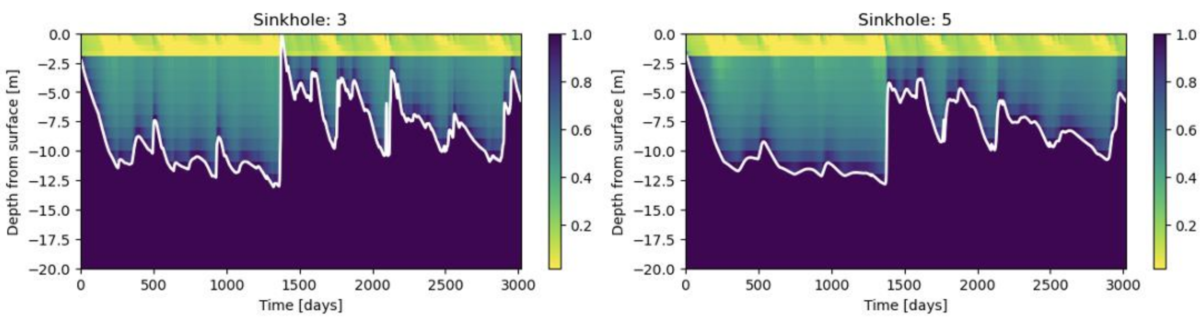

Figure 46. Temporal variation of groundwater table (white line) and soil water content (color map) across different depths (meters) for sinkholes 3 and 5 *Over Time* (Days).

Subtask 6.2: Conclusions

The primary goal in FIU Year 4 was to create an ATS model of Basin 6 to study the impact of sinkholes on surface and shallow subsurface processes. This involved developing a mesh of Basin 6 using Watershed Workflow, followed by two transient ATS models—one with sinkholes and one without. Key parameters analyzed included runoff, infiltration, evapotranspiration, water content, and groundwater levels. The results showed that sinkholes significantly reduce runoff, enhance infiltration, and increase evapotranspiration. The response of individual sinkholes varies by location within the river network, elevation, and surrounding subsurface soils. Extreme, multi-day rainfall events caused the most notable changes in groundwater globally in the basin and at sinkholes.

Future work will focus on calibrating and validating the Basin 6 model using field data from soil sampling and pressure transducers installed as part of Task 6.3. This effort aims to improve model accuracy and extend it to represent the entire Nash Draw, incorporating deeper subsurface features such as brine lakes and additional sinkholes. The expanded model will assess the long-term effects of climate variability on regional hydrology and its potential influence on WIPP. This approach will provide valuable insights into halite dissolution rates and their implications for WIPP performance and safety.

A professional abstract titled *"Simulating Hydrology and Climate Impacts on Groundwater Recharge in Basin 6 near the WIPP with the Advanced Terrestrial Simulator (ATS)",* based on the research being conducted under this task, was submitted to WM2025 and accepted for an oral presentation.

Subtask 6.2: References

Advanced Terrestrial Simulator. (2019). SDOE Office of Science (SC), Biological and Environmental Research (BER) (SC-23). [Online]. Available: https://github.com/amanzi/ats.

Beauheim, R. L. (2009). Collection and integration of geoscience information to revise the WIPP hydrology conceptual model. In *Approaches and challenges for the use of geological information in the safety case for deep disposal of radioactive waste*.

Chaturvedi, L. (1993). WIPP-related geological issues. In Carlsbad Region, New Mexico and West Texas, New Mexico Geological Society Forty-fourth Annual Field Conference, Carlsbad, NM (pp. 331-338).

Coon, E. T., Moulton, J. D., & Painter, S. L. (2016). Managing complexity in simulations of land surface and near-surface processes. Environmental modelling & software, 78, 134-149.

Coon, Ethan T., and Pin Shuai. "Watershed Workflow: A toolset for parameterizing data-intensive, integrated hydrologic models." Environmental Modelling & Software 157 (2022): 105502.: https://doi.org/10.1016/j.envsoft.2022.105502

Corbet, T. F., & Knupp, P. M. (1996). *The role of regional groundwater flow in the hydrogeology of the Culebra Member of the Rustler Formation at the Waste Isolation Pilot Plant (WIPP), southeastern New Mexico* (No. SAND-96-2133). Sandia National Lab, Albuquerque, NM (United States).

Goodbar, A. K., Powers, D. W., Goodbar, J. R., & Holt, R. M. (2020). Karst and sinkholes at Nash Draw, southeastern New Mexico (USA).

Hart, D. B., McKenna, S. A., & Beauheim, R. L. (2009). *Calibration of the WIPP culebra transmissivity fields* (No. SAND2009-7334C). Sandia National Lab.(SNL-NM), Albuquerque, NM (United States); Sandia National Laboratories,, Carlsbad, NM.

Hayes, A. (2019). *Culebra Hydrologic Model in WIPP Performance Assessment* (No. SAND2019-4432PE). Sandia National Lab.(SNL-NM), Albuquerque, NM (United States).

J. Moulton *et al.*, "High-level design of Amanzi, the multi-process high performance computing simulator," *Office of Environmental Management, United States Department of Energy, Washington DC,* vol. 495, p. 585, 2012.

Zeitler, T. R. (2016). *WIPP Performance Assessment* (No. SAND2016-8142PE). Sandia National Lab.(SNL-NM), Albuquerque, NM (United States)

Subtask 6.3: Fieldwork and Data Collection to Support Hydrological Model Calibration and Validation (NEW)

Subtask 6.3: Introduction

This subtask involves the collection of in-situ field data in the Basin 6 study area just west of the Waste Isolation Pilot Plant (WIPP) in New Mexico and supports the Basin 6 Advanced Terrestrial Simulator (ATS) model development under Subtask 6.2. There is a need to obtain detailed soil data within Basin 6 of the Nash Draw as in situ observations of soil texture, organic content and physical properties are limited. Information derived from soil pits nearby or from large scale soil texture datasets is available, but it is currently unknown how representative these datasets are for Basin 6. Knowledge of surface flow locations and availability of surface flow measurements in Basin 6 are also scarce; however, this information is needed to better understand the regional hydrology.

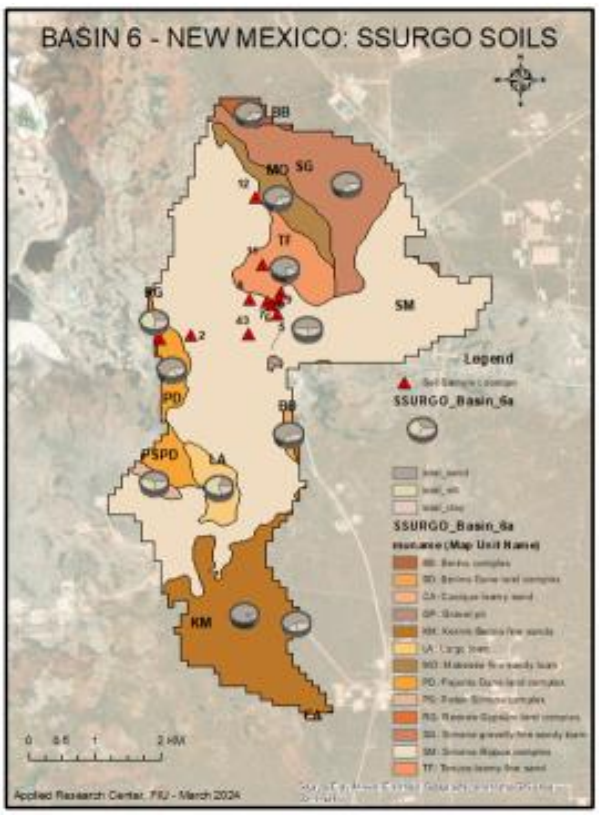

Figure 47. SSURGO soil map units with % sand, silt, and clay content in Basin 6 of the Nash Draw region. Soil sample locations are shown in red.

The work executed under this subtask will provide site specific information on soil physical properties for various locations and at various depths within the Basin 6 study domain. This data will be compared with large-scale publicly available soil texture datasets (i.e., STATSGO2, SSURGO and SoilGrids) typically used for the development of hydrological models. The location and magnitude of surface flow at various points along the Basin 6 river network will also be recorded in addition to water level measurements, which will be acquired via the deployment of piezometers in areas considered to be potential points of subsurface infiltration, such as sinkholes, swallets and gulleys. The data derived under this subtask can subsequently be used for calibration and validation of the ATS model being developed under Subtask 6.2.

Subtask 6.3: Objectives

The objective of this subtask is to obtain detailed soil texture information for various locations and at various depths within Basin 6 of the Nash Draw and determine specific locations and magnitude of surface flow via the strategic deployment of piezometers in areas considered to be potential points of significant subsurface infiltration. The data derived can subsequently be incorporated in the ATS model being developed under Subtask 6.2 for model calibration and validation and to estimate the various hydrological flow parameters within the unsaturated zone as used by ATS. This will help assess the performance of the ATS model developed. Furthermore, the texture observations will be used to evaluate the quality of large-scale publicly available soil texture datasets (i.e., STATSGO2, SSURGO, and SoilGrids).

Subtask 6.3: Methodology

To achieve the aforementioned objectives, the past year's activities involved (1) the analysis of soil samples collected in FIU Year 3 in Basin 6, NM west of the WIPP during the summer of 2023; (2) a revisit to the Basin 6 study domain in the summer of 2024 to extend fieldwork activities to include the collection of additional soil samples, download of the water level measurements recorded from the HOBO U20L water level data loggers (piezometers) that were deployed in 2023, and installation of 3 additional piezometers in sinkholes or noted areas of significant depression; and (3) analysis of the additional soil samples collected in 2024 as part of the FIU Year 4 scope of work.

In May 2023, for a small domain along the central valley of Basin 6, 48 soil samples were collected for determination of the soil physical properties. In Year 4, FIU executed test procedures for analysis of the soil samples according to the workplan *"In-Situ Data Collection in Basin 6, NM to Support Development of a Hydrological Model using the Advanced Terrestrial Simulator (ATS)"* developed in FIU Year 3. The workplan procedures were sourced from established protocols and standards, including the California Department of Pesticide Regulation Environmental Monitoring Branch for bulk density, ASTM for organic content and sieve analysis, and Woessner and Poeter's textbook for porosity testing. The results of the soil analysis were compiled in a report titled *"Soil Parameter Variability in Basin 6"* (Deliverable 2023-P2-D2).

Figure 48 shows a process flowchart for the laboratory analysis of the 48 soil samples collected in Year 3. The soil sample analysis focused on the determination of key physical properties, including bulk density, porosity, organic content, and soil texture, providing more site specific in situ soil characterization.

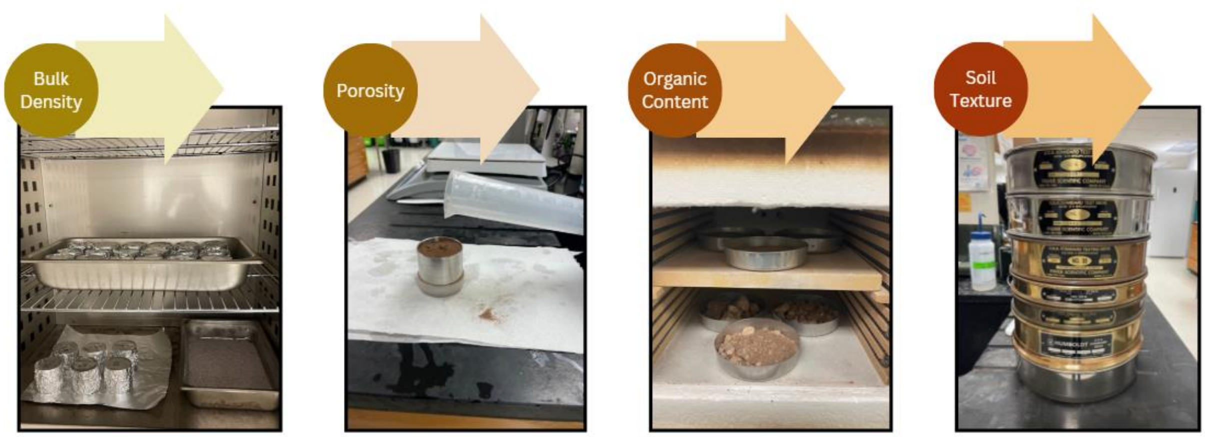

Figure 48. Flow chart of the soil analysis laboratory procedure.

For the Year 4 fieldwork, potential locations for the collection of soil samples and deployment of the additional piezometers were identified prior to visiting the Basin 6 study site using ArcGIS tools. The locations of the new and existing piezometers and soil sampling sites, as well as verified sinkholes, were then mapped, as seen in Figure 49. These locations, though predetermined, were subject to change based on in situ field conditions.

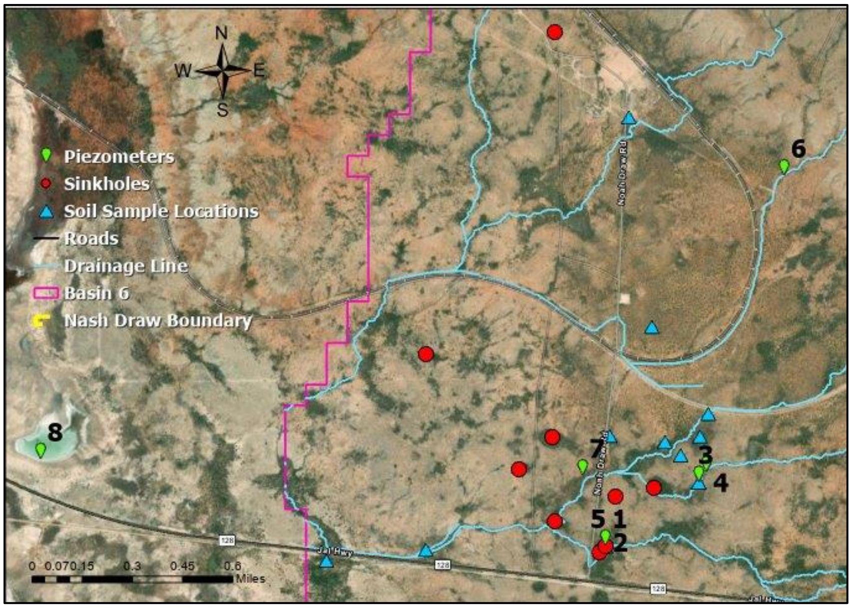

Figure 49. GIS map of field sampling locations in Basin 6. Green pin drop symbols show the deployment locations of the pressure transducers. Red dots show various sinkhole locations. Blue triangles are the locations where soil samples were collected.

Preparations for the Year 4 field work also included the purchase of 3 new HOBO water level data loggers (Figure 50, left) and the Eijkelkeamp soil sampling rings (Figure 50, right) used in Year 3 were cleaned for reuse. The HOBO U20L water level data loggers (piezometers) were tested to ensure they were operational and will provide accurate readings. The battery life and data storage were also determined, which is important as it determines how long the HOBO units can be left in the field to collect data. For example, if the time interval is five minutes, then the units can be left in the field for 75 days (about 2 and a half months) before they run out of data storage. The battery life of the HOBO U20L loggers is five years, which is adequate for this fieldwork campaign.

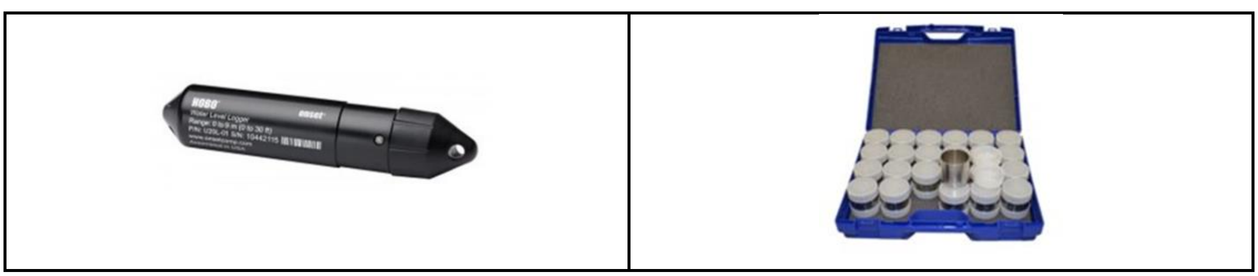

Figure 50. HOBO water level data logger (let) and Eijkelkamp soil sampling rings (right).

Subtask 6.3: Results and Discussion

Laboratory Analysis of Soil Samples Collected in FIU Year 3

The results from analysis of the 48 samples collected in Year 3 were compiled in a report titled *"Soil Parameter Variability in Basin 6"* that was submitted in March 2024 as Deliverable 2023-P2-D2. The average bulk density of the samples was 1.26 g/cm³, with lower values observed in samples collected closer to the surface. The average porosity was 41%, attributed to the presence of aggregates and small rocks. The mean organic content was 2.08%, though significant variation in organic content was observed across different locations and depths. On average, the samples contained 97.73% sand, indicating that the majority of the soil composition was sand. These results were then compared to existing federal databases. Figure 51 provides a direct comparison between the soil analysis data and the SSURGO dataset.

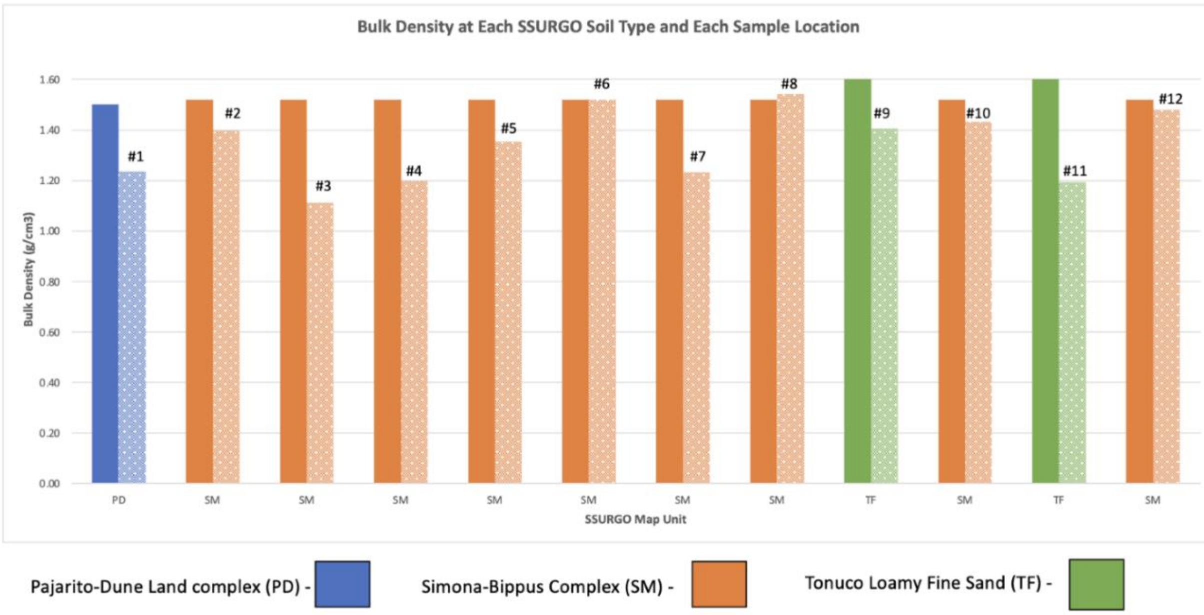

Figure 51. Graph of soil bulk density (g/cm^3) for each SSURGO map unit and each soil sample location within these units.

FIU Year 4 Fieldwork

The Year 4 fieldwork in Basin 6 was conducted on May 31 – June 3, 2024 by an FIU field team comprised of a senior research scientist and a DOE Fellow. Fieldwork support was provided by Dr. Anderson Ward, a Compliance Certification Manager from the DOE Carlsbad Field Office and Dr. Dennis Powers, a Consulting Geologist and subject matter specialist on the Nash Draw hydrogeology. Fieldwork activities included:

1. Collection of water level measurements from the 5 HOBO U20L pressure transducers installed in Summer 2023, routine maintenance of the devices, and redeployment in the same locations. These pressure transducers recorded data on the water levels in two sinkhole locations, a ponding location downstream of flow, and a V-shape upstream flow of the ponding location.
    - Location #1 → Sinkhole within sinkhole cluster.
    - Location #2 → Largest sinkhole within the Location #1 cluster.
    - Location #3 → A site of ponding water at the end of an upstream flow path.
    - Location #4 → The upstream flow path of Location #3.
    - Location #5 → Site near Location #2 placed above surface to monitor atm. pressure.

    Initial steps were taken to analyze the data obtained from the pressure transducers, as the data was downloaded from the units and uploaded to the HOBOware Pro software. The transducers will continue to collect data from Basin 6 into FIU Year 5. Figure 52 shows the pressure transducer measurements for the period August to October 2023. The graph displays the date and temperature variations for each location.

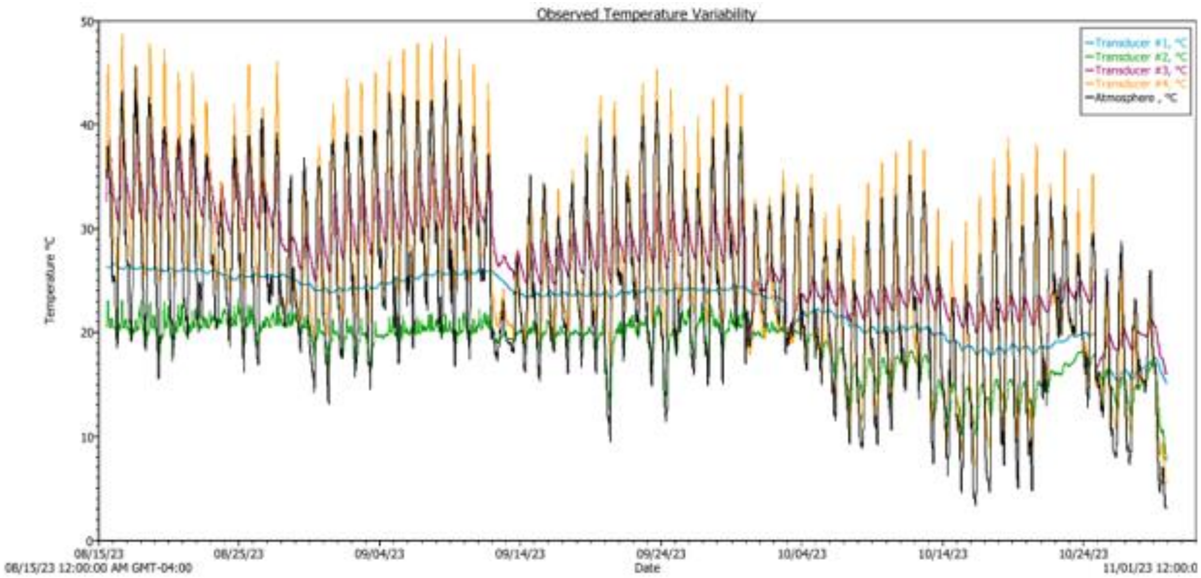

Figure 52. Temperature variation at each pressure transducer location for the months of August through October 2023 collected in FIU Year 4.

2. Deployment of 3 additional HOBO U20L water level loggers (pressure transducers) within the Basin 6 study area.

   - Location #6 → A trapezoidal channel.
   - Location #7 → West of Nash Draw Road, where the washout is located.
   - Location #8 → Within a salt lake.

   Figure 53 is an image of the setup for the first additional pressure transducer at Location #6. The pressure transducer is within the PVC pipe being held by a non-stretch wire. This location is in a trapezoidal channel with a bottom width of approximately 11.8 feet and a top width of approximately 22.1 feet. At Location #6, soil samples 1-4 of Box 1 were taken at depths ranging from the surface to 12 inches.

Figure 53. Pressure transducer at Location #6.

In Figure 54, an image of the setup for the second additional pressure transducer (Location #7) is seen. This location is west of Nash Draw Road by the washout. Multiple soil samples were taken at or within close proximity to Location #7.

Figure 54. Pressure transducer at Location #7.

Figure 55 shows an image of the setup for the third additional pressure transducer (Location #8). This location is within a salt lake. Soil samples were also taken at the salt lake or the surrounding area.

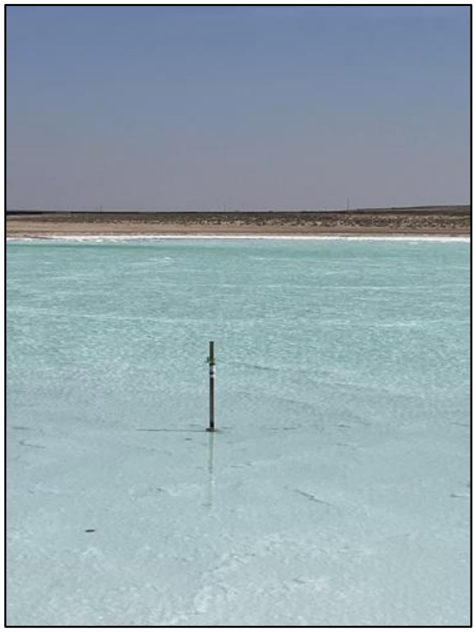

Figure 55. Pressure transducer at the salt lake (Location #8).

3. Collection of 32 additional soil samples at various strategic locations within the Basin 6 study area at depths from surface to 6.5 feet below the ground surface.

   In Figure 56, an image of the soil variation near the trapezoidal channel at Location #6 is seen. The soil samples taken relative to this location were taken upstream where the subsurface was exposed. The exposed subsurface showed variation in color, which seemed to correlate with the amount of gravel present.

Figure 56. Soil variation near Location #6.

Laboratory Analysis of Soil Samples Collected in FIU Year 4

FIU has completed the analysis of the Year 4 soil samples to determine porosity, bulk density, organic content, and soil texture and the results are undergoing an internal review. The laboratory procedure developed in Year 3 was slightly revised to reorder the process workflow for improved accuracy. The new sequence—porosity, followed by bulk density, organic content, and soil texture—was implemented to enhance the precision of the porosity measurement. In the analysis of the Year 3 soil data, conducting the bulk density test first disrupted the sample's natural state, which affected the accuracy of the porosity analysis. By testing porosity first, the soil sample remains in its undisturbed, natural condition, providing a more accurate representation of its in-situ porosity.

An Excel spreadsheet was created (Table 4) that contains the box number (#1 or #2), sample number (#1 - #24), location coordinates of the sample, the depth of the sample below the surface, and any comments or descriptions about the sample and its location. An Excel table was also created to record pertinent information for the pressure transducers such as the location number (#1-8) of the transducer, location coordinates, transducer serial number, dimensions of the sinkhole or feature of interest within which the transducers were placed, and the description.

Table 4. Results from Laboratory Analysis of Soil Samples Collected in Year 4

ID	Porosity	Bulk Density (g/cm^3)	Organic Content	Sand	Silt	Clay
Box #1						
1	0.36	1.63	0.94%	99.97%	0.03%	0.00%
2	0.36	1.56	0.82%	99.88%	0.12%	0.00%
3	0.34	1.53	0.97%	99.73%	0.25%	0.02%
4	0.30	1.51	0.80%	99.82%	0.18%	0.00%
5	0.36	1.46	1.10%	98.55%	1.45%	0.00%
6	0.29	1.58	1.50%	98.08%	1.92%	0.00%
7	0.38	1.24	1.33%	98.00%	2.00%	0.00%
8	0.36	1.17	1.45%	94.92%	5.08%	0.00%
9	0.34	1.66	0.51%	99.50%	0.50%	0.00%
10	0.38	1.49	0.55%	99.65%	0.35%	0.00%
11	0.27	1.40	1.60%	98.62%	1.38%	0.00%
12	0.44	1.33	1.98%	95.81%	4.19%	0.00%
13	0.32	1.64	0.59%	99.60%	0.40%	0.00%
14	0.30	1.56	0.61%	99.68%	0.32%	0.00%
15	0.33	1.62	0.45%	99.83%	0.17%	0.00%
16	0.33	1.45	0.44%	99.79%	0.21%	0.00%
17	---	---	---	---	---	---
18	0.28	1.00	18.60%	99.44%	0.56%	0.00%
19	0.40	1.06	17.21%	99.38%	0.62%	0.00%

20	0.30	1.68	0.75%	99.64%	0.36%	0.00%
21	0.33	1.72	0.70%	99.64%	0.36%	0.00%
22	0.33	1.39	1.10%	98.39%	1.61%	0.00%
23	0.31	1.53	0.92%	98.72%	1.28%	0.00%
24	0.34	1.42	1.08%	98.28%	1.72%	0.00%
Box #2						
1	0.34	1.46	2.63%	97.52%	2.48%	0.00%
2	0.32	1.50	1.65%	97.56%	2.44%	0.00%
3	0.33	1.44	2.18%	95.50%	4.50%	0.00%
4	0.32	1.47	1.73%	96.91%	3.09%	0.00%
5	0.42	1.12	18.43%	99.50%	0.50%	0.00%
6	0.39	1.10	15.50%	99.28%	0.72%	0.00%
7	0.4	1.24	9.56%	99.58%	0.42%	0.00%
8	0.33	1.46	2.62%	97.10%	2.90%	0.00%

Subtask 6.3: Conclusions

The soil and water level data derived from the field and laboratory work conducted thus far under this subtask only covers a very small area within Basin 6, and it is currently unclear how representative these are for the larger Basin 6 study domain. FIU therefore intends to continue collecting additional soil samples and water level measurements, broadening the geographic area within the Basin 6 domain where data is recorded to derive a more representative dataset of soil physical properties and surface flow. An infiltrometer has also been purchased and will be used in FIU Year 5 to record additional information to supplement the soil and water level data. Collectively, the data will aid in determining the soil surface and shallow subsurface characteristics at the hillslope scale as well as within the dry bed river network in Basin 6.

Subtask 6.3: References

Goodbar, A., Powers, D., Goodbar, J. and R. Holt (2020). Karst and sinkholes at Nash Draw, southeastern New Mexico (USA). DOI: 10.5038/9781733375313.1026.

Litzinger, A., Lawrence, A., Hazenberg, P., Lagos, L., Moulton, D., Zhang, Y., Ward., A. (2023) Work Plan: In-Situ Data Collection in Basin 6, NM to Support Development of a Hydrological Model using the Advanced Terrestrial Simulator (ATS). FIU-ARC-2023-800013918-04c-002.

Litzinger, A., Lawrence, A., Hazenberg, P., Lagos, L., Moulton, D., Zhang, Y., Ward., A. (2024) Technical Report: Soil Parameter Variability in Basin 6. FIU-ARC-2023-800013918-04c-002.

California Department of Pesticide Regulation Environmental Monitoring Branch Standard Operating Procedure for Soil Bulk Density Determination Using the Eijkelkamp Soil

Sampler (SOP# FSSO001.01, 02/18/2014), https://www.cdpr.ca.gov/docs/emon/pubs/ /fsso00101.pdf.

ASTM D2974 – 20ε1, Standard Test Methods for Determining the Water (Moisture) Content, Ash Content, and Organic Material of Peat and Other Organic Soils.

ASTM C136-06, Standard Test Method for Sieve Analysis of Fine and Coarse Aggregates.

Hydrogeologic properties of earth materials and principles of groundwater flow / William W. Woessner, Eileen P. Poeter - Guelph, Ontario, Canada, 2020. 205 p. ISBN: 978-1-7770541-2-0

CONFERENCE PARTICIPATION, PUBLICATIONS, AWARDS & ACADEMIC MILESTONES

Peer-reviewed Publications

In preparation for submission to a Journal TBD: Litzinger, A., Gutierrez-Zuniga, G., Risher, E., Moulton, D., Zhang, Y., Xu, Z., Ward, A., Lawrence, A., Lagos, L., Hazenberg, P. (2024) The Role of Sinkholes and the River Network on Local and Regional Scale Groundwater Recharge in Basin 6, Using Amanzi-ATS.

In preparation for submission to Journal of Hydrology: Zhou, Y., Alam, M., Lawrence, A., Morales, J., Looney, B. B., Seaman, J. C., Kaplan, D., Parker, C.J., Lagos, L. and P. Hazenberg. (2023) Hydrologic Model Development to Understand Flow and Shear Stress Variability during Extreme Precipitation Events in the Tims Branch Watershed, SC.

Doughman, M., Katsenovich, Y, O'Shea, K, Hilary P. Emerson, H. P., Szecsody J, Kenneth Carroll, K, and N. Qafoku, 2024, Impact of Chromium (VI) as a Co-Contaminant on the Sorption and Co-Precipitation of Uranium (VI) in Sediments Under Mildly Alkaline Oxic Conditions, *Journal of Environmental Management*, 349, 119463 doi.org/10.1016/j.jenvman.2023.119463

Katsenovich, Y, Drozd, V, Shambhu Kandel, S, Lagos, L, and M. Asmussen, 2024. The corrosion behavior of borosilicate glass in the presence of cementitious waste forms, *Dalton Transactions*, 53, 12740 DOI: 10.1039/D4DT00855C

Dickson, J., Estrada, C., Katsenovich, Y., Lagos, L., Johs, A., and E. Pierce, 2024. Sorption Kinetics and Stability of Conventional Adsorbents for Mercury Remediation. *Journal of Environmental Chemical Engineering* doi.org/10.1016/j.jece.2024.113664

Conference Presentations

Oral Presentations (presenter is underlined)

Yelena Katsenovich, Hilary Emerson, Jim Szecsody, Nikolla Qafoku, and Leonel Lagos, *"The Reoxidation Behavior of Tc(IV) and U(IV) in Perched Water of the Hanford Site Vadose Zone after Treatment with Strong Reductants"*. Waste Management Symposia 2024, March 10 - 14, 2024, Phoenix, AZ

P. Hazenberg, A. Litzinger, H. Aziz, Z. Xu, B. Looney, H. Gonzalez Raymat, H. Wainwright, C. Eddy-Dilek, R. Gudavalli, L. Lagos, A. Lawrence, *The Stability of Existing Contamination within the Savannah River Site's Braided River Network as Impacted by Heavy Precipitation and Changes in Climate - 24501*, Waste Management Symposia 2024, March 10 - 14, 2024, Phoenix, AZ.

Vadym Drozd, *"Borosilicate glass dissolution in the presence of cementitious waste forms",* Goldschmidt 2024 (Invited Talk), 18-23 August 2024, Chicago, IL.

Poster Presentations (presenter is underlined)

Aubrey Litzinger (DOE Fellow), David Moulton, Zexuan Xu, Anderson Ward, Pieter Hazenberg, Angelique Lawrence, Ravi Gudavalli, and Leonel Lagos, *"Exploring the Surface and Subsurface Hydrology of Basin 6 Near the WIPP Using Watershed Workflow and the Advanced Terrestrial Simulator (ATS)",* Roy G. Post Scholarship 2024 Winner Poster Session, WM2024 Conference March 10-14, 2024, Phoenix, Arizona, USA.

Hannah Aziz (DOE Fellow), Evaluating the Spatial Distribution of Contaminants Over Time in the SRS F-Area & their Potential Fate & Transport" (Poster Presentation), WM2024 Conference March 10-14, 2024, Phoenix, Arizona, USA.

DOE Fellows prepared and presented posters at 2023 DOE Fellows poster exhibition and competition:

- Exploring Regional Hydrology Near the WIPP Using Watershed Workflow and the Advanced Terrestrial Simulator - **Aubrey Litzinger**
- Evaluating the Spatial Distribution of Contaminants Over Time in the SRS F-Area & their Potential Fate & Transport – **Hannah Aziz**

Awards

DOE Fellow, Aubrey Litzinger, who supports the research on Tasks 3 and 6, was a recipient of a Roy G. Post Scholarship and presented a poster of her Task 6 research during the Roy G. Post Scholarship 2024 Winner Poster Session at the 2024 Waste Management Symposia.

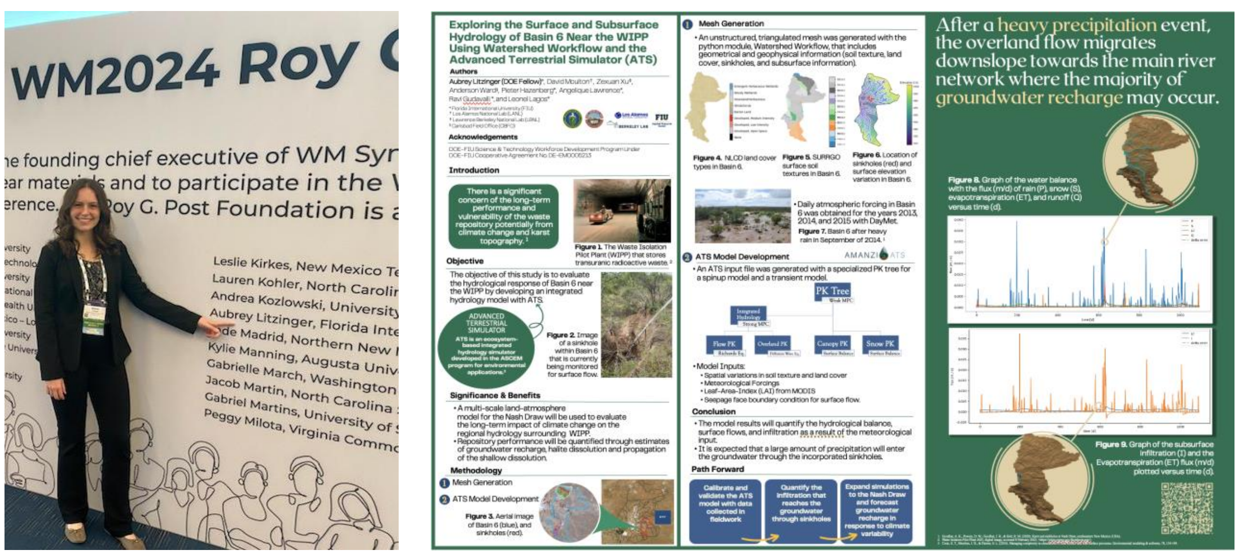

Figure 57. DOE Fellow and Roy G. Post Scholarship 2024 Winner, Aubrey Litzinger (left). Aubrey's poster was based on her research in Basin 6, NM (right).

Figure 58. ARC Research Specialist II, Angelique Lawrence (top photo), being awarded "Mentor of the Year" and DOE Fellow, Aubrey Litzinger (bottom photo), receiving a "special recognition" award at the Annual DOE Fellows Induction Ceremony held in November 2023 at FIU's Modesto Maidique Campus.

Academic Milestones

DOE Fellow Mariah Doughman successfully passed her Ph.D. defense. Her dissertation is titled *"Evaluation and Sensing of problematic Pollutants in the Environment"* (Abstract in APPENDIX D). Upon graduation in summer 2024, Mariah joined Pacific Northwest National Laboratory as a Postdoctoral Associate.

Figure 59. Mariah Doughman receiving her PhD in Chemistry at FIU's commencement ceremony (left) and with her mentor, Dr. Yelena Katsenovich (right).

Former DOE Fellow, Juan Morales, graduated with a PhD in Environmental Health Sciences in March 2024. A part of his dissertation titled *"Long-Term Monitoring Of Heavy Metals Using Numerical Modeling And Molecular Indices"* was based on the Task 3.1 research in the Tims Branch watershed at Savannah River Site, Aiken, SC (Abstract in APPENDIX E). Juan was also the recipient of the Dean's Award for Academic Excellence. He joined the Marine Corps in 2022.

Figure 60. Former DOE Fellow, Juan Morales, during FIU's Spring 2024 commencement ceremony (left) and in his Marine Corps uniform (right).

DOE Fellow, Hannah Aziz, graduated with a BS in Environmental Engineering in Spring 2024 and was accepted into a PhD program at Northwestern University beginning in the Fall of 2024.

Figure 61. Hannah Aziz with family at FIU's commencement ceremony.

Community Outreach

The Environmental Modeling Group teamed with the ARC Robotics team to host 8 AP Human Geography students and their teacher, Ms. Laura Massa, from Palmer Trinity School located in Palmetto Bay, Miami and conducted a presentation titled “Mapping Contaminants: A Real-World Application of GIS in Human Geography” on Nov. 17, 2023 as a form of ARC Outreach to the Miami-Dade community. The Environmental Modeling Group’s presentation was focused on the use of Geographic Information Systems (GIS) to map contaminants at U.S. Department of Energy sites across the country and in developing hydrological models to predict the potential transport and spread of those contaminants under extreme meteorological conditions. The ARC Robotics team then presented several indoor and outdoor robotic scanning and mapping technologies which contain various types of cameras and sensors, some of which we use to collect GIS data. The robotic technologies demonstrated included a ground penetrating radar (GPR) mounted on a rover and a drone equipped with a 20MP camera which are being used to scan outdoor terrain, a mini rover used to scan the inside of radioactive waste storage tanks, and the Spot® robot dog from Boston Dynamics.

Figure 62. AP Human Geography Students from Palmer Trinity School viewing robotic scanning and mapping technologies used to collect GIS data at the Applied Research Center.

ACKNOWLEDGEMENTS

Funding for this research was provided by U.S. DOE Cooperative Agreement #DE-EM0005213. FIU's Applied Research Center would like to acknowledge the commitment of DOE-EM to this specific Environmental Remediation Science and Technology project and to all the collaborators at DOE-EM HQ and the National Labs for support of the research being conducted as part of the DOE-FIU Cooperative Agreement. The partnership between DOE EM and FIU has also resulted in the development and training of outstanding minority STEM students that will benefit this country as a whole.

APPENDICES

Please note that the reports included in the Appendices have been written in manuscript format to submit them for publication in peer-reviewed journals. Posting these documents on the web would risk identification by plagiarism detection software, such as Turnitin, making them ineligible for publication due to a self-plagiarism issue. A one-year moratorium is anticipated on these peer-reviewed journal publications. Once published, the FIU Year End Report will be updated and posted on the FIU-DOE research website: (https://doeresearch.fiu.edu/SitePages/Welcome.aspx).

APPENDIX D and APPENDIX E contain the abstracts of DOE Fellow dissertations based on research conducted under the DOE-FIU Cooperative Agreement. For the full version of these documents, please refer to FIU's Digital Commons Institutional Repository (https://digitalcommons.fiu.edu/etd/) or contact the DOE-FIU Cooperative Agreement PI, Dr. Leonel Lagos (lagosl@fiu.edu).

APPENDIX A

The following documents are available at the DOE Research website for the Cooperative Agreement between the U.S. Department of Energy Office of Environmental Management and the Applied Research Center at Florida International University: https://doeresearch.fiu.edu/SitePages/Welcome.aspx

FIU Year 4 Annual Research Review Presentations:

1. FIU Research Review - Project 1
2. FIU Research Review - Project 2
3. FIU Research Review - Project 3 - D&D IT ML
4. FIU Research Review - Project 4
5. FIU Research Review - Project 5
6. FIU Research Review - Project 4-5 – Carlos Rios
7. FIU Research Review - Project 4-5 – Fellow Aris
8. FIU Research Review - Project 4-5 – Fellow Aubrey
9. FIU Research Review - Project 4-5 – Fellow Melissa
10. FIU Research Review - Project 4-5 – Fellow Ocampo
11. FIU Research Review - Project 4-5 – Fellow Victor
12. FIU Research Review - Project 4-5 – Fellow Theophile
13. FIU Research Review - Wrap Up - Project 1
14. FIU Research Review - Wrap Up - Project 2
15. FIU Research Review - Wrap Up - Project 3 – D&D IT ML
16. FIU Research Review - Wrap Up - Project 4
17. FIU Research Review - Wrap Up - Project 5

APPENDIX B

Full version of Subtask 1.4: Experimental Support of Lysimeter Testing, *Prepared in Manuscript Format for Subsequent Publishing.*

APPENDIX C

Full version of Subtask 2.1: Environmental Factors Controlling the Attenuation and Release of Contaminants in the Wetland Sediments at Savannah River Site, *Prepared in Manuscript Format for Subsequent Publishing.*

APPENDIX D

ABSTRACT OF THE DISSERTATION

EVALUATION AND SENSING OF PROBLEMATIC POLLUTANTS IN THE ENVIRONMENT

by
Mariah Springer Doughman

Florida International University, 2024
Miami, Florida

Professor Kevin E. O'Shea, Major Professor

Uranium waste generated during plutonium production at the Hanford Site, a U.S. Department of Energy legacy nuclear site in Washington State, was released to and contaminated the subsurface. Monitored natural attenuation is a common approach for remediation of contaminants released to the subsurface. However, when contaminants are commingled, their transport may be challenging to predict due to competitive reactions.

The objective of this study was to understand the fate of uranium in conditions similar to those at Hanford in the presence of chromium and iodine as co-contaminants. Column and batch experiments, along with thermodynamic equilibrium speciation modeling were conducted to investigate the impact of chromium and iodine on uranium attenuation mechanisms in carbonate-rich sediments. Experiments were performed under slightly alkaline conditions (pH~8) in the presence of major groundwater components (calcium, magnesium, sodium, potassium, carbonate, chloride, and sulfate) with varying uranium:chromium:iodine molar ratios.

Speciation results indicated the presence of relatively weak adsorbing, aqueous calcium uranyl carbonate species (neutral and negatively charged). For the lower molar ratios of uranium:chromium:iodine, uranium adsorption decreased in the presence of co-contaminants. For the higher molar ratios of uranium:chromium, batch and column results suggest that uranium adsorption slightly increased in the presence of chromium. This could be due to the increase in ionic strength and/or a potential change in the U(VI) speciation which likely favored the formation of charged species that could adsorb strongly. Understanding the fate of uranium under Hanford subsurface like conditions is critical in the development of effective passive remediation strategies of complex contaminated sites with uranium and other co-contaminants.

Per and polyfluoroalkyl substances (PFAS) are contaminants that are also commonly found at DOE sites. Currently, there is a need for a cost-effective rapid assay for field monitoring. The objective of this study was to determine if PFAS could be detected using a β-cyclodextrin: fluorophore complex. Results indicated that fluorescence modulation of the complex is observed with the addition of PFAS and binding constants of the compounds to the cavity of β-cyclodextrin were determined. This demonstrates the possible utilization of this system in the field at Hanford and similar DOE sites.

APPENDIX E

ABSTRACT OF THE DISSERTATION

LONG-TERM MONITORING OF HEAVY METALS USING NUMERICAL MODELING AND MOLECULAR INDICES

by
Juan C. Morales

Florida International University, 2024
Miami, Florida

Major Professor: Alok Deoraj; Co-Major Professor: Quentin Felty

Climate change is anticipated to intensify storm events, leading to increased river streamflow. In the case of the Tims Branch Watershed (TBW) this heightened flow raises concerns about toxic legacy discharges. The TBW was contaminated with uranium (U) and other heavy metals from a Cold War-era nuclear fuel facility. Our study aims to monitor heavy metal transport and aquatic toxicology in the TBW to understand the potential human health risk during frequent storm events. The transport of heavy metals was modeled in the Tims Branch discharge. A significant proportion of elevated suspended sediment concentrations (SSC), carried by particles with a hydrodynamic diameter greater than 1 μm, is influenced by critical current velocity, sediment mass, and resuspension rate. Measured observations aligned well with modeled simulations, revealing that SSC can exceed 40 $mg \cdot l^{-1}$ during high-streamflow events in the Tims Branch River. Our water quality component modeled the flux of U within Average Recurrence Intervals (ARIs) ranging from 1 to 500 years at critical locations in the Tims Branch stream. The 500-year ARI peak discharge rate was found to transport the greatest quantity of U-sorbed sediment. The organic carbon partition coefficient (Koc) played a crucial role in U mobility calibration, with a value of 833,333 $l \cdot kg^{-1}$. Considerably higher U flux ($mg \cdot s^{-1}$) during the 500-year ARI was observed, resulting in transport to the TBW outlet (3550% increase in simulated storm conditions) and the Steed Pond outlet (1327% increase compared to base streamflow). The transport models are helpful in monitoring heavy metals downstream, but it is important to determine their toxicological relevance. Therefore, we used nuclear respiratory factor 1 *(nrf1)*, and its target genes in zebrafish as biological surrogates for assessing aquatic toxicity. Our results revealed significant modifications to *nrf1* mRNA expression associated with arsenic (As) and cadmium- (Cd) exposed females, and mercury (Hg) exposed male zebrafish. Transcriptomic data from zebrafish exposed to heavy metals were used to generate probabilistic graphical models using Bayesian Networks with Java Objects (BANJO). Bayesian Networks showed *nrf1* toxicity signatures from arsenic and cadmium exposures aligned with stress response pathways. Moreover, enriched stress pathways including apoptotic signaling, transcription regulation, and catalytic activity, were observed across all male zebrafish groups. *nrf1* and its target genes such as *chac1, dnajb11, gstp1,* and *hspa8* demonstrated toxicity responses to As, Cd, and Hg exposure in both sexes. These insights have critical implications for the long-term monitoring of heavy metal transport, particularly during episodic rain events and their potential adverse health outcome. Our estimations can support the as Our estimations can support the assessment of heavy metal deposition hotspots, planning, and decision-making for the TBW and elsewhere.